Lateral Path Tracking in Limit Handling Condition using SDRE Control

Master's thesis in Product Development

ERIK WACHTER

Department of Applied Mechanics
CHALMERS UNIVERSITY OF TECHNOLOGY

Göteborg, Sweden 2016

MASTER'S THESIS IN PRODUCT DEVELOPMENT

Lateral Path Tracking in Limit Handling Condition using SDRE Control

ERIK WACHTER

Department of Applied Mechanics
Division of Vehicle Engineering & Autonomous Systems
CHALMERS UNIVERSITY OF TECHNOLOGY

Göteborg, Sweden 2016

Lateral Path Tracking in Limit Handling Condition using SDRE Control
ERIK WACHTER

Master's thesis 2016:63
ISSN 1652-8557
Department of Applied Mechanics
Division of Vehicle Engineering & Autonomous Systems
Chalmers University of Technology
SE-412 96 Göteborg
Sweden
Telephone: +46 (0)31-772 1000

Cover:
TNO BMW car lab doing a drift on the skid pad in Lelystad

Chalmers Reproservice
Göteborg, Sweden 2016

Lateral Path Tracking in Limit Handling Condition using SDRE Control
Master's thesis in Product Development
ERIK WACHTER
Department of Applied Mechanics
Division of Vehicle Engineering & Autonomous Systems
Chalmers University of Technology

Abstract

Tires operated at or close to their friction limits show a highly nonlinear force response. This state is called limit handling condition. The objective of this research is to minimize lateral path tracking error whilst the tires operate in limit handling. The State Dependent Riccati Equation (SDRE) technique is employed to develop a feedback-feedforward steering controller. It gives a systematic approach to take into account model nonlinearities such as combined slip tire characteristics. Furthermore the controller was implemented on real-time hardware and tested on a test track. The controller shows reliable path tracking performance up to the friction limits and also for conditions with large body sideslip angle, also referred to as "Drifting". Additionally a linear throttle controller was implemented to achieve autonomous body slip control on top of the path control. Experimental evaluation of this controller also showed promising results in terms of combined position and vehicle state control.

Keywords: Lateral Control, Path Tracking, Steering Controller, Autonomous Drifting

Preface

This is the final report of a Master Thesis Project. It represents one requirement in order to complete a Masters study programme at Chalmers University of Technology and acquire the title Master of Science. In this case the project was proposed by TNO in Helmond, Netherlands, which provided the assignment and resources to conduct the project.

Acknowledgements

Firstly, I would like to express my sincere gratitude to my supervisor Dr. Mohsen Alirezaei for the continuous support of my graduation project. His guidance, and the countless discussions together with him, have always been very positive and productive.

Besides my supervisor I would like to thank my examiner Prof. Dr. Fredrik Bruzelius. His valuable feedback gave direction to the research and broadened my horizon at the same time.

I want to thank TNO for providing the assignment and for giving me excellent opportunities to conduct the experiments. Thanks to all the collogues who made the time at TNO a very positive experience. In particular to mention are the other graduate students at TNO: Robbin, Niels, Jorrit, Wouter, Koos, Manikandan, Sujit, Chyannie and Manigandan, who made the year in Eindhoven such a great time.

Especially I want to thank my parents and family, who not only supported me during the time of my graduation project, but throughout all the endeavours of my Master studies.

Nomenclature

Acronyms

CG	Center of Gravity
DYC	Direct Yaw Control
FB	Feedback
FF	Feedforward
LH	Left Hand
LQR	Linear Quadratic Regulator
MF	Magic Formula
MPC	Model Predictive Control
OS	Oversteer
PID	Proportional Integral Differential
RE	Riccati Equation
RH	Right Hand
SDC	State Dependent Coefficient
SDRE	State Dependent Riccati Equation
SMC	Sliding Mode Control
US	Understeer

Greek Symbols

α_i	Tire sideslip angle of tire or axle i
β	Body sideslip angle
δ	Steering angle at the front wheel(s)
λ_i	Longitudinal tire slip of the respective tire i
ζ	Solution of the Hamiltonian
μ	Tire-road friction coefficient
ω	Rotational wheel speed
ψ	Heading angle
ρ	Curvature of the actual trajectory
ρ_{des}	Desired/reference curvature that is to be tracked
ρ_{path}	Path curvature

Roman Symbols

$\mathbf{A}$	System dynamics
$\mathbf{B}$	System inputs
$\mathbf{K}$	Feedback control gain matrix
$\mathbf{P}$	Solution of the Riccati Equation
$\mathbf{Q}$	State weighting matrix
$\mathbf{R}$	Input weighting matrix
$\mathbf{u}$	Input
$\mathbf{x}$	Vehicle state
$e_{x/y}^{\vec{g}}$	Axis of the global frame of reference
$e_{x/y}^{\vec{v}}$	Axis of the vehicle frame of reference
a_x	Longitudinal acceleration
a_y	Lateral acceleration
a_{tot}	Total/cornering acceleration: $\sqrt{a_x^2 + a_y^2}$
$C_{\alpha,i}$	Lateral stiffness of tire or axle i
$C_{\lambda,i}$	Longitudinal stiffness of tire or axle i
d	Distance along a path/arc length
e_ψ	Heading error
e_ρ	Curvature Error
e_{la}	Look-ahead error
$F_{x,i}$	Longitudinal tire force of respective tire or axle i

$F_{y,i}$	Lateral tire force of tire or axle i
$F_{z,i}$	Vertical tire force of respective tire or axle i
g	Gravitational constant: 9.81 m/s^2
h_{CG}	Vehicle CG height
I_z	Vehicle inertia around z-axis
J	Quadratic cost performance index
K_{US}	Understeering gradient
L	Look-ahead point
l	Wheelbase
l_f	Distance from CG to front axle
l_r	Length from CG to front axle
l_t	Track width
m	Vehicle mass
M_z	Moment around vehicle z-axis
R	Corner radius
r	Yaw rate
r_w	Wheel radius
t	Time
v/v_{tot}	Total velocity
v_x	Longitudinal velocity
v_y	Lateral velocity
X	Cartesian coordinate in respective axis
x_{la}	Look-ahead distance
Y	Cartesian coordinate in respective axis

Contents

Part I
Introduction

1 Background

Road traffic injuries are the leading cause of death among people between five and 29 years old in Europe [09]. This is the reason for a consistent demand to increase road safety. One way to reduce the number of accidents is to introduce safety systems to road vehicles. Figure 1.1 shows the roadmap of passive and active systems and how they provide to the aim of minimizing traffic fatalities.

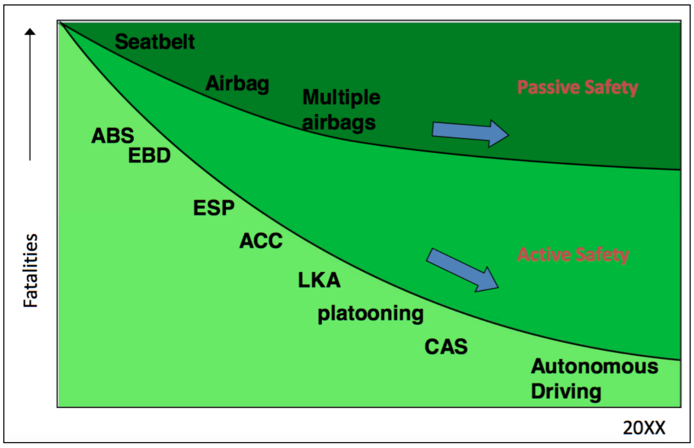

Figure 1.1: *Roadmap to minimizing of road traffic fatalities via Autonomous Driving [Ali15]*

The causes behind traffic accidents are 72% purely due to human error [Tho+13]. Therefore the ultimate aim is to take the responsibility from the human driver and introduce fully autonomous driving. Therefore one necessity is to have reliable autonomous action of the vehicle in any driving scenario. A particularly extreme case in that sense is collision avoidance. While autonomous driving cars are intended to avoid safety critical situations in the first place these can occur when non-predictable objects pop up on the intended track of the vehicle, for example approaching traffic or dropped cargo.

If the required stopping distance then is too small, evasive manoeuvring and exploitation of the vehicle handling limits might be necessary to reduce risk of a collision. To guarantee reliable and safe autonomous action up to the limits of handling marks one of the pieces in the puzzle, that has to be put into place to complete the roadmap towards autonomous driving.

2 Problem

Active yaw rate control using differential braking, that allowed to keep a vehicle stable in dangerous driving conditions, was firstly introduced to passenger cars in 1995 [Lie+]. It became enforced by law to be standard safety feature for new cars in the EU from 2014 on [Par09]. The system supports the driver in the sence of helping to keep the vehicle controllable via preventing skidding and spinning out. Logic controllers distribute braking torque over all four wheels in a predefined manner, in order that large sideslip angles are avoided and tires are controlled to stay in the linear regime. Therefore the drivers demanded yaw rate might be compromised [Raj12]. Supporting the driver in dangerous situations with this system it is still his responsibility to steer the car and track his desired path.

The essence of autonomous driving is that the vehicle will take responsibility of tracking the desired path. Facilitating active steering, a number of different controllers have been proposed and are already employed in passenger cars for lane following assistance systems. Mainly linear controllers have been employed for safe lane following in highway like environments. The main characteristics of highway driving in fact is that highway lanes make smooth bends. Therefore small steering inputs together with low yaw rates are expected.

Evasive maneuvering like in a collision avoidance scenario happens in a short time horizon and requires large actuator inputs together with high yaw rates. Tires will operate close to their friction limits and can partly be oversaturated, coming together with large sideslips. In this condition tire force characteristics become highly nonlinear making it hard to stabilize the vehicle, which is therefore called limit handling condition. Controllability via steering input becomes very much limited in these conditions [Hin13]. Authority over yaw dynamics at high sideslip manoeuvres can be gained using differential braking as additional actuator to the steering.

There is few controllers developed for specific cases of limit handling scenarios like collision avoidance in a structured urban environment [Gra+], for autonomous drifting experiments [Hin13] or for following a racing line [Kri12]. However the variability and generality of the control approaches is limited since they were designed for specific scenarios or are only valid for limited sideslip angles. A further step is to put emphasis on path tracking under limit handling conditions when following an avoidance path. Therefore the command of the existing actuators have to be intelligently distributed to achieve maximum tracking performance with minimum vehicle excitation in varying environmental conditions. Figure 2.1 shows the problem schematically.

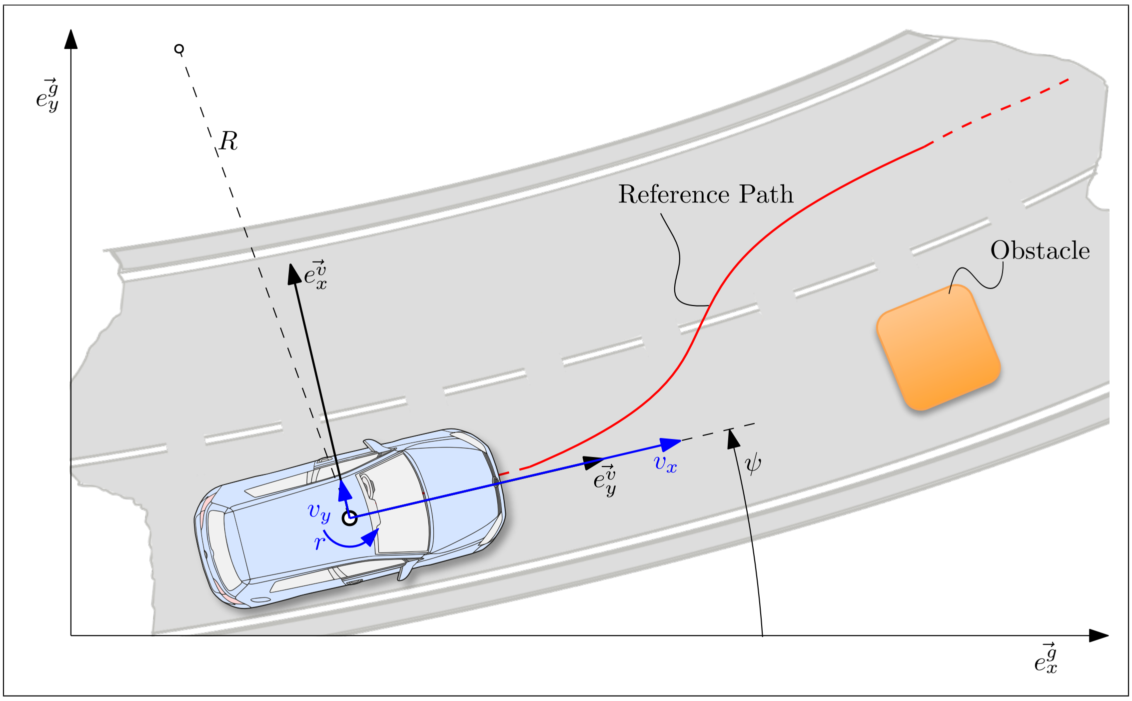

Figure 2.1: *Problem visualization: The vehicle is required to do an evasive manoeuvre for reducing risk of a collision.*

The vehicle shown has to track the reference path in an evasive fashion, otherwise a risk for collision is prevailing. In this specific scenario the reference path is a quick lane-change, whereas case dependent the path can have any shape.

3 Delimitations

In this research the goal is to control the lateral motion of a vehicle in limit handling condition, whilst following a desired path. To achieve this, the control approach relies on existing and cost effective sensors for detecting the position with reference to the path.

Forward-looking sensors like camera and radar are the available tools for active safety applications in today's vehicles. Furthermore research shows that vehicle states and friction estimates can be estimated in real-time using standard sensors available in production cars, such as gyroscpopes and wheel speed sensors [Hoe16]. State information is taken for granted for possible control schemes in this research. Also the path planning is done independently, so the method will rely on available path information, which is computed offline. Summarized the delimitations are:

- Reference path is available, see also Section 9.1 for delimitations on the path,
- path information from Radar and Camera are available for path tracking task and
- vehicle state feedback is available in real-time.

There is a Toyota Prius available at TNO for experimental investigation. With this prospect vehicle and tire parameters are taken from the Prius as well. Therefore calculations, simulations and results in this thesis are done on behalf of the Prius, see Appendix A. In case other parameters are used it is pointed out explicitly. However in the process of the thesis work it was concluded that for experimentation of limit handling scenarios a different vehicle would be more suitable. Therefore, from Chapter 22 simulation and experimentation is done on behalf of a BMW 5 series, see Appendix B.

4 Report Outline

Before developing the lateral motion controller, it is necessary to discuss fundamentals and recent research results in this field. In Part II relevant fundamentals in lateral vehicle motion are treated with special emphasis on the nonlinear nature of tire-road friction. Also a definition of the limit handling operation regime is given. Subsequently in Part III the path tracking control problem is defined together with an investigation of related problem formulations from literature. Taking the problem description in mind a survey of control method alternatives is done.

In Part IV the development of the SDRE controller is described together with an explanation of the control method itself. Together with the SDRE feedback controller also feedforward terms are used and therefore described in here. Part V contains the explanation of relevant scenarios for testing the controller. Results of computer simulation are shown and discussed. Also a basic investigation of body sideslip control is done. Part VI describes necessary adaptions made for controller implementation into a real car for testing. Also testing results are shown. The report finishes off with conclusions about the project and recommendations for future work.

Part II
Lateral Vehicle Motion

Relevant fundamentals about lateral vehicle dynamics with special emphasis on vehicle stability and tire-road friction are to be discussed in this part. These are prerequisites for designing the lateral path tracking controller. Vehicle dynamics are discussed on behalf of a well suited lateral model using the convention as it can be seen in Figure 2.1. The vehicle moves in a global frame of reference $\vec{e^g}$. The vehicle reference frame $\vec{e^v}$ is fixed to the center of gravity (CG) of the vehicle and aligned with the vehicle in a sense that $\vec{e^v_x}$ points towards the front and $\vec{e^v_x}$ points towards the left, each in positive direction respectively. The vehicle translates with longitudinal and lateral velocity, v_x and v_y, respectively. The orientation of the vehicle ψ changes due to the yaw rate r, whereas positive yaw rate means turning to the left. This convention is used throughout the whole report together with SI units. Furthermore for generation of graphs shown in this chapter the Toyota Prius parameters are used, see Appendix A. Concluding in this part the explanation of the limit handling operating regime is given.

5 Linearized Model

Looking at a generic four wheel vehicle with front wheel steering, the wheels of each axle can be modelled into one wheel per axle for simplification. A bicycle like planar model is the result, see Figure 5.1. It has three degrees of freedom, these beeing longitudinal velocity v_x, lateral velocity v_y and yaw rate r. The steering input is depicted by δ. The length from CG to front and rear axle are represented by l_f and l_r respectively. Negotiating a turn with this bicycle model, a particular relation between steering angle and turning radius can be found.

$$\delta = \arctan\left(\frac{l}{R}\right) \tag{5.1}$$

This purely kinematic relation holds for low velocities with approximately zero lateral acceleration. The governing assumption is that the velocity vectors at the front and rear wheel point in the direction of the wheel respectively [Raj12].

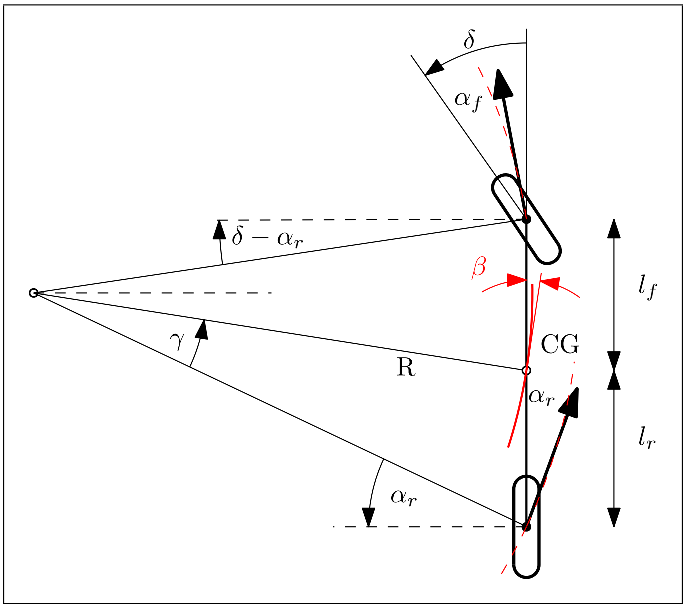

Figure 5.1: *Bicycle model cornering with lateral acceleration present*

For higher vehicle speeds this assumption can no longer be made. Lateral acceleration is present, yielding tire lateral forces. Result is a lateral velocity component of each wheel meaning that the velocity vector no longer points in the direction of the wheel. The slip angle is defined as the angle between the orientation of a wheel and the orientation of the velocity vector of that wheel [Raj12]. Figure 5.1 shows a bicycle model cornering with lateral acceleration present and points out the slip angles.

$$\alpha_f = \delta - \arctan\left(\frac{v_y + l_f r}{v_x}\right) \tag{5.2}$$

$$\alpha_r = \arctan\left(\frac{-v_y + l_r r}{v_x}\right) \tag{5.3}$$

Experimental data shows that tire lateral force is proportional to the tire slip-angle, for small slip angles [Raj12] [Gil92].

$$F_{y,i} = C_{\alpha,i}\alpha_i \tag{5.4}$$

The tire lateral stiffness C_α is tire specific and depends on different parameters like vertical load, tire pressure, size, type and number of plies. When assuming longitudinal speed to be constant a two degree of freedom model can be obtained using Newtons second law. Force and moment balance at the center of gravity yield

$$m\ddot{y} = m(\dot{v_y} + v_x r) = F_{y,f} + F_{y,r} \tag{5.5}$$

$$I_z\ddot{\psi} = I_z\dot{r} = l_f F_{y,f} - l_r F_{y,r} \tag{5.6}$$

Using Equation 5.4 for calculating tire forces, $F_{y,f/r}$, the two degree of freedom bicycle model is obtained.

$$\begin{bmatrix} \dot{v_y} \\ \dot{r} \end{bmatrix} = \begin{bmatrix} -\frac{C_{\alpha,f}+C_{\alpha,r}}{mv_x} & -v_x + \frac{l_r C_{\alpha,r} - l_f C_{\alpha,f}}{mv_x} \\ \frac{l_r C_{\alpha,r} - l_f C_{\alpha,f}}{I_z v_x} & -\frac{l_r^2 C_{\alpha,r} - l_f^2 C_{\alpha,f}}{I_z v_x} \end{bmatrix} \begin{bmatrix} v_y \\ r \end{bmatrix} + \begin{bmatrix} \frac{C_{\alpha_f}}{m} \\ \frac{l_f C_{\alpha_f}}{I_z} \end{bmatrix} \delta \tag{5.7}$$

From this system in the form of $\dot{\mathbf{x}} = \mathbf{Ax} + \mathbf{Bu}$, fundamental stability properties of lateral vehicle motion can be obtained as follows.

6 Steady-state Cornering and Stability

Applying a step input in steering will lead to lateral slip on the front wheel, which in turn creates lateral force and the model will enter a turn. Lateral acceleration of the model occurs when entering a turn. As a result, also the rear wheel will create lateral slip. Geometrical properties, mass, tire stiffness and longitudinal velocity will decide if the vehicle can stable negotiate the turn. If assumed that $R \gg l$ the geometric relation for steering can be obtained from Figure 5.1.

$$\delta = \frac{l}{R} + \alpha_f - \alpha_r \tag{6.1}$$

Steady-state cornering implies constant lateral acceleration and zero change in yaw rate, $r = v_x/R$.

$$a_{y,SS} = v_x r \tag{6.2}$$

$$= \frac{v_x^2}{R} \tag{6.3}$$

A relation for steering input necessary to negotiate a turn with radius R dependent on longitudinal velocity v_x is obtained for steady-state condition [Raj12].

$$\delta = \frac{l}{R} + K_{US}\frac{v_x^2}{R} \tag{6.4}$$

where

$$K_{US} = \frac{m}{l}\left(\frac{l_r}{C_{\alpha,f}} - \frac{l_f}{C_{\alpha,r}}\right) \tag{6.5}$$

K_{US} depicts the Understeering Gradient. Depending on it, the required steering input to negotiate a turn with radius R will differ from the pure geometrical contribution L/R. There exist three different cases [Raj12].

1. **Neutral steer**, $K_{US} = 0$
   Negotiating a turn with constant radius R does not require a change in steering input as speed is varied.

2. **Understeer**, $K_{US} > 0$
   Negotiating a turn with constant radius R does require an increase in steering input as speed is increased.

3. **Oversteer**, $K_{US} < 0$
   Negotiating a turn with constant radius R does require a decrease in steering input as speed is increased.

Figure 6.1 shows steering input as a function of lateral acceleration in g for the respective cases. The speed at which the steering input is zero for oversteering case is called critical speed v_{crit}.

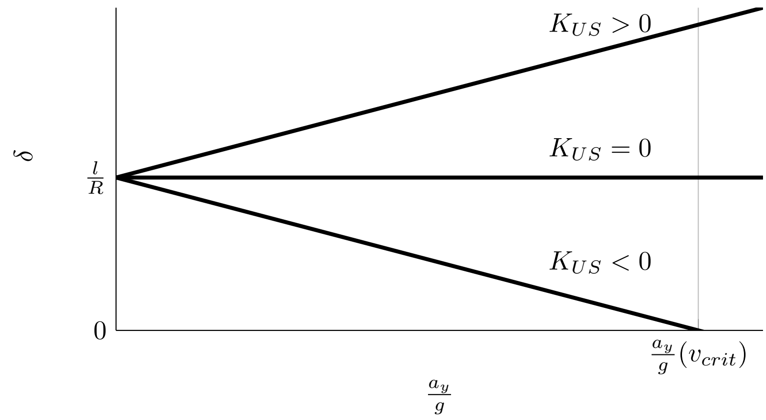

Figure 6.1: *Required steering input with respect to lateral acceleration in order to negotiate a turn with radius R*

At this speed the bicycle model becomes unstable and can no longer negotiate the turn. This relation represents the Hurwitz stability criteria of the bicycle model from Equation 5.7. Furthermore due to the lateral velocity component a body sideslip β adheres to the model.

$$\beta = \arctan\left(\frac{v_y}{v_x}\right) \approx \frac{v_y}{v_x}, \quad \text{for } v_x \gg |v_y| \tag{6.6}$$

As seen from Figure 5.1, the body sideslip angle represents the heading error with respect to the vehicle trajectory. This means a mismatch between heading vector and velocity vector of the CG and equals zero only if α_r is equal to the angle $\gamma = l_r/R$. This is the case at the exact speed, when v_x fulfils

$$\frac{l_r}{R} = \frac{l_f}{C_{\alpha,r} l} \frac{m\ v_x^2}{R} \tag{6.7}$$

This error however is predefined, since the slip angles at rear and front are completely determined for fixed radius R and speed v_x [Raj12].

7 Tire Characteristics and Limit Handling

Lateral motion at higher accelerations involves significant tire lateral slip, and the linear model does not hold any more. Tire forces show a particular and highly nonlinear friction characteristic for increasing lateral slip. Additionally to lateral slip, which yields lateral tire force, as introduced in Section 5, there is longitudinal slip, yielding longitudinal tire force. It is defined as normalized relative movement between tire running surface and road,

$$\lambda = \frac{\omega\ r_w - v_x}{v_x}. \tag{7.1}$$

Furthermore, lateral and longitudinal tire forces are mutually dependent. A lot of research has been spent on the tire and yielded several types of mathematical models for tire force calculation. The range spans from empirical models (using experimental data only) to theoretical models (using physical models). All types support their specific purpose, while inheriting different levels of accuracy and complexity. A widely used and practical model is the semi-empirical Magic Formula (MF) tire model [Pac12]. A MF model is shown in Figure 7.1.

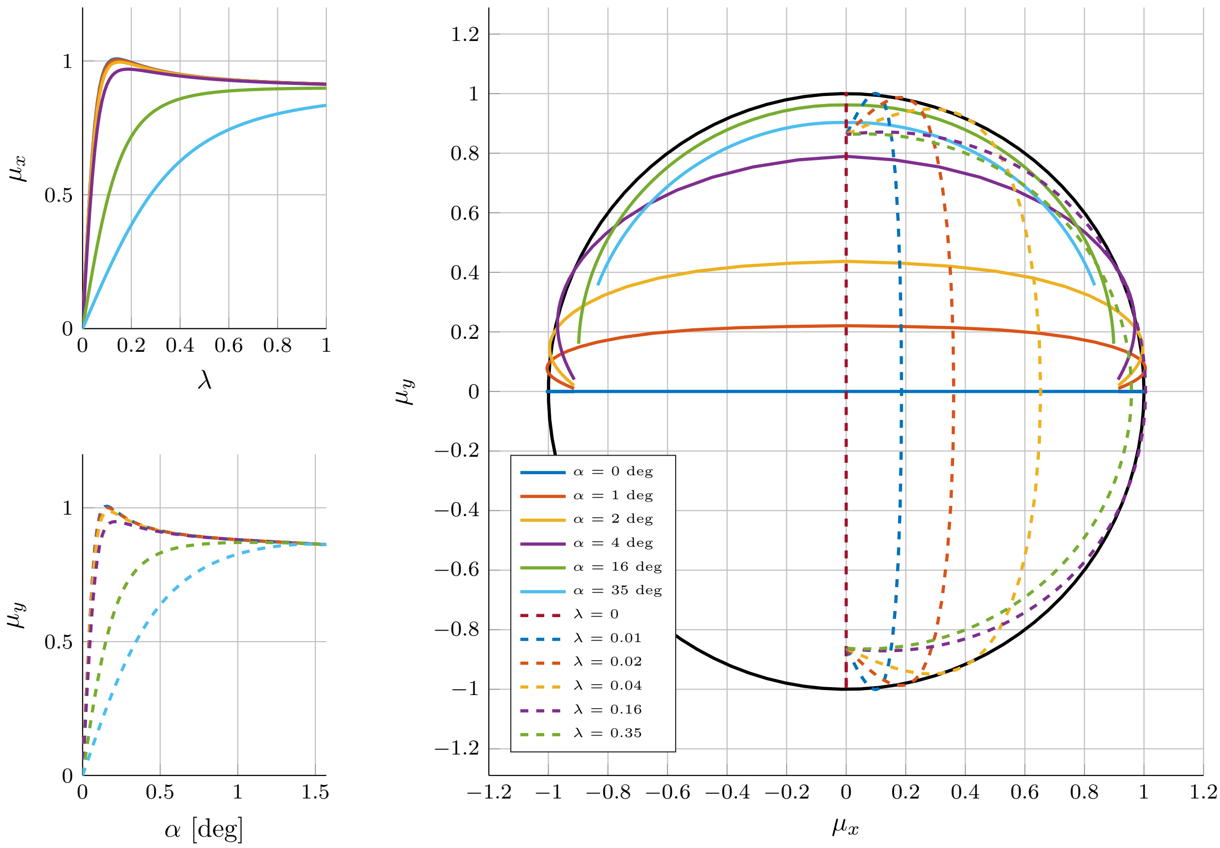

Figure 7.1: *Left: Magic Formula lateral and longitudinal slip curve for a typical passenger car tire, Right: Combined lateral and longitudinal slip friction circle*

The governing dependency of longitudinal/lateral tire-road friction, $\mu_{x/y} = \frac{F_{x/y}}{F_z}$, on longitudinal/lateral tire slip, λ/α, is shown. Firstly, pure slip scenarios are considered, where $\alpha = 0$ for the μ_x-graph and $\lambda = 0$ for the μ_y-graph. At about zero slip, both curves show an approximately linear stiffness, which decays to zero and yields the tire friction peak at about 10% slip. The peak is followed by a large saturation range, which represents the physical limitation of tire-road friction. However, for combined slip scenarios, lateral capabilities of the tire are compromised by the longitudinal slip and vice versa. This is expressed in terms of the so called friction circle on the right. Friction values do not exceed it. Therefore, in order to exploit the full capabilities of a vehicle in an evasive manoeuvre, the applied control system should account for this combined slip behaviour. Furthermore, the saturation at large tire sideslip should be considered, as changes in steering have then a highly reduced impact onto change of yaw rate. This behavior is different in comparison to maneuvering within the linear range. It makes the vehicle hardly controllable for average drivers [Raj12]. This condition is therefore called limit handling.

First active lateral stability control systems were introduced in commercial cars in the 1990s. Examples are the ESP from Mercedes and the DSC3 from BMW. In the meanwhile these systems became state of the art and even compulsory for new production cars in Europe. They are aimed to keep the vehicle in a handling envelope, which is safe for the driver when doing lateral manoeuvres. Facilitating differential braking between left and right wheels yaw moment is controlled in order to limit yaw rate depending on the desired corner radius [Raj12]. The vehicle is prevented from spinning out (exceeding desired curvature), and tire saturation of only one axle is avoided to sustain controllability for the driver [Lie+]. Direct Yaw Control (DYC) Systems only facilitate the brake system and do not take path tracking into account. Application of active steering additionally to the differential braking can take the responsibility of path following from the driver in emergency cases. Such evasive manoeuvres require the control system to make optimal use of the tire potential in every time instance, and therefore take combined slip behaviour into account.

8 Cornering with Saturated Tires

Lateral motion at the friction limits can be investigated when taking tire nonlinearities into account. This can be done using the bicycle model and incorporating a nonlinear tire model for pure lateral slip. Also the influence of steering angle on lateral front axle force can be taken into account.

$$\begin{bmatrix}\dot{\beta}\\ \dot{r}\end{bmatrix} = \begin{bmatrix}\frac{F_{y,f}\cos\delta + F_{y,r}}{mv_x} - r\\ \frac{l_f F_{y,f}\cos\delta - l_r F_{y,r}}{I_Z}\end{bmatrix} \tag{8.1}$$

where the relation between lateral velocity and sideslip is $\beta = v_y/v_x$. The nonlinear tire model of the Prius is represented through $F_{y,i} = f(\alpha_i)$. Figure 8.1 shows a phase portrait of the model for one fixed set of steer angle $\delta = 3$ deg and speed $v_x = 15$ m/s. As demonstrated in literature there are three equilibria appearing [Ono+13] [Klo10] [Hin13].

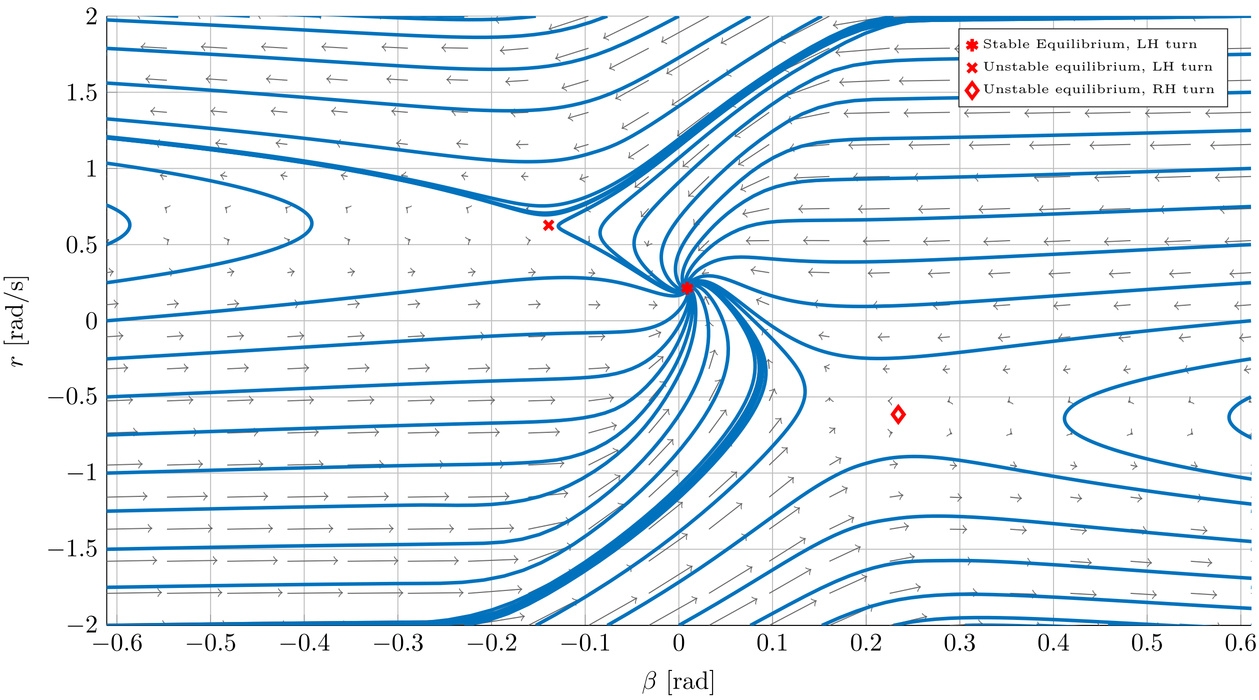

Figure 8.1: *Phase portrait of lateral vehicle dynamic model (Equation 8.1) with Prius parameters for v_x = 15m/s and δ = 3 deg*

One of them appears to be a stable equilibrium where the system trajectories converge to in a certain envelope for limited sideslip and yaw rate. Two appear to be open loop unstable drift equilibria. One appears for positive, left hand (LH) turning with moderate absolute sideslip and one appears for right hand (RH) turning (negative yaw rate) and large absolute sideslip angle. Both are located in the phase plane where the vehicle is highly excited and at the edge to spin out, which can be seen from the divergence in sideslip. A well known example, where cornering techniques using these so called drift equilibria are applied, is rallye racing. For rally drivers it is quite common to corner with the rear tires of their racecar saturated and working the vehicle at the edge of the stable handling envelope. This is directly opposing the DYC principle which aims to avoid tire saturation in order to keep the vehicle stable and controllable for the driver.

A successful drifting controller using linearization about one of these equilibria could be presented [VHG10].

Based on human driver data, it was investigated how the control strategy for producing such a manoeuvre would look like. It usually consists of two sequences, an open and a closed loop sequence. During the open loop sequence the driver ramps, then holds a relatively large and constant steering input, bringing the car near the limits of handling. Initiation of the drift is done by saturating the rear tires using rear brake. Due to the combined slip characteristic, a sudden drop in rear lateral force yields an increase in yaw moment. Then the yaw rate peaks, yielding an increase in lateral velocity magnitude and sideslip magnitude as well. This marks an initial condition and from then on closed loop activity occurs where the driver actively avoids a vehicle spinout via increasing counter steering and actively avoids an exit of the drift via reducing counter steering.

The control scheme presented follows the same process as the drivers intuition. An open loop sequence brings the vehicle over a threshold value of v_y. Then the steering controller is activated. The feedback controller is designed based upon a linearized bicycle model of the desired equilibrium, using constant stabilizing gains for lateral velocity and yaw rate error. Longitudinal velocity is controlled using rear drive torque. Generally for drifting to sustain necessary forward velocity, longitudinal slip needs to be generated on the saturated rear tires, to gain longitudinal force.

Three governing characteristics of the drift equilibria were proposed [Hin13]. The first one is that the sideslip is highly sensitive to yaw rate variations. The impact of steering input on sideslip is mainly outweighed by the effect of it via yaw dynamics. Secondly, the front tires work around their maximum friction potential meaning that controllability through steering is limited. Thirdly, the rear drive force holds main control authority as a result of the combined slip characteristic at rear tire saturation. Also by [EP09] and [Vel+09] it was concluded that sufficient drive torque plays a prominent role for drifting. It is also possible to find cornering equilibria for vehicles only equipped with differential drives and without steering input. There exist multiple equilibria for any cornering radius in combination with a certain longitudinal speed [VFT09].

Especially in sharp, hair-pin turns and on low friction surfaces, using this practice they achieve maximum performance (minimum time on track) [Hin13]. In longer turns even a steady-state condition with large sideslip can be observed. Dynamic programming showed that rallye driving techniques correspond to the minimum-time cornering solution when a fast exit of the turn is most important [Efs08] [E V]. However this is not always the case and one more reason why this cornering technique is mostly used for races on dirt and loose surfaces is that tire behaviour is different on solid surfaces, in comparison to loose gravel for instance. For the latter case, tire force does not experience a typical decline at large slip, to the contrary it even increases slightly. This effect presumably rather originates from the tire interacting with loose objects than from pure slipping on a solid surface, see Figure 8.2.

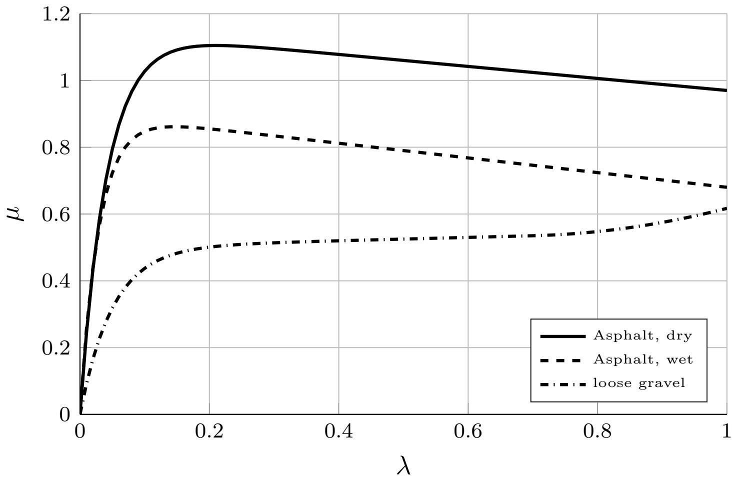

Figure 8.2: *Dependence of tire force between different grounds, according to [Trz08]*

However, for drifting on solid grounds, there is ultimately not more grip to be expected (for normal car tires). The total friction is limited as seen from the concept of the friction circle. Though, for sharp turns there can still be an advantage using rear tire saturation. The maximum cornering acceleration resulting from the friction limits can not be achieved for sharp turns when only using steering input. This effect is called steering effectiveness in literature [Fra08]. A thorough explanation of it can not be found however. It might appear from the reason that for very sharp turns a limit in achievable yaw rate exists, r_{max}. Using the relations for longitudinal and lateral acceleration, $a_y = \dot{v_y} + v_x r$ and $a_x = \dot{v_x} - v_y r$ respectively, and assuming steady-state cornering the following relation for cornering acceleration can be obtained.

$$a_{tot} = \sqrt{(v_x r)^2 + (-v_y r)^2} = r v_{tot} \tag{8.2}$$

For sharp turns v decreases and the required yaw rate r tends to infinity. As well the cornering radius R becomes very small and turning transfers to a kinematic problem, where the slip angle of the rear tire drops close to zero. Imagine the geometrical cornering problem, as seen in Figure 8.3. The term $-v_y + l_r r$ converges to zero, as does the rear lateral slip.

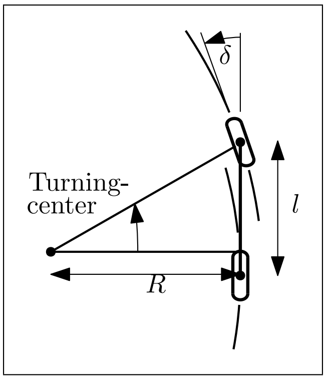

Figure 8.3: *Kinematic Turn*

In these cases it is beneficial to saturate the rear tires and force them into larger sideslip angle. This can be compared to rear wheel steering and allows for exploitation of sharp turns which is also referred to as doughnuts. Furthermore another investigation gives also a different view on the term steering effectiveness. Solving the system of Equation 8.1 for the cornering equilibria with the maximum cornering acceleration $a_{tot,max}$ dependent on speed v_x, yields the graph in Figure 8.4.

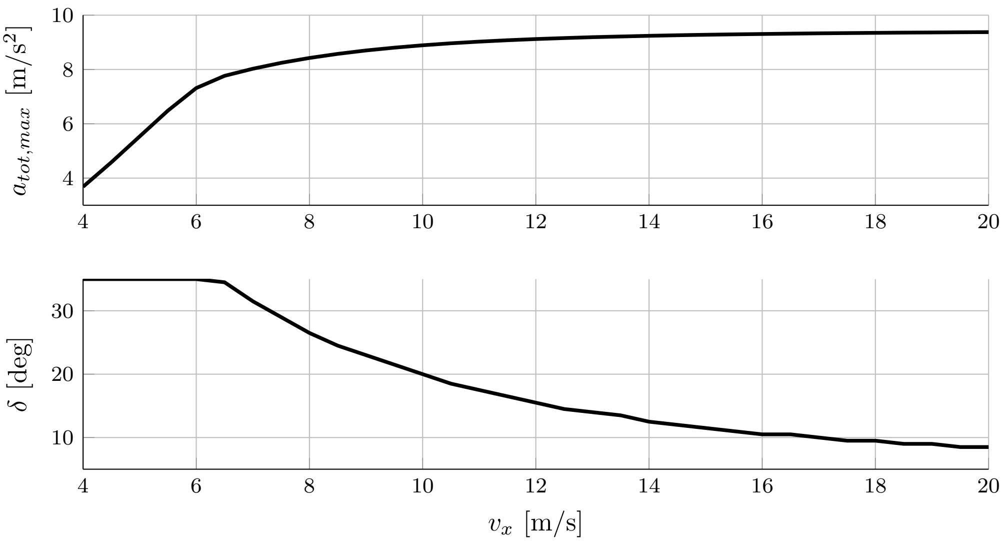

Figure 8.4: *Equilibria with maximum cornering acceleration of the nonlinear bicycle from Equation 8.1*

.

It can be seen that for v_x smaller than 12 m/s the maximum cornering acceleration drops significantly. When looking at the corresponding steering input, it can be seen that with increasing steering angle the maximum available cornering acceleration drops. The reason is that due to turning the front wheel the lateral force component of the front tire contributing to cornering reduces with the factor $\cos\delta$. For speed v_x smaller than 6 m/s, steering reaches the considered mechanical steering limit of 35 degree. This lets the maximum cornering acceleration drop further. This investigation shows that for speeds below 12 m/s, there might be the advantage of increased body sideslip in terms of drifting, yielding to reduced steering effort and in turn increased maximum cornering performance.

The following points became apparent from the literature study.

1. Increasing the β-r handling envelope, in which the vehicle can be stabilized allows accounting for external disturbances, that could otherwise make the vehicle unstable when it is already in limit handling condition
2. Large sideslip manoeuvres are connected to higher yaw rates as seen from Figure 8.1 which can be beneficial in certain transient conditions. This could be for instance that collision avoidance requires entering a sharp turn or changing direction. Deliberate tire saturation could be beneficial and increase handling capabilities in these scenarios.
3. Drifting trims could increase maximum cornering acceleration for certain grounds and for low speeds, when steering effectiveness comes into play.

Therefore considering drifting handling regimes is relevant for the limit handling lateral controller in this research. Further research is necessary in order to show the benefits quantitatively.

Part III
Path Tracking Control Problem

In this part the task of path tracking in limit handling is broken down to the underlying control problem. In the first place this task implies the vehicle has to track a certain reference, which in turn was designed having underlying capabilities of the vehicle itself in mind. The reference should be output of a high level path planning algorithm, which takes data from the environment sensors like camera and radar into account. The focus in this research is to exploit the performance for tracking a reference path given from a high level path planner. This path is assumed to be given and can be somewhat arbitrary, as it results from arbitrary avoidance situations in real traffic.

However, when assuming tire-road contact to be the only mechanical connection between vehicle and environment, then there is a strict physical limit to the arbitrariness and therefore achieveability of the path. This should be clarified first and gives delimitations on the project. Furthermore, related control problem formulations from literature are investigated in order to find the best suiting formulation for path tracking in limit handling condition. Also control alternatives are compared to see which one suits best for the control problem.

9 Definition of Reference Path

It must be defined, in which physical quantity the reference path appears as input and what means path achievability.

9.1 Curvature Achievebility

A path is represented in terms of a curvature, $\rho = 1/R$, and as a function of distance d along the path itself, $\rho_{path} = f(d)$. Assuming constant speed v, the relation between two-dimensional Cartesian coordinates X, Y and path curvature ρ_{path} is as follows.

$$X = \int v \cos \psi dt \tag{9.1}$$

$$Y = \int v \sin \psi dt \tag{9.2}$$

$$\psi = \int \rho_{path}(t) v dt \tag{9.3}$$

Assuming a vehicle to have point mass properties, it could achieve a maximum horizontal acceleration of $a_{max} = \mu_{v,max} g$, where $\mu_{v,max}$ is the maximum friction coefficient. The latter one is mainly dependent on the peak tire-road friction coefficient, but also other factors. For instance due to weight transfer and suspension dynamics not all tires can work at their peak friction in every condition. Nevertheless, for simplification purpose it can be seen as a constant and be taken as the peak lateral value from the friction ellipse. Assuming the vehicle to be travelling along a steady-state arc with constant speed, a maximum curvature for the vehicle can be found.

$$\frac{1}{\rho_{max}} \geq \frac{v^2}{a_{max}} \tag{9.4}$$

Figure 9.1 shows the relation graphically for different $\mu_{v,max}$. A path is generally inachieveable if the desired curvature at any instance of the path, ρ_{des}, exceeds ρ_{max}. However, for actual paths where curvature and speed are not constant, desired yaw rate of the vehicle changes.

$$r_{des}(t) = v(t) \rho_{des}(t) \tag{9.5}$$

Is the vehicle already moving at its friction limits or close to it, it will most probably not be able to follow a required (significant) change in curvature. With tires working on their friction limits, there is simply not

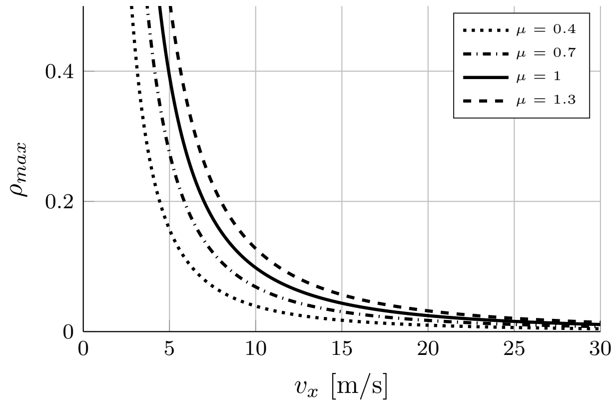

Figure 9.1: *Maximum curvature a vehicle (with point mass properties) can achieve dependent on friction*

enough yaw moment that can be created quick enough. So the scope of this project is to increase achievability of paths with $|\rho_{des}| \lessapprox \rho_{max}$. The heading of the vehicle should be changed as quick as possible, whilst retaining positional constraints to the path when tires operate at or close to the friction limits.

9.2 Curvature as a Function of Time

In an avoidance path, rate of change in desired curvature is large in comparison to normal highway driving. A path can be seen as a connection of transient parts, where one part resembles the change from one steady-state condition (cornering equilibrium) to another. In this situation the vehicle will deviate from the path if it can't gain a large enough curvature rate. Figure 9.2 shows a qualitative curvature profile over time, where a change from one equilibrium to another is negotiated. When speed along the path is considered to be constant, then time axis also represents distance d along the path.

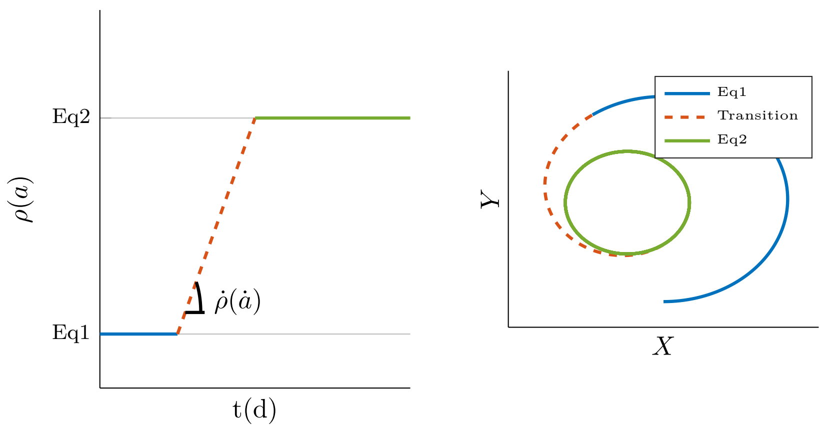

Figure 9.2: *Transition between one curvature equilibrium to another dependent on time t, or distance d, for constant speed along the path*

The curvature rate $\dot{\rho}$ of the vehicle can be seen as the ability to change its course.

$$\rho = \frac{r}{v} \tag{9.6}$$

$$\dot{\rho} = \frac{d}{dt}\frac{r(t)}{v(t)} \tag{9.7}$$

$$\dot{\rho} = \frac{\dot{r}}{v} - \rho\frac{\dot{v}}{v} \tag{9.8}$$

where v is the total velocity of the vehicle.

$$v_{tot} = \sqrt{v_x^2 + v_y^2}\ , \quad \forall v_x \geq 0 \tag{9.9}$$

It follows

$$\dot{\rho} = \frac{\dot{r}}{v_{tot}} - \rho \frac{v_x \dot{v}_x + v_y \dot{v}_y}{v_{tot}^2} \tag{9.10}$$

where when assuming $\dot{v}_x = 0$ and using $\dot{v}_y = \dot{\beta} v_x$

$$\dot{\rho} = \frac{\dot{r}}{v_{tot}} - \frac{\dot{\beta}}{v_{tot}^2} \rho v_x v_y \tag{9.11}$$

Assume a vehicle with $v_x > 0$ negotiating a positive turn, $\rho > 0$, in steady-state condtition, $v_y = constant$. Therefore $\dot{\rho}$ is directly proportional to $\dot{r}$ and $-\dot{\beta} v_y$. So the ability of a vehicle to change its course is directly dependent on its capabilities in yaw acceleration and changing sideslip. These two quantities need to be optimized in order to track a path as agile as possible. As seen from Equation 5.6, yaw acceleration is dependent on the yaw moment that can be created around the z-axis of the vehicle.

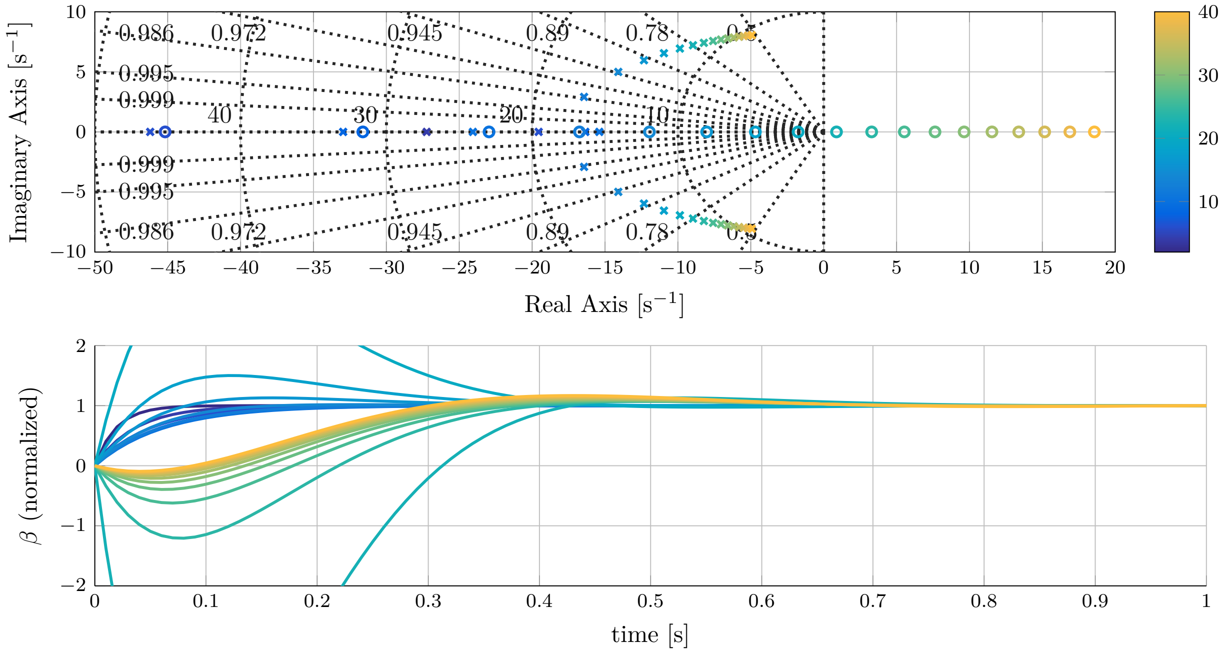

Figure 9.3: *Pole zero map and step response of β for open loop bicycle model*

As it is desired in this project to use differential wheel inputs, these can be used to create additional yaw moment and should increase path tracking performance. However for change in sideslip this relation is not as trivial. Some insight brings investigation of the open-loop bicycle model, see Equation 5.7. Figure 9.3 shows a pole-zero-map and normalized step response for $\beta = v_y/v_x$ and changing v_x. Since the Prius has a positive understeering gradient the state is open-loop stable, but for velocities greater than 20 m/s the response looses phase due to a positive zero. This behavior is far from optimal, but it lies within the nature of the bicycle model, that following a steering input, firstly the front axle builds up slip and force. Thus the initial response is positive sideslip.

It should be checked to what extent the response in sideslip can be altered using differential wheel slip inputs. These actuators act as an additional input for the state r. A four wheeled vehicle is assumed, where the two inner wheels (with respect to the turn) produce yaw moment via negative slip. It represents the use of selective braking actuation. The resulting additional yaw moment is

$$M_{z,\lambda} = \frac{2 C_\lambda l_t}{I_z} \lambda \tag{9.12}$$

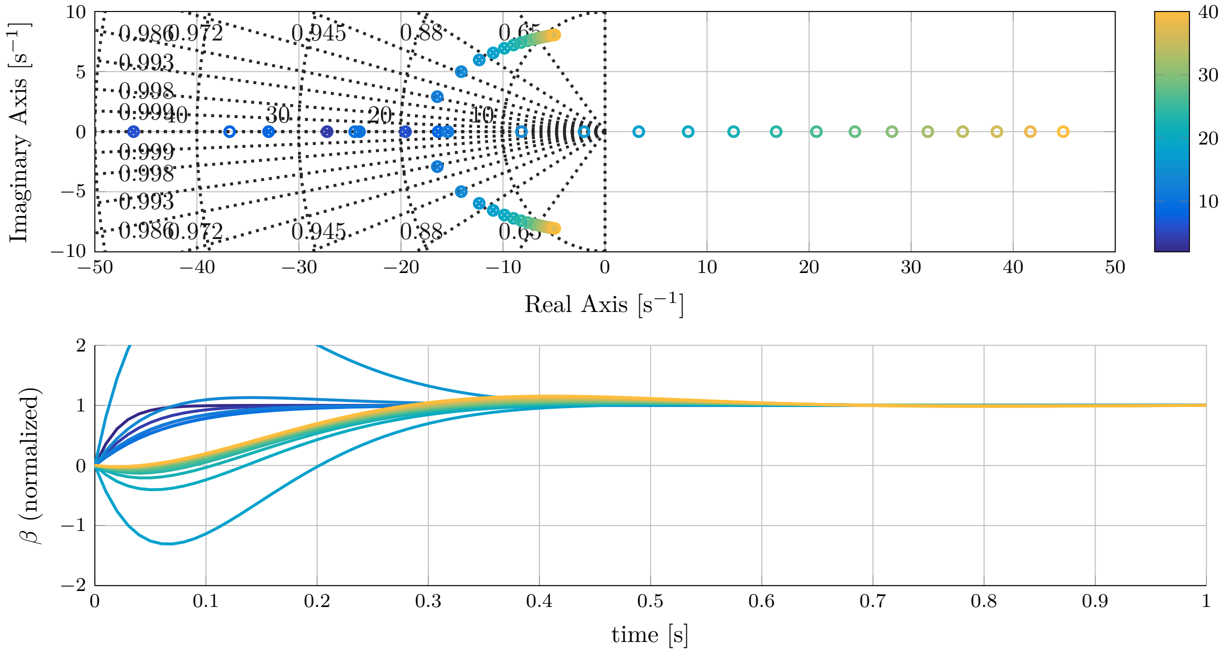

Figure 9.4: *Pole zero map and step response of β for open loop bicycle model with additional actuators*

where C_λ represents the linearized longitudinal tire stiffness and l_t represents the half track width of the vehicle. The term **Bu** from Equation 5.7 can be altered to

$$\begin{bmatrix} \frac{C_{\alpha_f}}{m} & 0 \\ \frac{l_f C_{\alpha_f}}{I_z} & \frac{2C_\lambda l_t}{I_z} \end{bmatrix} \begin{bmatrix} \delta \\ \lambda \end{bmatrix} \tag{9.13}$$

When adding the two transfer functions $\delta \to \beta$ and $\lambda \to \beta$ together, the influence of the additional input can be investigated. Figure 9.4 shows the pole-zero-map and step response.

The new transfer function shows three zeros, of which one still remains in the right half plane, see Figure 9.4. The non-minimum phase characteristic for higher velocities persists, but since two zeros remain in the left half plane and are located closer to the origin, these act as dominant and improve the transient behaviour of β. This can be seen in a less oscillatory transient part compared to the system with only steering input. Also the system reacts in a way that further increase of yaw moment input would further reduce the impact of the positive zeros, and therefore further decouple yaw motion from lateral motion. This shows how wheel slip inputs alter the characteristics in terms of body slip response.

9.3 Curvature Response

The actual response in terms of curvature can be assessed for the linear bicycle, using $\dot{\rho} = \frac{\dot{r}}{v_x}$. Different actuator combinations should be analysed to see the influence on the curvature response of the bicycle model. Five relevant setups are compared.

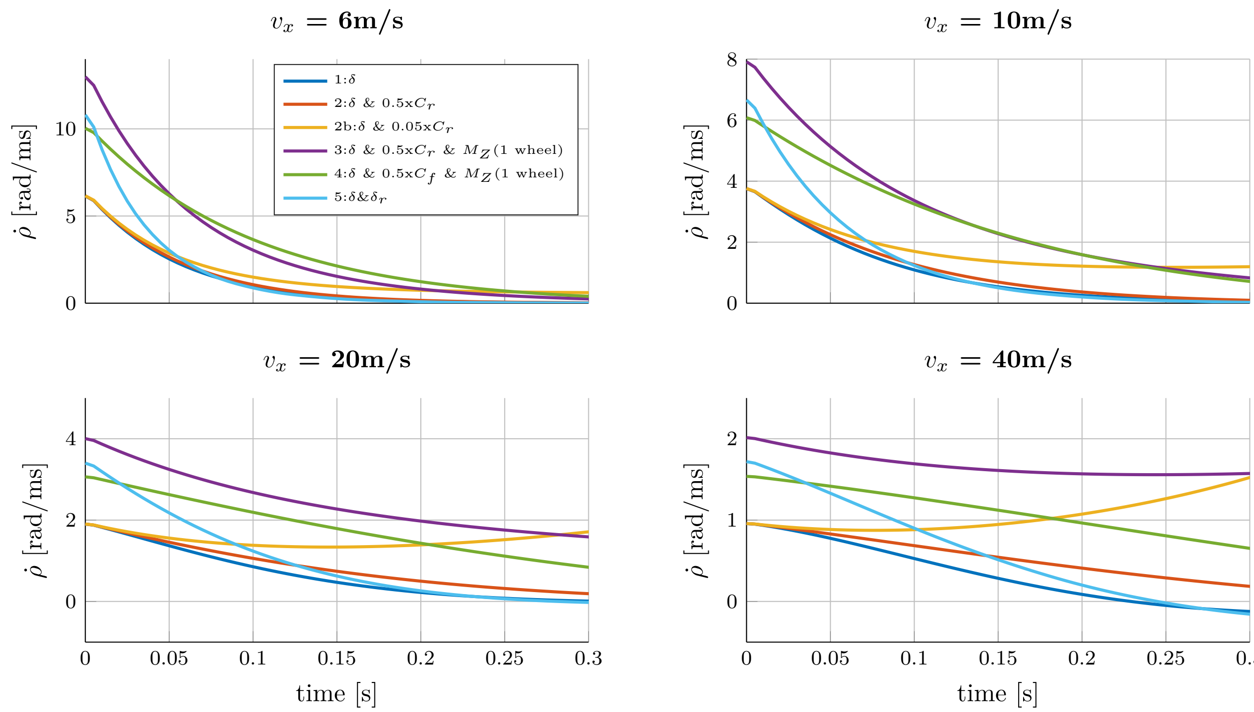

Figure 9.5: *Step response in curvature for different actuator combinations*

1. **Front wheel steering input δ_f:** This resembles the standard input for the bicycle model.

2. **Front wheel steering input, δ_f together with wheel slip input λ on the rear axle:** As both wheels of the rear axle get the same slip, representing rear wheel drive propulsion torque, the rear cornering stiffness will drop due to the tire combined slip behavior. This in terms of the bicycle model will represent a vehicle with smaller understeering gradient, therefore rather oversteering. Two cases are considered, one with rear cornering stiffness reduced by 50% (Line 2 in plot) and one case with rear cornering stiffness reduced by 95% (Line 2b in plot). The latter one represents a fully saturated rear axle, which can only be generated with large longitudinal tire slip $|\lambda_r|$, due to driving or braking toque.

3. **Front wheel steering input δ_f and wheel slip λ on the inner wheel (with respect to the turn), on the rear axle in order to generate additional yaw moment, according to Equation 9.13:** This represents the case with differential braking actuation. Only one wheel is considered and represents a minimum in available actuators (worst case). It is considered that this wheel is part of the rear axle, and also the rear axle cornering stiffness is reduced by 50% to represent the combined slip characteristic.

4. **Same as Setup 3, but additional yaw moment is generated with λ at the inner wheel of the front axle:** Respectively is the front axle cornering stiffness reduced by 50% (to represent combined slip tire characteristics).

5. **Front wheel steering input δ_f and rear wheel steering input δ_r:** This represents a costly option that is not relevant for small and middle class production cars at this moment, but is considered as a benchmark.

Figure 9.5 shows a step response in curvature of the above mentioned setups. The setup numbers correspond with the figure. Focus is the initial curvature response, since it indicates on how quick a vehicle can change its course.

It can be seen that Setup 1,2 and 2b show an identical initial response. Decreased understeering gradient yields a response with a smaller decrease in curvature. It even shows instability in terms of diverging curvature response for Setup 2b, with further decreased understeering gradient. This shows an oversteering vehicle, where the critical speed v_{crit} is exceeded in all four plots. However it can be seen that there is no variation in initial response, and that the rear tire saturation does not influence initial response.

To change initial response additional actuators are necessary, as the graph for Setup 3 shows. With creating additional yaw moment on the rear axle, Setup 3 reaches the maximum response at all speeds. In comparison, Setup 4 performs less good, where the additional yaw moment is created on the front axle. This is a relevant observation, since it suggests to prioritize the use of additional actuation for the rear axle. The reason lies within the decrease in front axle cornering stiffness. For equal initial steering input this yields less initial lateral force. Figure 9.6 shows the response in slip angle of front and rear axle for only steering input. It can be seen that the steering input yields instant slip on the front axle and thus lateral force. For the rear axle slip needs to build up first, before lateral force can be created.

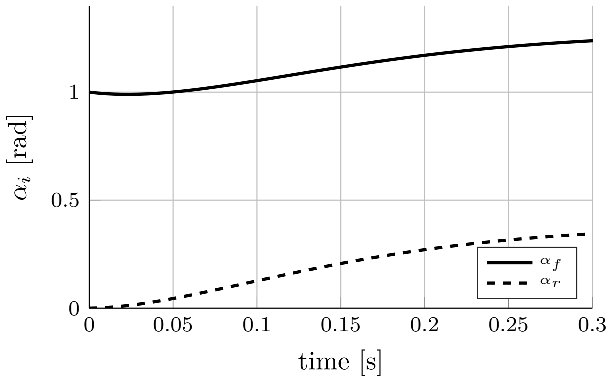

Figure 9.6: *Step response of slip angles for front and rear axle after step input in steering for speed of 20 m/s*

Concluding, it can be seen that the initial response in curvature is only dependent on the front axle for the bicycle model. Therefore, lowering the front axle cornering stiffness would yield a lower response. Setup 5 with rear wheel steering shows also good performance, but still for all speeds lower performance than Setup 3. Overall the results only represent a tendency of how the setups perform with respect to each other. An investigation with a fully nonlinear model is required as well. Not only the change in stiffness, but also tire force saturation plays a role when entering a turn and using large actuator inputs.

10 Path Following Scheme

An error definition that imposes positional constraint to the reference path is required to tell if the vehicle is located on the path as desired, or if it is deviating from the path. Different approaches for this control problem have been discussed in literature. Rajamani et al. [Raj12] shows how to obtain the feedforward steering angle for path following. Nevertheless, a feedback scheme is necessary to react to disturbances and uncertainties. This resembles the manner in which human drivers sense the road curvature ahead of the vehicle and provide output feedback for their steering task [HM90] [LL94].

A variety of driver steering models has been developed so far [HM90]. A dynamic model approach using measurements ahead of the vehicle has been investigated by [OUH95]. A fixed controller is used with its gain proportional to the lateral error at a certain look-ahead distance. Depending on the longitudinal velocity the look-ahead distance can always be chosen large enough to provide closed-loop stability. This is generally valid for look-ahead scheme systems [Koš96]. It has been investigated that adding or increasing the look-ahead distance creates more damping in the system, because it increases the phase margin [Koš96].

Further studies were done with emphasis on performance improvements for path following systems using the control law at a look-ahead distance, or at the center of gravity of the vehicle [GTP96] [PT90]. The latter one examines performance limitations with the use of lateral displacement sensors at front and rear bumper for so called look-down systems. Furthermore, the vision processing delay plays a big role when using output feedback strategies. There is a tradeoff between look-ahead distance and minimum curvature that can be tracked. Using an observer estimating the vehicle states, full state-feedback is possible, and the delay does not need to be modeled explicitly [Koš96]. Figure 10.1 shows the vision based model, which uses look-ahead distance concept to calculate error state feedback. The measure y_{la} points out the lateral error at the look-ahead distance.

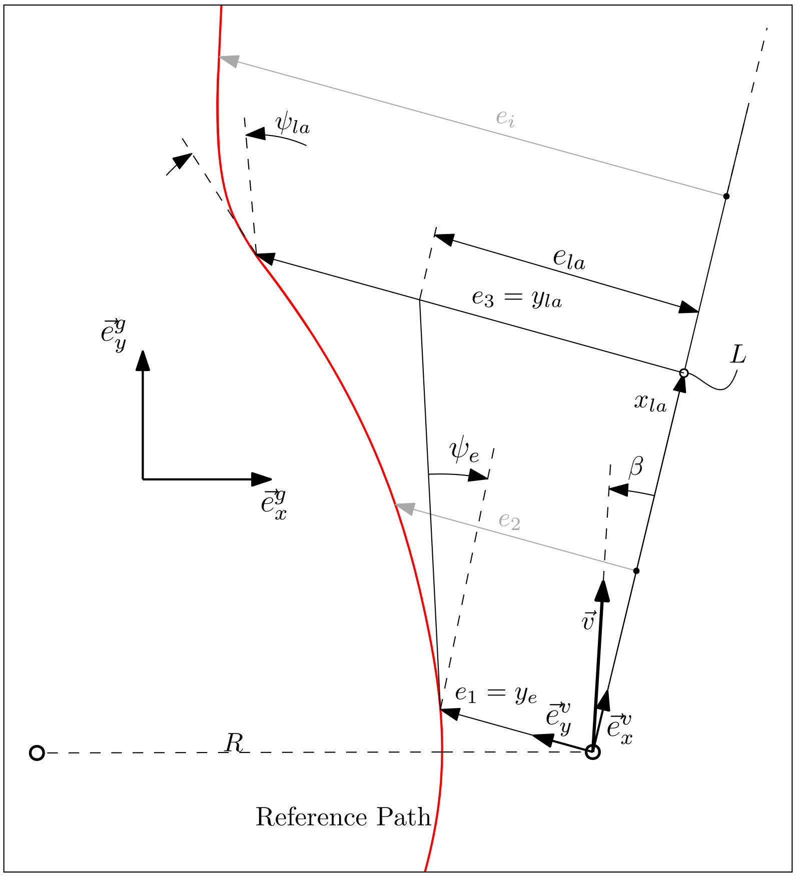

Figure 10.1: *Different error definitions for the path tracking control problem*

The red line resembles processed measurement points of the vision based sensor system, showing the path to follow. Point L represents the virtual control point. It is located inline with the longitudinal velocity vector at the look-ahead distance x_{la}. Additionally, the heading error at the look-ahead distance, ψ_{la}, can be controlled [Koš+98]. Using this second error takes vehicle orientation into account and is therefore beneficial, as it indicates whether the vehicle is going to deviate from the path. This provides additional damping. However, measuring both errors at a position ahead of the vehicle yields to significant corner cutting for corners with small radius.

An alternative error definition, preventing this behavior, is used by [RSG00]. The idea is to measure both error signals not at the look-ahead distance, but at the CG. Therefore the lateral offset is represented by the shortest distance between the CG and the reference path and the heading error is as well defined at the CG. These definitions are represented by y_e and ψ_e, respectively. Look-ahead distance can be incorporated into this concept as seen in Figure 10.1 as well. The resulting error e_{la} is obtained.

$$e_{la} = y_e + x_{la} sin(\psi_e) \tag{10.1}$$

It is constructed by defining a line tangent to the reference path, at the path point intersecting with a line through $\vec{e}_y^{\,v}$. Then e_{la} is defined as the distance between this tangent line and $\vec{e}_x^{\,v}$, measured at the look-ahead distance. This error definition avoids the effect of cutting corners, but therefore will the controller only receive an error if the vehicle has already departed from the desired path. Consequently the vehicle will only then negotiate back towards the reference path. This is typical behaviour for feedback control.

A combination of these two concepts was proposed for a driver steering model [SCS00]. The heading error, ψ_e, at the vehicle CG would be taken into account, and additionally a weighted sum out of multiple look-ahead errors e_i at respective look-ahead distances. Using at least four error states with this approach, there is also more path information required from ahead of the vehicle.

As discussed in Chapter 8 for collision avoidance manoeuvres relatively large lateral velocities are to be expected. Therefore it seems natural to put the virtual control point in line with the total velocity vector $\vec{v}$. It provides more accurate information about where the vehicle is going to be in the near future, based on where the vehicle is currently moving towards, for the case when significant sideslip is present. However, this approach can lead to decreased stability margins [KG15].

11 Efficient Use of Actuators

Active steering systems are discussed so far. In this chapter it should be mentioned how additional actuators, in terms of differential brakes, can enhance path tracking performance, and what requirements that puts onto suitable controllers. Differential braking can improve tracking performance since it allows for the creation of additional yaw moment as described in Chapter 9.3. Therefore the control problem is getting more complex since there will be five actuators instead of only one steering actuator. For the yaw moment necessary to negotiate a turn, this imposes the existence of multiple solutions of actuator distribution that yield the same result [VFT09]. This task is said to be under determined when only having to fulfil the yaw moment objective.

As discussed in [HC13], conventional DYC systems are mostly build upon logical controllers, that determine a lumped braking torque for wheels, either at two sides or one side instead of all four independently. Systems show hierarchical approaches, in the first step determining target yaw moment, and secondly control distribution to the wheels. To achieve optimum performance an optimization has to be solved requiring a well defined objective.

Ono et al. defines the objective as to minimize the work load of each tire, and shows global optimality of this approach [Ono+06]. For a similar control system Tjønnås and Johansen choose to minimize steering angle and slip ratios, and also show theoretical optimality for limited model errors [TJ10]. However, two major drawbacks arise from the control distribution problem, which is firstly that the feedback system might not be stable. This occurs due to the fact that there are dynamics between tire forces and traction/braking torques, which are mostly not modeled. The second fact is that optimization incorporates numerical search techniques which inhibit heavy computational burdon [HC13] [Ono+06] [TJ10].

Alirezaei et al. also minimizes combined slip for a DYC system, but using optimal control. With the State Dependent Riccati Equation (SDRE) technique the actuator inputs fulfil a performance index. Practical experiments of a double lane change manoeuvre show minimized impact on longitudinal dynamics and driving comfort beyond keeping the vehicle stable, with minimized sideslip [Ali+13].

12 Nonlinear Control Methods

Summarized from the literature research there is relevant requirements on the desired control approach:

1. Tire nonlinearities and combined slip tire behaviour play a big role for evasive manoeuvring. Drifting might allow for higher yaw rates and a controller is necessary, that can deal with nonlinear state relationships. The initiation of a drift is usually done by saturating the rear tires via applying of braking torque. A certain intelligence of the controller is necessary to accomplish this task. Again this figures the use of a rather sophisticated vehicle model within the (model based) controller.

2. The path following error scheme implies the use of classic feedback control to minimize lateral error. It makes use of measuring the error at a look-ahead distance in order to have built in damping. Special emphasis lies in the tuning of the look-ahead distance. Possibly a velocity dependent function becomes necessary. Tracking performance has to be evaluated and it must be checked if a feed forward controller is required.

3. As there are five actuators available for tracking the desired path, a law must be developed on how to distribute actuator inputs efficiently. Out of this overactuated system an optimization problem arises.

> The solution of the latter one allows for optimum performance of the collision avoidance system. This point is particularly important, since a collision avoidance manoeuvre is a safety critical task.

Relevant nonlinear control methods are briefly examined in this chapter, also with emphasis on the application. To choose the most suitable method for this project, the methods are evaluated with respect to the criteria of: Control performance/optimality, ease of design, implementation, possibility of real time implementation and robustness.

12.1 Feedback Linearization

For this method state feedback is required. The aim is to cancel out nonlinear terms in the differential equations of the system by multiplying the state feedback with respective coefficients. An additional linear term is added to the state feedback that can be shaped as a controller stabilizing the system [Kha02]. The advantage is that linear control laws can be applied.

Hsu et al. uses a feedback linearized system to guide a steer by wire vehicle smoothly along the limits of friction using steering saturation when driver inputs exceed slip thresholds and the vehicle leaves the linear range [HG05]. Liaw et al. did a theoretical study on stabilization of vehicles around unstable equilibria using steering as only input, limited to constant longitudinal speed [LC08]. For the specified conditions the stable region in state-space could be enhanced. However, feedback linearization may obscure the underlying dynamics at a drift equilibrium, but it does not eliminate these dynamics [Hin13].

In contrast it has been shown that feedback linearization can lead to unnecessary high actuator inputs and cause instability in the presence of actuator saturation or uncertainties [Clo+]. Therefore it is rather prawn to error caused by uncertainties in the system, and not always can any nonlinearities be cancelled to apply linear control methods. Thus implementation may be simple, but lack of performance and stability is likely.

12.2 Gain Scheduling Linear Quadratic Regulator (LQR) Control

Gain scheduling uses classic linear control theory for stable pole placement. For known states the closed-loop poles can be placed arbitrarily resulting in a controllable system. Nonlinear systems can be linearized around arbitrary points in state-space and respective gains stabilizing the system in the desired envelope can be defined. This is done offline and the gains are stored in a look-up table, from which the controller in operation picks the set of gains corresponding to the current working point. Using a linearized vehicle model these gains can be obtained using Linear Quadratic Regulator (LQR) technique. This optimal control method regulates errors to zero by minimizing the cost function

$$J = \frac{1}{2} \int_{t_0}^{t_f} (\mathbf{x}^T \mathbf{Q} \mathbf{x} + \mathbf{u}^T \mathbf{R} \mathbf{u}) dt \tag{12.1}$$

The optimal feedback gains are obtained solving the corresponding Riccati equation. Therefore a linear system in the form of $\dot{\mathbf{x}} = \mathbf{A}\mathbf{x} + \mathbf{B}\mathbf{u}$ is necessary. The main issue with gain scheduling is that for any parameter changes a new set of gains has to be computed offline. For instance if only three parameters are varied within the lateral model, like speed in 20 increments, friction coefficient in 4 increments and look-ahead distance in three increments, the number of set of gains would already be $20 \times 4 \times 3 = 240$. Xiong et al. uses a linear model together with a cornering stiffness estimator and shows successful application of the approach for a double lane change manoeuvre [Xio+12].

However, if the model should incorporate highly nonlinear relations like it is the case for tire models the system needs to be linearized around a sufficient amount of points in state space and this increases the variety of necessary sets of gains further, especially if there is a number of actuators involved. What makes this method impractical at the end, is a huge testing effort that corresponds to a large amount of gain sets. Even though the method is easy to apply, practicality is limited and therefore the performance is significantly limited.

12.3 State Dependent Riccati Equation (SDRE) Technique

When using the State Dependent Riccati Equation (SDRE) technique the same objective function as for gain scheduling will be solved in order to minimize state error and control input. The difference comes with solving the State Dependent Riccati Equation. The system matrices are state dependent, $\mathbf{A}(\mathbf{x})$ and $\mathbf{B}(\mathbf{x})$ respectively. This is achieved via writing the systems nonlinear differential equations in linear like state dependent coefficient (SDC) form. The RE is then computed on-line in order to calculate the optimized actuator inputs [ime08].

The SDRE method of nonlinear control design comprises promising advantages for employment in a collision avoidance system [Ali+13]. First of all the method can incorporate nonlinear dynamics in terms of the SDC form. Within this variable framework it is easy to incorporate modeling changes and change amount and kind of actuators. Furthermore, fulfilling the performance index, minimum actuator effort is expected. The system description within the SDRE is nonunique which requires more emphasis on finding a suitable solution, but this also gives desireable degrees of freedom for tuning and stabilizing the system. This degree of freedom should be used for instance to tune the radius of robustness against parameter uncertainty [NS11]. Stability can be shown within the domain of interest. Since there exist a number of numerical methods to solve the algebraic Riccati equation (ARE) in real-time, experimental validation is feasible.

12.4 Model Predictive Control (MPC)

Model Predictive Control (MPC) has been used for path tracking applications. It resembles a finite horizon optimal control scheme. A plant model is used to iteratively predict future evolution of the states. With this, it computes the input sequence such that the predicted states satisfy given constraints and minimize a user-defined objective function [And+10].

Falcone et al. uses a linear time varying vehicle model together with additional stabilizing constraints within a MPC approach [Fal+10]. Even though experiments show, that the model can handle counter steering in case of excessive sideslip, the objective is to recover saturated tires into the linear region, and not make full use of the friction limits. One remaining drawback of MPC is the relatively high computational burden. The challenge resides in the real-time solution of a Nonlinear Programming problem, which typically takes 20 - 50 ms [Fal+08]. Research has made great progress, but still the necessity of controller model simplifications remains in order to make the effort real time feasible. Falcone et al. simplifies the model by lumping differential brake actuators together [Fal+08]. Reducing the problem size through model simplification is a challenging trade-off between model complexity and accuracy.

For path tracking in limit handling condition Gray et al. shows, that in certain emergency conditions a collision can only be avoided when having the vehicle operate around drift equilibria [Gra+]. In their study a set of motion primitives is used to calculate feasible avoidance manoeuvres offline. To accomplish these motion primitives an MPC approach according to [Fal+08] is chosen and successfully tested for low velocities on icy surface. This principle focuses on highly structured driving environments like they occur in urban driving. Expected performance with MPC is good as literature shows, only could there be a significant drawback if model complexity has to be reduced in order to allow for real-time implementation.

12.5 Sliding Mode Control (SMC)

Sliding Mode Control (SMC) represents a variable structure control system. As the name suggests for such systems the control law is deliberately changed during the control process according to defined rules depending on the state of the system. So called switching functions guide the state along a line or surface in state space. This is done in a way that it drives states towards the desired equilibrium. By introducing a rule for switching between two control structures, which independently do not provide stability, a stable closed-loop system can be obtained [ES98]. However, this method is prone to high frequency switching between two different control structures, as the system trajectories repeatedly cross the switching line or surface. This high frequency motion is described as chattering.

Hsu et al. [HC13] proposes an approach to reduce chattering in an optimal controller for path following, and shows positive results in theory. An SDC related approach which would only define a safe envelope of vehicle condition in state space is used by Bobier et al. [BG13]. If detected that the vehicle is close or outside the safe envelope, control action is taken, whereas inside the envelope there is no control action taken, and the driver controls the vehicle. Pang et al. [PW] focuses on the improvement of robustness and integrated sliding mode control with the State Dependent Riccati Equation.

12.6 Other Approaches

Talvala et al. [TKG11] and Kritayakirana et al. [Kri12] use feedforward steering input together with feedback lanekeeping and yaw damping error for lateral control of a vehicle. The aim is to exploit the full tire potential whilst following a racing line. The current potential is obtained via friction circle concept. It is shown that lane keeping can be robust with simple lookahead control schemes, even at the friction limits. The heading error with respect to the desired path is minimized and therefore the vehicle is recovered out of tire saturation by counter steering.

A different approach to the path tracking problem is described by Gordon et al. [GBD02]. Using convergent vector fields for any location of the vehicle with respect to the reference path a desired vehicle mass center velocity is obtained. The vector field is build considering nonlinear tire friction and vehicle properties. Stable and robust control is possible even in the case of limit handling. Though, heavy offline analysis is necessary. Using differential flatness technique Peters et al. [PI11] reduces the nonlinear bicycle to a point mass containing yaw dynamics. The resulting system shows instability for body sideslip angles exceeding the unstable drift equilibria.

12.7 Discussion

Control problem definitions from literature were discussed and a task description for the lateral control in limit handling was given. Also different suitable control methods were proposed, which are Feedback Linearization, Linear Quadratic Regulator (LQR), State Dependent Riccati Equation (SDRE) Technique, Model Predictive Control (MPC), Sliding Mode Control (SMC) and two miscellaneous approaches. Results of this investigation are summarized in Table 12.1.

Table 12.1: Properties of discussed control methods

Method	**Performance/ optimality**	**Ease of implementation**	**Real-time implementation**	**Robustness**
Feedback Lin.	-	+	+	+
LQR	0	-	+	-
SDRE	+	+	0	0
MPC	+	+	-	0
SMC	0	0	+	+

LQR was taken as reference, since there is most knowledge available about this control method, and it is seen as baseline here. Performance of LQR is very much dependent on how much datapoints are available in the look-up table. Is this number to small then interpolation becomes necessary and penalizes performance and optimality. Therefore, this value was set to ”0” as neutral value. For a larger set of gains calculated, implementation becomes a serious issue, especially if the complex nonlinearities of the tire should be considered. In our case that is a strong requirement. So this value is set to ”-”. Anyway, real-time implementation is easy for LQR, since the controller is calculated off-line and therefore a ”+” is chosen. Robustness is a weak property for the LQR approach, since not only the parameter uncertainty is neglected in the control approach, but also does the underlying linearized controller model not match effects like tire saturation.

In comparison, Feedback Linearization has the biggest drawback in terms of performance/ optimality. It is no optimal control approach. The SDRE technique shows a drawback in terms of real-time implementation. For high controller model fidelity this can become an issue. Also robustness could be considered as a weak point here, but due to the degree of freedom in the model parameterization, robustness can be addressed to some extent. MPC has a drawback in terms of real-time implementation. Whereas it shows great performance, as good as the SDRE approach, all solutions found in literature dealt significant compromising of model accuracy for real-time implementability. Finally SMC shows uncertain drawbacks in terms of performance/ optimality since chattering is to expect when using SMC. Furthermore it is not necessary optimal and uncertainty lies within the implementation. To meet the performance requirements, adaption of the SMC would be necessary, which makes implementation more complicated and uncertain.

Due to this result the choice is made for the SDRE control approach, especially because good performance is expected and this can be seen as major requirement. It shows the capability to systematically handle model nonlinearities, work in a wide operating region and minimize actuator effort together with control error. Whereas there is no guarantee for robustness towards parameter uncertainty, this can be assessed for a certain radius of interest and tweaked adapting the parameterization of the system. Thus, SDRE is chosen, as it shows an overall well suiting characteristic for path tracking in limit handling conditions.

Part IV
Modelling and Controller Development

The buildup of the controller is explained in this part. Figure 12.1 shows the layout of the developed controller. Obtaining the state dependent control gain $\mathbf{K}(\mathbf{x})$ is done using the SDRE technique. Multiplication with the path tracking error $\mathbf{e}$ yields the feedback control input.

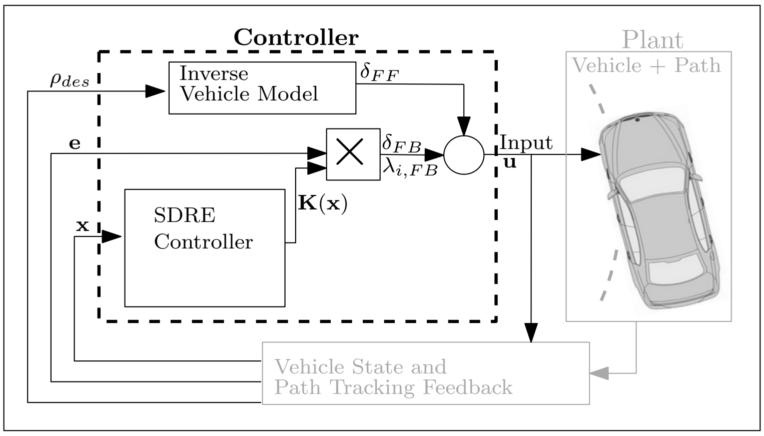

Figure 12.1: *Controller Layout*

There is also a feedforward steering term, which is a function of the desired path curvature ρ_{des}. The latter one together with path tracking error $\mathbf{e}$ and vehicle state information $\mathbf{x}$ are considered to be given from a state estimator. Input $\mathbf{u}$ to the plant is steering δ and wheel slip λ_r. However, firstly the plant model is described, from which eventually the controller model will be derived.

13 Plant Model

The plant model should represent the real system as accurate as possible, but not more than required. Unnecessary complexity increases effort in setting up and computing the simulation. The plant model is comprised of a vehicle model for calculating the evolution of the vehicle states dependent on the actuator inputs. The second part is a camera model for detecting the predefined path which is given in a global reference frame and expressing it in terms of vehicle coordinates. The third block represents post-processing of the camera information to obtain error states. This schematic can be seen in Figure 13.1.

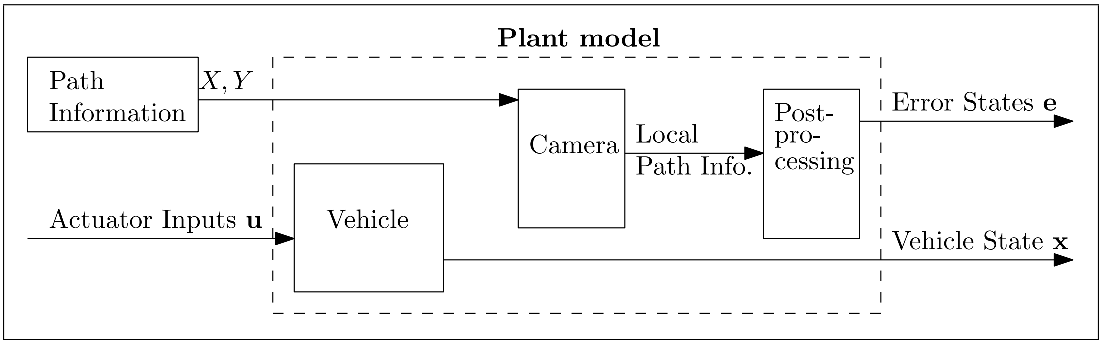

Figure 13.1: *Plant model with inputs and outputs*

The subfunctions of these models are broken down further.

13.1 Camera and Post-Processing

The camera model produces a polynomial, which represents the path close to the vehicle with a certain radius of interest. Therefore it would pick up global path points ahead of the vehicle and transfer them into local coordinates. This represents the method how the real mobile camera gives path information to the lane following controller, see Figure 13.2.

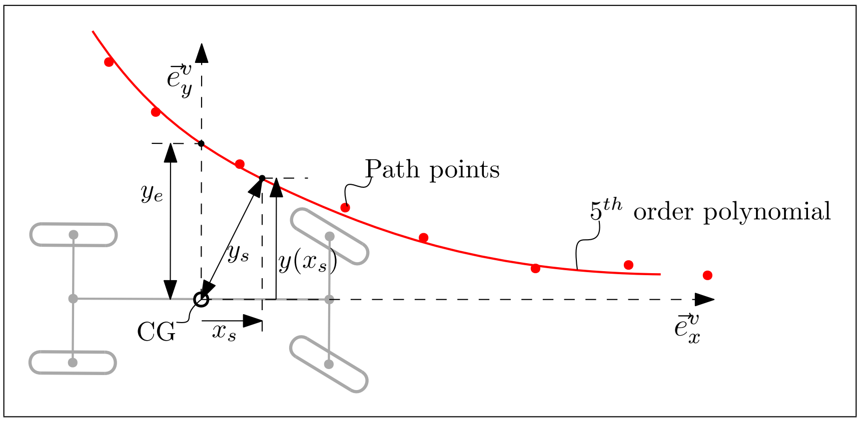

Figure 13.2: *Path polynomial in vehicle reference frame and measurement of lateral displacement*

The lateral error y_e, as discussed in Chapter 10, can be obtained evaluating the polynomial at $x = 0$.

$$y(x) = c_0 + c_1 x + c_2 x^2 + c_3 x^3 + ... + c_i x^i \tag{13.1}$$

Heading error,

$$e_\psi(x) = \arctan\left(\frac{dy_e(x)}{dx}\right) \tag{13.2}$$

Curvature [Wei16],

$$\rho(x) = \frac{\frac{d^2 y(x)}{dx^2}}{\left(1 + \left(\frac{dy(x)}{dx}\right)^2\right)^{\frac{3}{2}}} \tag{13.3}$$

Using this convention for significant body sideslip and or large heading with respect to the path, y_e becomes large even though the vehicle is close to the path. If the lateral error should rather represent the shortest distance from CG to the path, then y_s is used instead of y_e, see Figure 13.2.

$$y_s = \sqrt{x_s^2 + y(x_s)^2}\,\mathrm{sign}(y(x_s)) \tag{13.4}$$

To find the candidate points for x_s, the term $(x_s^2 + y(x_s))^2$ has to be minimized. Therefore,

$$\frac{d}{dx}(x^2 + y(x)^2) = 0 \text{ and } \frac{d^2}{dx^2}(x^2 + y(x)^2) > 0 \tag{13.5}$$

has to be fulfilled. From the candidate points the one closest to the origin represents x_s.

13.2 Vehicle

The vehicle model incorporates evaluation of the vehicle states, v_x, v_y, and r, dependent on its inputs, δ and λ_i. A planar two-track vehicle model is considered and can be seen in Figure 13.3.

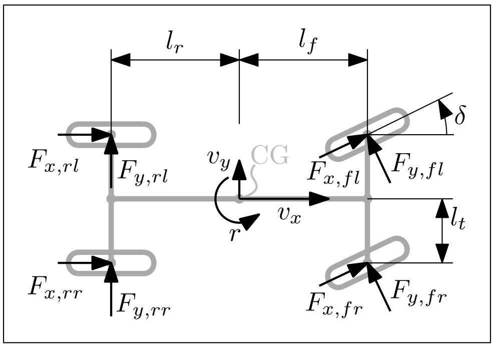

Figure 13.3: *Two-track vehicle model*

The state derivatives can be computed dependent to the tire forces $F_{x/y,i}$, which are oriented in wheel reference frame, inline with the wheel. The front tire forces are brought into chassis frame of reference via correction for steering δ on the front wheels. It follows

$$\begin{aligned}\begin{bmatrix}\dot{v}_x\\ \dot{v}_y\\ \dot{r}\end{bmatrix} &= \begin{bmatrix}0 & r & 0\\ -r & 0 & 0\\ 0 & 0 & 0\end{bmatrix}\begin{bmatrix}v_x\\ v_y\\ r\end{bmatrix}\\ &+ \begin{bmatrix}\frac{1}{m} & 0 & 0\\ 0 & \frac{1}{m} & 0\\ 0 & 0 & \frac{1}{I_Z}\end{bmatrix}\begin{bmatrix}\cos\delta & \cos\delta & 1 & 1\\ \sin\delta & \sin\delta & 0 & 0\\ \substack{l_f\sin\delta\\ -l_t\cos\delta} & \substack{l_f\sin\delta\\ +l_t\cos\delta} & -l_t & l_t\end{bmatrix}\begin{bmatrix}F_{x,fl}\\ F_{x,fr}\\ F_{x,rl}\\ F_{x,rr}\end{bmatrix}\\ &+ \begin{bmatrix}\frac{1}{m} & 0 & 0\\ 0 & \frac{1}{m} & 0\\ 0 & 0 & \frac{1}{I_Z}\end{bmatrix}\begin{bmatrix}-\sin\delta & -\sin\delta & 0 & 0\\ \cos\delta & \cos\delta & 1 & 1\\ \substack{l_f\cos\delta\\ +l_t\sin\delta} & \substack{l_f\cos\delta\\ -l_t\sin\delta} & -l_r & -l_r\end{bmatrix}\begin{bmatrix}F_{y,fl}\\ F_{y,fr}\\ F_{y,rl}\\ F_{y,rr}\end{bmatrix}\end{aligned} \tag{13.6}$$

The tire forces are a function of lateral and longitudinal slip, as well as tire load: $F_{x/y,i} = f(\lambda_i, \alpha_i, F_{z,i})$. They are obtained using the combined slip Magic Formula tire model [Pac12].

$$\begin{aligned}F_{x,i} &= G_{x,i}(\lambda_i, \alpha_i)F_{x0,i}(\lambda_i, F_{z,i})\\ F_{y,i} &= G_{y,i}(\lambda_i, \alpha_i)F_{y0,i}(\alpha_i, F_{z,i})\end{aligned} \tag{13.7}$$

Pure slip forces are represented by $F_{x0,i}(\lambda_i, F_{z,i})$ and $F_{y0,i}(\alpha_i, F_{z,i})$, which have the following shape:

$$y_{mf} = D_{mf}\sin(C_{mf}\arctan(B_{mf}x_{mf} - E_{mf}(B_{mf}x_{mf} - \arctan(B_{mf}x_{mf})))) \tag{13.8}$$

where output y_{mf} represents pure slip tire force and input x_{mf} represents longitudinal slip λ or lateral slip α respectively. The coefficients are there to fit the slip curve properties:

- B_{mf} the stiffness,
- C_{mf} the shape,
- D_{mf} the peak value and
- E_{mf} the curvature [Pac12].

The combined slip relation is represented through the weighting functions $G_{x,i}(\lambda_i, \alpha_i)$ and $G_{y,i}(\lambda_i, \alpha_i)$. Required parameters are determined via curve fitting of experimental data. The Prius tire parameters are provided by TNO, a detailed description is not relevant for this research. The slip angles α_i are derived in the same fashion as it is shown in Chapter 5. Additionally there is the term $l_t r$ appearing in the equations, due to the track width contribution of the two-track model.

$$\alpha_{fl} = \delta - \arctan\left(\frac{v_y + l_f r}{v_x - l_t r}\right) \qquad \alpha_{fr} = \delta - \arctan\left(\frac{v_y + l_f r}{v_x + l_t r}\right) \tag{13.9}$$

$$\alpha_{rl} = \arctan\left(\frac{-v_y + l_r r}{v_x - l_t r}\right) \qquad \alpha_{rr} = \arctan\left(\frac{-v_y + l_r r}{v_x + l_t r}\right) \tag{13.10}$$

Static load transfer due to longitudinal and lateral acceleration is taken into account when calculating the vertical tire loads. The static loads

$$F_{z,f,l/r,static} = \frac{l_r}{l}\frac{mg}{2} \tag{13.11}$$

$$F_{z,r,l/r,static} = \frac{l_f}{l}\frac{mg}{2} \tag{13.12}$$

together with longitudinal and lateral load transfer

$$\Delta F_{z,long,l/r} = \frac{ma_x h_{CG}}{2l} \tag{13.13}$$

$$\Delta F_{z,lat,front} = \frac{l_r m a_y h_{CG}}{2l_t l} \tag{13.14}$$

$$\Delta F_{z,lat,rear} = \frac{l_f m a_y h_{CG}}{2l_t l} \tag{13.15}$$

are added as follows

$$F_{z,fl} = F_{z,f,l/r} - \Delta F_{z,long,l/r} - \Delta F_{z,lat,front} \tag{13.16}$$

$$F_{z,fr} = F_{z,f,l/r} - \Delta F_{z,long,l/r} + \Delta F_{z,lat,front} \tag{13.17}$$

$$F_{z,rl} = F_{z,f,l/r} + \Delta F_{z,long,l/r} - \Delta F_{z,lat,rear} \tag{13.18}$$

$$F_{z,rr} = F_{z,f,l/r} + \Delta F_{z,long,l/r} + \Delta F_{z,lat,rear} \tag{13.19}$$

(13.20)

Roll-Stiffness distribution due to load transfer is not taken into account and there is no influence of suspension or aerodynamic resistance considered within the plant model. Compliance of the suspension system is represented within the tire stiffness, which is adapted accordingly in order to fit the real understeering gradient.

14 State Dependent Riccati Equation

A nonlinear system representable in the control-affine form $\dot{\mathbf{x}}(t) = \mathbf{f}(\mathbf{x}) + \mathbf{B}(\mathbf{x})\mathbf{u}(t)$ and holding an equilibrium in the origin, $f(0) = 0$, can be driven there by minimizing the infinite time quadratic performance index [ime08] [CDM96].

$$J = \frac{1}{2}\int_{t_0}^{\infty} (\mathbf{x}^T\mathbf{Q}(\mathbf{x})\mathbf{x} + \mathbf{u}^T\mathbf{R}(\mathbf{x})\mathbf{u})dt \tag{14.1}$$

Matrices $\mathbf{Q}(\mathbf{x})$ and $\mathbf{R}(\mathbf{x})$ are positive semi-definite and diagonal and generally state dependent. They represent state and input weightings, where the respective elements are chosen to be:

- q_i, the maximum expected or acceptable value of $1/x_i^2$ and
- r_i, the maximum expected or acceptable value of $1/u_i^2$

for practical applications. The Hamiltonian then relates the performance index together with the path constraint of the system in the form of $\mathbf{A}(\mathbf{x})\mathbf{x} + \mathbf{B}(\mathbf{x})\mathbf{u}$ [Pad].

$$H = \frac{1}{2}(\mathbf{x}^T\mathbf{Q}\mathbf{x} + \mathbf{u}^T\mathbf{R}\mathbf{u}) + \zeta^T(\mathbf{A}(\mathbf{x})\mathbf{x} + \mathbf{B}(\mathbf{x})\mathbf{u}) \tag{14.2}$$

Furthermore

$$\dot{\zeta} = -\frac{\partial H}{\partial \mathbf{x}} = -(\mathbf{Q}\mathbf{x} + \mathbf{A}(\mathbf{x})^T\zeta) \tag{14.3}$$

and the optimal control equation is

$$\frac{\partial H}{\partial \mathbf{u}} = \mathbf{R}\mathbf{u} + \mathbf{B}(\mathbf{x})^T\zeta = 0 \tag{14.4}$$

Control can be obtained and results to

$$\mathbf{u} = -\mathbf{R}^{-\mathbf{1}}\mathbf{B}(\mathbf{x})^T\zeta \tag{14.5}$$

Apparently a unique solution exists, where $\zeta(t)$ is a linear function of $\mathbf{x}(t)$ [Ber95].

$$\zeta(t) = \mathbf{P}(t)\mathbf{x}(t) \tag{14.6}$$

Using Equation 14.3, 14.5 and 14.6, the differential Riccati Equation can be obtained.

$$\dot{\mathbf{P}} + \mathbf{P}\mathbf{A}(\mathbf{x}) + \mathbf{A}(\mathbf{x})^T\mathbf{P} - \mathbf{P}\mathbf{B}(\mathbf{x})\mathbf{R}^{-1}\mathbf{B}(\mathbf{x})^T\mathbf{P} + \mathbf{Q} = 0 \tag{14.7}$$

For infinite time horizon and $\{\mathbf{Q}(\mathbf{x}), \mathbf{R}(\mathbf{x})\}$ = constant, it can be shown that $\dot{\mathbf{P}} \to 0$ [Pad]. Furthermore $\mathbf{Q}(\mathbf{x})$ and $\mathbf{R}(\mathbf{x})$ are considered to be constant throughout the time step where a solution is attempted. The result is the algebraic Riccati Equation (ARE).

$$\mathbf{P}\mathbf{A}(\mathbf{x}) + \mathbf{A}(\mathbf{x})^T\mathbf{P} - \mathbf{P}\mathbf{B}(\mathbf{x})\mathbf{R}(\mathbf{x})^{-1}\mathbf{B}(\mathbf{x})^T\mathbf{P} + \mathbf{Q}(\mathbf{x}) = 0 \tag{14.8}$$

The nonlinearity of the system is represented by state dependent system matrices $\mathbf{A}(\mathbf{x})$ and $\mathbf{B}(\mathbf{x})$, so it is called State Dependent Riccati Equation (SDRE). It has to be computed on-line in order to obtain the control

$$\mathbf{u} = -(\mathbf{R}^{-1}\mathbf{B}^T\mathbf{P})\mathbf{x} = -\mathbf{K}\mathbf{x} \tag{14.9}$$

A solver, that is tested on real-time hardware is to be used to obtain matrix $\mathbf{P}$ for this research [AJJ16]. Since solving the Riccati Equation for high-order systems can be computationally demanding, the complexity and therefore fidelity of the controller model is somehow limited.

15 Controller Model

The SDRE controller obtains the control gain matrix $\mathbf{K}$ dependent on vehicle state feedback. Furthermore there is a feedforward control intended, which is described in Chapter 19. Figure 15.1 shows the layout of the feedback-feedforward controller.

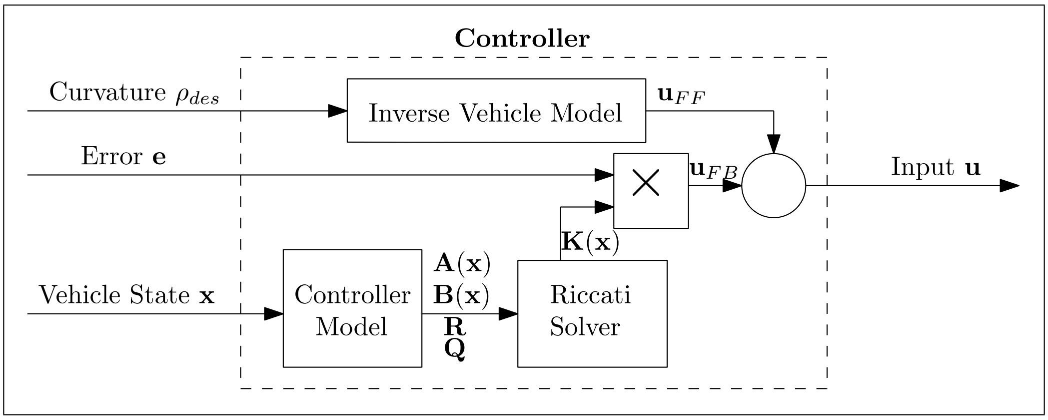

Figure 15.1: *Controller Model*

For model based control, controller performance depends to a large extent on controller model fidelity, which will be discussed first. Besides a representation of the vehicle, also error dynamics are part of the controller model. Furthermore, to fit the model into the SDRE framework, it needs to be brought into parameterized form. This will be discussed in the subsequent chapter, together with related implementation issues.

15.1 Vehicle Model Fidelity

The more accurate the model represents the plant, the better can the controller adapt to the inherent plant dynamics and obtain control gains accordingly. But high model fidelity also leads to a more complex controller model, which in turn yields increased computational effort for the Riccati solver. This is the case especially if the order of the system is increased, and decreases reliability. Furthermore, increased complexity in the controller means increased effort for tuning is required. There is a tradeoff to be made. The model should take into account the governing nonlinearities, but not more than necessary. Therefore, the dynamics taken into account are chosen as follows.

1. **Combined slip tire model**
   Tire saturation is expected for cornering at the limits of handling. In these conditions lateral force capabilities are compromised by longitudinal slip of the tire. Since longitudinal slip of the tires will be distributed via the controller it is particularly important to account for this behaviour in order to not compromise lateral tracking performance. Instead with purposefully distribution the slip inputs are supposed to improve lateral tracking performance.

2. **Two-track property of the vehicle**
   In order to be able to distribute wheel slip inputs for all four wheels, it is required that the model represents four independent tires with respective lateral slip, longitudinal slip and vertical load. See Chapter 13.2 for a representation of the two-track model.

3. **Load transfer**
   For manoeuvres, where the vehicle is operated at the edge of instability, especially longitudinal load transfer can have significant importance. It allows for change in distribution of lateral force between front and rear axle and therefore change the yawrate [VTL07].

Therefore, the controller model becomes identical fidelity as the plant model described in Chapter 13.2. It has three degree-of-freedom: v_x, v_y and r.

15.2 State for Tracking Curvature

The discussion in Chapter 9.2 gave the motivation to also include a curvature state into the controller. It can be translated into an error state when subtracting the curvature of the actual (vehicle) trajectory from the desired (path) curvature.

$$e_\rho = \rho_{des} - \rho \tag{15.1}$$

Together with Equation 9.9 and 9.10 the state equation can be written down.

$$\dot{e_\rho} = -\frac{\dot{r}}{v_{tot}} - e_\rho \frac{v_x \dot{v_x} + v_y \dot{v_y}}{v_{tot}^2} + \rho_{des} \frac{v_x \dot{v_x} + v_y \dot{v_y}}{v_{tot}^2} + \dot{\rho_{des}} \tag{15.2}$$

It can be seen that the curvature error state is dependent on all vehicle state equations. It has to be checked if this state can improve path tracking performance in certain conditions.

15.3 Heading and Lateral Error Dynamics

The error dynamics of the positional errors describe how the vehicle moves with respect to the path. As a result of the literature review in Chapter 10, there were chosen to be two error states: a lateral error at a certain look-ahead distance, e_{la}, and a heading error at the CG, e_ψ. Figure 15.2 shows the geometrical definition of these errors as it is used in the controller model.

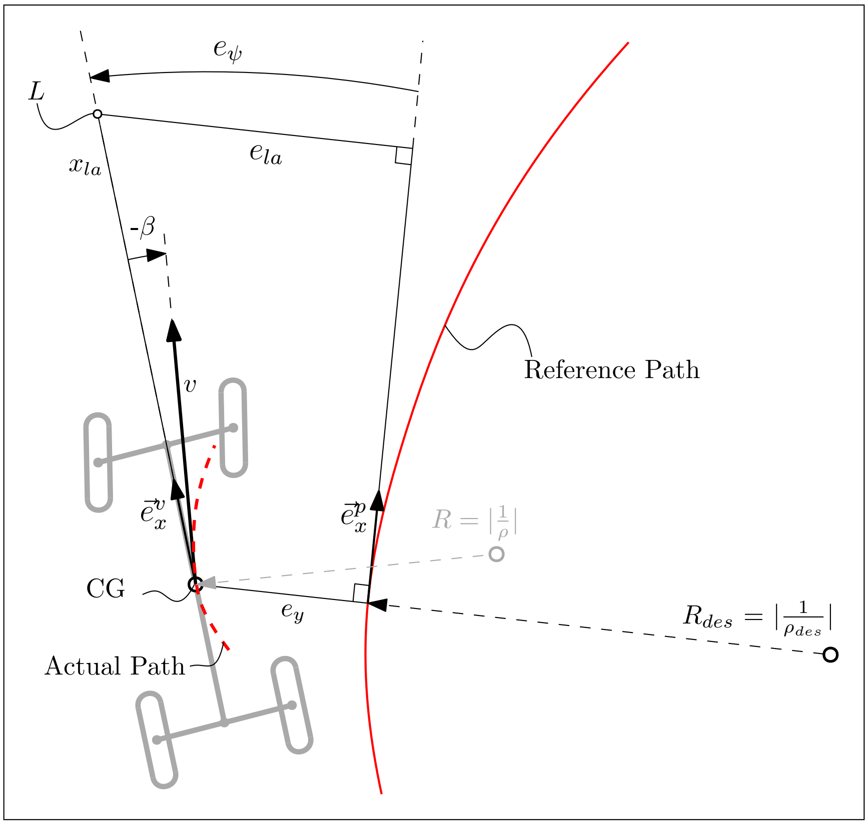

Figure 15.2: *Error definition*

It is of importance to notice that the lateral error at the CG was defined to span the shortest distance between CG and path, e_y, see also y_s in Chapter 13.1. There is zero error whenever the CG is located on the path and the vehicle heading equals the path heading. The derivation is as follows. The heading error e_ψ determines the deviation between path heading and vehicle heading at the CG. Therefore the component of the vehicles velocity that points in the direction of the path, $v_x \cos e_\psi + v_y \sin e_\psi$, is relevant.

$$\dot{e}_\psi = -(v_x \cos e_\psi + v_y \sin e_\psi)\rho_{des} + r \tag{15.3}$$

The lateral error e_y describes the offset, respectively the shortest distance, at the CG and therefore the component of the velocity perpendicular to the path, $v_y \cos e_\psi + v_y \sin e_\psi$, is relevant.

$$\dot{e}_y = v_y \cos e_\psi + v_x \sin e_\psi \tag{15.4}$$

The look ahead error e_{la} resembles a weighted sum of both, using look-ahead distance x_{la}.

$$e_{la} = e_y + x_{la} \sin e_\psi \tag{15.5}$$

and therefore

$$\begin{aligned} \dot{e}_{la} &= \dot{e}_y + x_{la} \frac{d}{dt} \sin e_\psi \\ &= v_y \cos e_\psi + v_x \sin e_\psi + x_{la} \cos e_\psi [-(v_x \cos e_\psi + v_y \sin e_\psi)\rho_{des} + r] \end{aligned} \tag{15.6}$$

Heading error and look-ahead error become states of the controller model. An alternative error definition, where heading error is measured with respect to the vehicle moving direction instead of the vehicle heading, is presented in Appendix D.

16 Controller Model SDC-Form

To solve the State Dependent Riccati Equation, it is required to have the system $\dot{\mathbf{x}}(t) = \mathbf{f}(\mathbf{x}, \mathbf{u})$ brought into a linear like form.

$$\dot{\mathbf{x}} = \mathbf{A}(\mathbf{x})\mathbf{x} + \mathbf{B}(\mathbf{x})\mathbf{u} \tag{16.1}$$

It follows a linear structure with the system matrices having State Dependent Coefficients (SDC), which is also referred to as Extended Linearisation [ime08]. For multi-variable systems, as considered in this research, the parameterization appears to be non-unique. Nonlinear terms $f_i(\mathbf{x})$ appearing in one of the state equations can be used as coefficients for arbitrary states x_j in this equation, of the form $f_i(\mathbf{x})/x_j$. Furthermore two distinct parameterizations fulfilling $\mathbf{f}(\mathbf{x}) = \mathbf{A_1}(\mathbf{x})\mathbf{x} = \mathbf{A_2}(\mathbf{x})\mathbf{x}$ can always be written in the form

$$\mathbf{A}(\mathbf{x},\theta) = \theta\mathbf{A_1}(\mathbf{x}) + (1-\theta)\mathbf{A_s}(\mathbf{x}) \tag{16.2}$$

This nonuniqueness property brings additional degree of freedom to the approach, as it will be discussed later. This section will focus on retrieving a generic SDC form for the controller model, that can be altered and adapted later for tuning purposes. Firstly, a SDC form of the vehicle state equations, v_x, v_y and r is derived, then also a parameterization of the error states e_ρ, e_{la} and e_ψ. They are assembled to one complete SDC representation at the end, of course. At the end of the chapter, there will be come back to some implementation and numerical issues that arise when using parameterization.

16.1 Tire Force Parameterization

The combined slip force calculation needs to be brought into a parametrized form. Therefore the tire forces $F_{x,i}$ and $F_{y,i}$ are respectively represented by a linear combination of longitudinal slip and lateral slip.

$$F_{x,i} = C_{x,i,\alpha}\alpha_i + C_{x,i,\lambda}\lambda_i \tag{16.3}$$
$$F_{y,i} = C_{y,i,\alpha}\alpha_i + C_{y,i,\lambda}\lambda_i \tag{16.4}$$

The factor $C_{x/y,i,\alpha/\lambda}$ is associated with slip stiffness and calculated in real-time dependent on the vehicle state and tire model. This allows to calculate tire forces in a separate model and the bulky functions do not have to be part of system matrices [Ali+13]. Figure 16.1 shows how this concept is schematically implemented into the model.

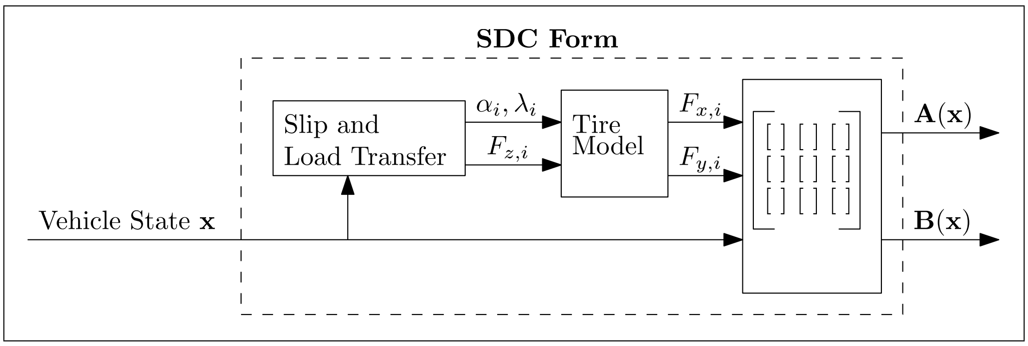

Figure 16.1: *SDC Form schematically: via the tiremodel tireforces are retrieved in real-time as an input for the system matrices*

The factorization is arbitrary and is one of the degrees of freedom of the SDC form. Most importantly the factorization has to be chosen in a fashion that it gives smooth values over the whole envelope of α and λ. With the following definition this could be achieved.

$$C_{x,i,\alpha} = F_{x,i}(\lambda_i, \alpha_i) \qquad C_{x,i,\lambda} = \frac{F_{x,i}(\lambda_i, \alpha_i)(1-\alpha_i)}{\lambda_i} \tag{16.5}$$

$$C_{y,i,\alpha} = \frac{F_{y,i}(\lambda_i, \alpha_i)(1-\lambda_i)}{\alpha_i} \qquad C_{y,i,\lambda} = F_{y,i}(\lambda_i, \alpha_i) \tag{16.6}$$

For the fact that the definitions of $C_{x,i,\lambda}$ and $C_{y,i,\alpha}$ would only be valid for nonzero slip, the latter one had to be saturated for values smaller than a defined threshold $h_{\lambda,th}$ and $h_{\alpha,th}$. Slips would be replaced by $f_\lambda(\lambda_i)$ and $f_\alpha(\alpha_i)$ respectively for simulation implementation.

$$f_\lambda(\lambda_i) = \begin{cases} \lambda_i, & \text{for } |\lambda_i| > h_{\lambda,th} \\ h_{\lambda,th}, & \text{for } |\lambda_i| \leq h_{\lambda,th} \end{cases} \tag{16.7}$$

and

$$f_\alpha(\alpha_i) = \begin{cases} \alpha_i, & \text{for } |\alpha_i| > h_{\alpha,th} \\ h_{\alpha,th}, & \text{for } |\alpha_i| \leq h_{\alpha,th} \end{cases} \tag{16.8}$$

Figure 16.2 shows $C_{x/y,i,\lambda/\alpha}$ plotted over the whole slip envelope.

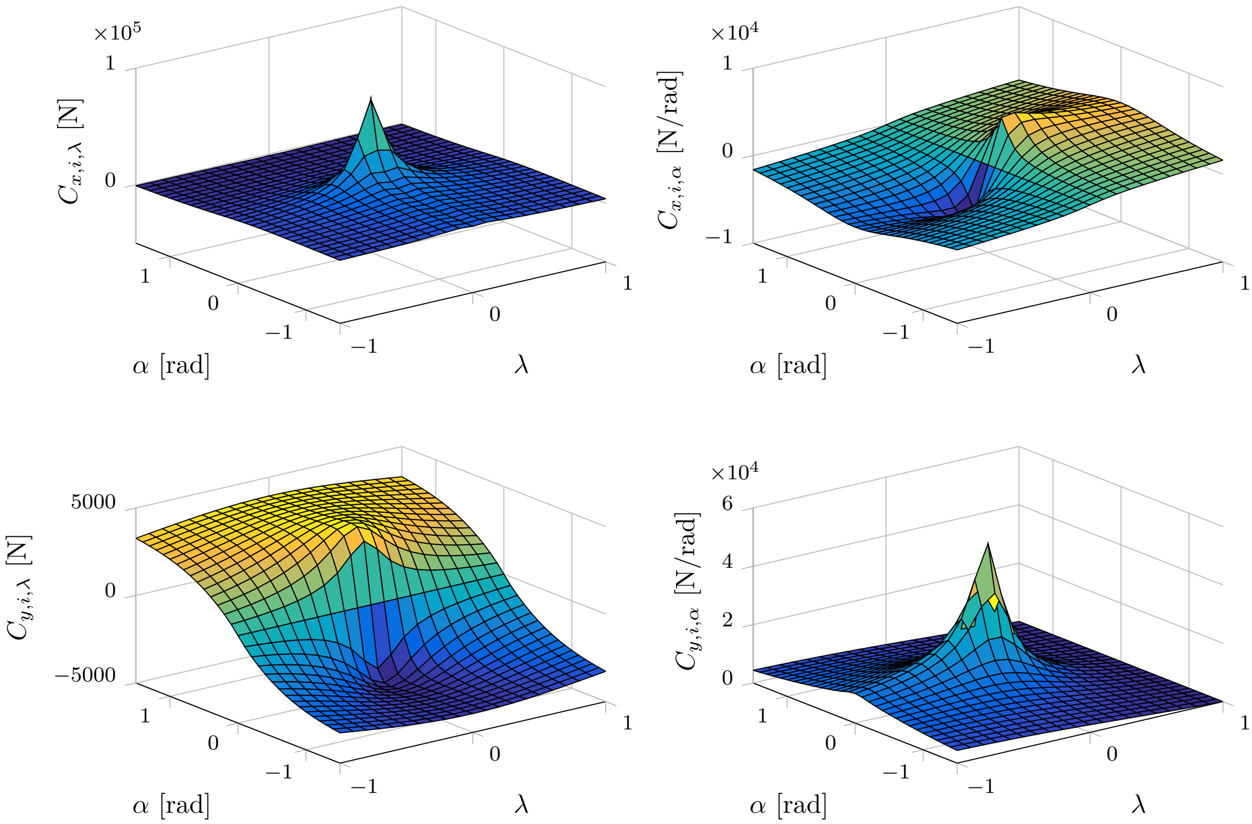

Figure 16.2: *The factors $C_{x/y,i,\alpha/\lambda}$ to be used for tire force calculation within the SDC form*

The alleged stiffness factors show smooth transition surfaces.

16.2 Vehicle Model Parameterization

The model described in Chapter 15.1 needs to be parameterized. As the representation in the strict form of $\dot{\mathbf{x}} = \mathbf{A}(\mathbf{x})\mathbf{x} + \mathbf{B}(\mathbf{x})\mathbf{u}$ yields confusingly large matrices, the state equations can be collapsed into multiple overseeable matrices. Furthermore $\mathbf{A}$ and $\mathbf{B}$ can be functions of both $\mathbf{x}$ and $\mathbf{u}$. For $\mathbf{x} = \begin{bmatrix} v_x & v_y & r \end{bmatrix}^T$ the system is written in the form of

$$\dot{\mathbf{x}} = \underbrace{\left[\mathbf{A_v}(\mathbf{x}) + \mathbf{A_m} \cdot \mathbf{A_s}(\mathbf{u}) \cdot \mathbf{A_t}(\mathbf{x}) \cdot \mathbf{A}_\alpha(\mathbf{x})\right]}_{\mathbf{A}_{veh}(\mathbf{x},\mathbf{u})} \cdot \mathbf{x} + \underbrace{\mathbf{A_m} \cdot \mathbf{A_s}(\mathbf{u}) \cdot \mathbf{B_t}(\mathbf{x}) \cdot \mathbf{B_u}}_{\mathbf{B}_{veh}(\mathbf{x},\mathbf{u})} \cdot \mathbf{u} \tag{16.9}$$

The matrices hold the following relations:

- $\mathbf{A_v}(\mathbf{x})$ the dependence of v_x and v_y on yawing motion,
- $\mathbf{A_m}$ the division by mass and inertia,
- $\mathbf{A_s}(\mathbf{u})$ the translation of tire reference frame to chassis reference frame via steering,
- $\mathbf{A_t}(\mathbf{x})$ the tire parameterization in terms of $C_{x/y,i,\alpha}$,
- $\mathbf{A}_\alpha(\mathbf{x})$ the arctan-terms of slip angle calculation,
- $\mathbf{B_t}(\mathbf{x})$ the tire parameterization in terms of $C_{x/y,i,\alpha/\lambda}$ and
- $\mathbf{B_u}(\mathbf{x}, \mathbf{u})$ the allocation of actuators to tire forces.

See the matrices as follows.

$$\mathbf{A_v}(\mathbf{x}) = \begin{bmatrix} 0 & r & 0 \\ -r & 0 & 0 \\ 0 & 0 & 0 \end{bmatrix} \tag{16.10}$$

$$\mathbf{A_m} = \begin{bmatrix} \frac{1}{m} & 0 & 0 \\ 0 & \frac{1}{m} & 0 \\ 0 & 0 & \frac{1}{I_Z} \end{bmatrix} \tag{16.11}$$

$$\mathbf{A_s}(\mathbf{u}) = \begin{bmatrix} \cos\delta & \cos\delta & 1 & 1 & -\sin\delta & -\sin\delta & 0 & 0 \\ \sin\delta & \sin\delta & 0 & 0 & \cos\delta & \cos\delta & 1 & 1 \\ \substack{l_f \sin\delta \\ -l_t \cos\delta} & \substack{l_f \sin\delta \\ +l_t \cos\delta} & -l_t & l_t & \substack{l_f \cos\delta \\ +l_t \sin\delta} & \substack{l_f \cos\delta \\ -l_t \sin\delta} & -l_r & -l_r \end{bmatrix} \tag{16.12}$$

$$\mathbf{A_t}(\mathbf{x}) = \begin{bmatrix} C_{x,\alpha,fl} & 0 & 0 & 0 \\ 0 & C_{x,\alpha,fr} & 0 & 0 \\ 0 & 0 & C_{x,\alpha,rl} & 0 \\ 0 & 0 & 0 & C_{x,\alpha,rr} \\ C_{y,\alpha,fl} & 0 & 0 & 0 \\ 0 & C_{y,\alpha,fr} & 0 & 0 \\ 0 & 0 & C_{y,\alpha,rl} & 0 \\ 0 & 0 & 0 & C_{y,\alpha,rr} \end{bmatrix} \tag{16.13}$$

$$\mathbf{A}_\alpha(\mathbf{x}) = \begin{bmatrix} -\arctan\left(\frac{v_y+l_f r}{v_x-l_t r}\right) & \frac{1}{v_x} & 0 & 0 \\ -\arctan\left(\frac{v_y+l_f r}{v_x+l_t r}\right) & \frac{1}{v_x} & 0 & 0 \\ \arctan\left(\frac{-v_y+l_r r}{v_x-l_r r}\right) & \frac{1}{v_x} & 0 & 0 \\ \arctan\left(\frac{-v_y+l_f r}{v_x+l_t r}\right) & \frac{1}{v_x} & 0 & 0 \end{bmatrix} \tag{16.14}$$

$$\mathbf{B_t}(\mathbf{x}) = \begin{bmatrix} C_{x,\alpha,fl} & 0 & 0 & 0 & C_{x,\lambda,fl} & 0 & 0 & 0 \\ 0 & C_{x,\alpha,fr} & 0 & 0 & 0 & C_{x,\lambda,fr} & 0 & 0 \\ 0 & 0 & C_{x,\alpha,rl} & 0 & 0 & 0 & C_{x,\lambda,rl} & 0 \\ 0 & 0 & 0 & C_{x,\alpha,rr} & 0 & 0 & 0 & C_{x,\lambda,rr} \\ C_{y,\alpha,fl} & 0 & 0 & 0 & C_{y,\lambda,fl} & 0 & 0 & 0 \\ 0 & C_{y,\alpha,fr} & 0 & 0 & 0 & C_{y,\lambda,fr} & 0 & 0 \\ 0 & 0 & C_{y,\alpha,rl} & 0 & 0 & 0 & C_{y,\lambda,rl} & 0 \\ 0 & 0 & 0 & C_{y,\alpha,rr} & 0 & 0 & 0 & C_{y,\lambda,rr} \end{bmatrix} \tag{16.15}$$

$$\mathbf{B_u} = \begin{bmatrix} 1 & 0 & 0 & 0 & 0 \\ 1 & 0 & 0 & 0 & 0 \\ 0 & 0 & 0 & 0 & 0 \\ 0 & 0 & 0 & 0 & 0 \\ 0 & 1 & 0 & 0 & 0 \\ 0 & 0 & 1 & 0 & 0 \\ 0 & 0 & 0 & 1 & 0 \\ 0 & 0 & 0 & 0 & 1 \end{bmatrix} \tag{16.16}$$

The arctan terms in matrix $\mathbf{A}_\alpha(\mathbf{x})$ in Equation 16.14 are chosen as a parameterization of v_x.

16.3 Error Dynamics Parameterization

According to Equation 15.2 the change in curvature error is

$$\dot{e_\rho} = -\frac{\dot{r}}{v} - e_\rho \frac{v_x \dot{v}_x}{v^2} - e_\rho \frac{v_y \dot{v}_y}{v^2} + \rho_{des} \frac{v_x \dot{v}_x}{v^2} + \rho_{des} \frac{v_y \dot{v}_y}{v^2} + \dot{\rho}_{des} \tag{16.17}$$

Since the dependency on vehicle state derivatives shows up in a linear combination, it can be brought into a similar matrix representation as the vehicle states, where matrices $\mathbf{A_s(u)}, \mathbf{B_t(x)}$, $\mathbf{B_u(x,u)}$ and the input $\mathbf{u}$ remain identical. This simplifies collecting all state equations into one big matrix representation at the end. For $\mathbf{x} = \begin{bmatrix} v_x & v_y & r & e_\rho \end{bmatrix}^T$, it follows

$$\begin{aligned}
\dot{e_\rho} = & \underbrace{[\mathbf{A}_{\mathbf{v},\rho}(\mathbf{x}) + \mathbf{A}_{\mathbf{m},\rho}(\mathbf{x}) \cdot \mathbf{A_s}(\mathbf{u}) \cdot \mathbf{A_t}(\mathbf{x}) \cdot \mathbf{A}_\alpha(\mathbf{x})]}_{\mathbf{A}_\rho(\mathbf{x},\mathbf{u})} \cdot \mathbf{x} + \underbrace{\mathbf{A}_{\mathbf{m},\rho}(\mathbf{x}) \cdot \mathbf{A_s}(\mathbf{u}) \cdot \mathbf{B_t}(\mathbf{x}) \cdot \mathbf{B_u}}_{\mathbf{B}_\rho(\mathbf{x},\mathbf{u})} \cdot \mathbf{u} \\
& + \underbrace{([\mathbf{E}_{\mathbf{v},\rho}(\mathbf{x}) + \mathbf{E}_{\mathbf{2},\rho}(\mathbf{x}) \cdot \mathbf{A_s}(\mathbf{u}) \cdot \mathbf{A_t}(\mathbf{x}) \cdot \mathbf{A}_\alpha(\mathbf{x})] \cdot \mathbf{x} + \mathbf{E}_{\mathbf{m},\rho}(\mathbf{x}) \cdot \mathbf{A_s}(\mathbf{u}) \cdot \mathbf{B_t}(\mathbf{x}) \cdot \mathbf{B_u} \cdot \mathbf{u})}_{\mathbf{E}_{\rho,1}(\mathbf{x},\mathbf{u})} \cdot \rho_{des} \\
& + \mathbf{E}_{\rho,\mathbf{2}} \dot{\rho}_{des}
\end{aligned} \tag{16.18}$$

where

$$\mathbf{A}_{\mathbf{v},\rho}(\mathbf{x}) = \begin{bmatrix} \frac{v_y r e_\rho}{v^2} & -\frac{v_x r e_\rho}{v^2} & 0 & 0 \end{bmatrix} \tag{16.19}$$

$$\mathbf{A}_{\mathbf{m},\rho}(\mathbf{x}) = \begin{bmatrix} -\frac{v_x e_\rho}{m v^2} & -\frac{v_y e_\rho}{m v^2} & -\frac{1}{I_Z v} \end{bmatrix} \tag{16.20}$$

$$\mathbf{E}_{\mathbf{v},\rho}(\mathbf{x}) = \begin{bmatrix} -\frac{v_y r}{v^2} & \frac{v_x r}{v^2} & 0 & 0 \end{bmatrix} \tag{16.21}$$

$$\mathbf{E}_{\mathbf{m},\rho}(\mathbf{x}) = \begin{bmatrix} \frac{v_x}{m v^2} & \frac{v_y}{m v^2} & 0 \end{bmatrix} \tag{16.22}$$

$$\mathbf{E}_{\rho,\mathbf{2}} = 1 \tag{16.23}$$

and $v = \sqrt{v_x^2 + v_y^2}$. For implementing into the controller all influences of ρ_{des} and $\dot{\rho}_{des}$ in terms of matrices $\mathbf{E}_{\rho,\mathbf{i}}$ are considered as a disturbance input to the system and therefore neglected when solving the RE.

Displacement and heading error, according to Equation 15.6 and 15.3, are brought into parametrized form as well. This appears to be less complex, since there is no dependence on input $\mathbf{u}$ in this state equations. For $\mathbf{x} = \begin{bmatrix} v_x & v_y & r & e_{la} & e_\psi \end{bmatrix}^T$ it follows

$$\begin{bmatrix} \dot{e_{la}} \\ \dot{e_\psi} \end{bmatrix} = \mathbf{A_e}(\mathbf{x})\mathbf{x} + \mathbf{E_e}(\mathbf{x})\rho_{des} \tag{16.24}$$

where

$$\mathbf{A_e}(\mathbf{x}) = \begin{bmatrix} \sin e_\psi & \cos e_\psi & x_{la} \cos e_\psi & 0 & 0 \\ 0 & 0 & 1 & 0 & 0 \end{bmatrix} \tag{16.25}$$

$$\mathbf{E_e}(\mathbf{x}) = \begin{bmatrix} -x_{la} \cos e_\psi (v_x \cos e_\psi + v_y \sin e_\psi) \\ -(v_x \cos e_\psi + v_y \sin e_\psi) \end{bmatrix} \tag{16.26}$$

As mentioned above, dependencies on road curvature in terms of $\mathbf{E_e}(\mathbf{x})$ are considered as disturbance input and therefore neglected.

16.4 Implementation and Numerical Issues

The system is assembled and brought into the form $\dot{\mathbf{x}} = \mathbf{A}(\mathbf{x})\mathbf{x} + \mathbf{B}(\mathbf{x},\mathbf{u})\mathbf{u}$ with all six states, so it can be used within the RE solver. Equations 16.9, 16.18 and 16.24 yield.

$$\begin{bmatrix} \dot{v}_x \\ \dot{v}_y \\ \dot{r} \\ \dot{e}_\rho \\ \dot{e}_{la} \\ \dot{e}_\psi \end{bmatrix} = \begin{bmatrix} \mathbf{A}_{veh}(\mathbf{x},\mathbf{u}) \\ \mathbf{A}_\rho(\mathbf{x},\mathbf{u}) \\ \mathbf{A_e}(\mathbf{x}) \end{bmatrix} \cdot \begin{bmatrix} v_x \\ v_y \\ r \\ e_\rho \\ e_{la} \\ e_\psi \end{bmatrix} + \begin{bmatrix} \mathbf{B}_{veh}(\mathbf{x},\mathbf{u}) \\ \mathbf{B}_\rho(\mathbf{x},\mathbf{u}) \\ \mathbf{0} \\ \mathbf{0} \end{bmatrix} \cdot \begin{bmatrix} \delta \\ \lambda_i \end{bmatrix} \tag{16.27}$$

Two rows of zeros in $\mathbf{B}$ appear since e_{la} and e_{ψ} are not dependent on $\mathbf{u}$.

For implementation into simulation it has to be taken into account, that the system is only valid for $v_x > 0$. In the first place, vehicles with $v_x < 0$ are driving backwards and neglected for this research. Furthermore conditions with $v_x = 0$ mean there is no movement in longitudinal direction or even stand-still, which are not interesting either. So requirement of $v_x > 0$ is achievable without loosing validity for the system in relevant scenarios.

Furthermore, the controllability matrix in the linear sense, $\mathbf{C_M} = \begin{bmatrix}\mathbf{B} & \mathbf{AB} & \mathbf{A}^2\mathbf{B} & \mathbf{A}^3\mathbf{B} & \mathbf{A}^4\mathbf{B} & \mathbf{A}^5\mathbf{B}\end{bmatrix}$ has only rank of five. Since the system itself is of order six it is not controllable. This originates from the fact, that that look-ahead error and heading error can not be controlled directly, but only via the control of the vehicle states. Adapting $\mathbf{A_e}(\mathbf{x})$ and generating a cross term between e_{la} and e_{ψ} can generate full rank in the controllability matrix. It needs to be mentioned here, that the linear system concept of controllability is not generally transferable to nonlinear systems. But for finding a valid SDC form, which yields a convergence of the Riccati solver, it has proven suitable. Generally to accomplish a parameterization with full rank, a single matrix element can be altered and made a coefficient of a different state x_i or input u_i. Thus the parameterization is nonunique, as the following example shows.

$$f(\mathbf{x}) = \frac{f(\mathbf{x})}{x_i} x_i \tag{16.28}$$

The nonlinear term $f(\mathbf{x})$ can be used as a coefficient to an arbitrary state x_i. Accordingly the term $\mathbf{A_e}(\mathbf{x})_{i=1,j=1} = \sin e_{\psi}$, being a coefficient of v_x, is altered to be a coefficient of e_{ψ}: $\frac{v_x \sin e_{\psi}}{e_{\psi}}$. The drawback here is that in case $e_{\psi} = 0$, the term yields division by zero. However since e_{ψ} appears in the numerator in terms of a sinus function, the limit for e_{ψ} converging to zero is finite,

$$\lim_{e_{\psi} \to 0} \frac{\sin e_{\psi}}{e_{\psi}} = 1 \tag{16.29}$$

Thus an auxiliary function can be defined to avoid division by zero.

$$f_a = \begin{cases} \frac{\sin e_{\psi}}{e_{\psi}}, & \text{for } e_{\psi} \neq 0 \\ 1, & \text{for } e_{\psi} = 0 \end{cases} \tag{16.30}$$

And therefore $\mathbf{A_e}(\mathbf{x})_{i=1,j=1} = 0$ and $\mathbf{A_e}(\mathbf{x})_{i=1,j=6} = v_x f_a$. With this adoption the system becomes controllable and represents a straightforward parameterization of the controller model. It is used as initial setup for simulation with further adoptions to be expected throughout the simulation and tuning process. Also to mention is that matrix $\mathbf{B_u}$ is used to allocate actuators and therefore relevant for defining the kind of drivetrain of the vehicle.

The controllability matrix is moreover a suitable tool in order to assess the conditioning of the system. One way to analyse this is calculating the condition number of $\mathbf{C_M}$, it being the ratio of the largest singular value of $\mathbf{C_M}$ to the smallest. It gives indication on how sensitive a solution attempted using the particular system is, when changing inputs to the system. A large conditioning number of $\mathbf{C_M}$ indicates a nearly singular system in terms of its SDC form. Also will the Riccati solver from a certain threshold not be able to retreive a solution. Tests showed that condition number larger than approximately 10^8 yield problems. Therefore the SDC form was checked for different states. States with low speed v_x yield large condition numbers due to the fact that v_x appears multiple times in terms of denominator inside $\mathbf{A}(\mathbf{x})$ and $\mathbf{B}(\mathbf{x})$. Respective terms tend to infinity for v_x tending to zero making the system singular. A saturation, $v_x > 5$ m/s, was implemented to account. This in turn yields to a less accurate system description inside the controller for low speeds. However since limit handling control for these low speeds is practically not relevant, less accuracy for this regime is acceptable.

17 Actuator Model and Longitudinal Controller

17.1 Actuator Saturation and Dynamics

Actuators in vehicles are underlying certain physical limitations, which are to be regarded in the model. In terms of steering a maximum steering angle $\delta_{max} = \pm 35$[deg] is taken into account. To model the steering actuator in the car, an identified model of the Prius is used in terms of the following second-order transfer function.

$$G_\delta = \frac{306.25}{s^2 + 24.5s + 306.25} \tag{17.1}$$

For the differential wheel actuators saturation in slip input was taken into account. For the lateral controller only differential braking and no drive torque input is considered. Therefore the limit slip inputs would be $\lambda_{i,max} = 0$ and $\lambda_{i,min} =$ -1. For representation of physical properties and inertia in the wheel when applying brakes, a first order system with a time constant of 0.1 seconds is included in the model.

$$G_\lambda = \frac{1}{0.1s + 1} \tag{17.2}$$

17.2 Longitudinal Controller

Lateral manoeuvre induce also longitudinal forces on the vehicle, forcing it to slow down. However, during the lateral manoeuvres to be tested, speed is desired to be kept constant in order to compare different controller setups with each other. For this task a longitudinal controller is used, which keeps the total velocity $v_{tot} = \sqrt{v_x^2 + v_y^2}$ constant. During a lateral manoeuvre with large sideslip, the lateral velocity makes a significant amount of the speed, with which the vehicle is travelling along its path. Therefore it was chosen to keep total velocity constant. Thus dependent on lateral velocity and desired total velocity the desired longitudinal velocity can be obtained.

$$v_{x,des} = \sqrt{v_{des}^2 - v_y^2}, \text{ for } |v_y| > |v_{des}| \tag{17.3}$$

The control error is

$$e_{v,x} = v_{x,des} - v_x \tag{17.4}$$

A PID controller is used to generate the wheel slip input dependent on the error.

$$\lambda(t) = k_p e_{v,x} + k_i \int_0^t e_{v,x}(\tau) d\tau + k_d \frac{de_{v,x}}{dt} \tag{17.5}$$

Both wheels of the driven axle therefore receive the same slip input from the cruise controller.

17.3 Axle Differential

Also an axle differential is modelled and represents a real passenger car drivetrain with open differential. An axle differential yields to equal drive torque on both wheels of one axle and therefore of course only works in case drive torque is applied to that axle. Thus the longitudinal force of each of the wheels is only as great as of the wheel with the least potential tractive force. Mainly is longitudinal potential of a wheel dependent on wheel load and friction, and therefore are these the limiting factors. In case of neglecting the function of the differential and giving equal slip to left and right wheel, the higher loaded one will create larger longitudinal forces and induce additional yawing moment, which would influence lateral motion.

The differential is modelled as part of the plant and uses longitudinal tire forces as input. The larger force of both is detected at the previous time step, and the slip input of the respective wheel is cut off in order that both wheels match in terms of longitudinal tire force. The differential is only active if both wheels have $\lambda > 0$ and can be applied to both front and rear axle, dependent on which one is chosen to be the driven one.

18 Linearized Controller Model

The fully nonlinear system was discussed so far. A linearized model is derived in this Chapter, which can be used for basic system analysis and linear control methods. The model is used to design an LQR controller from it, as a benchmark for the SDRE controller. For normal driving, in the linear operating range of the tires, nonlinear and linear controller should perform similar. Furthermore, also for limit handling scenarios the benchmark should be used as a reference, to judge in which way the nonlinear controller changes the response of the system. A four-degree-of-freedom linearized model is derived from the full model.

Vehicle states are described with the bicycle model according to Equation 5.7. Underlying assumptions are: small steering angle, lumped linear tire stiffness, constant velocity and steering as the only input. There is only steering input considered, because wheel slip input has a highly nonlinear influence onto lateral dynamics. This comes through the combined slip tire characteristics, and wheel slip input is neglected through assuming a linear tire. The error state equations are obtained from linearization of Equation 15.3 and 15.6 around the origin.

$$\dot{e}_\psi = r - v_x\rho_{des} \tag{18.1}$$

$$\dot{e}_y = v_y + v_x e_\psi \tag{18.2}$$

$$\dot{e}_{la} = v_y + v_x e_\psi + x_{la} r - x_{la} v_x \rho_{des} \tag{18.3}$$

The four-degree-of-freedom model follows.

$$\begin{bmatrix} \dot{v}_y \\ \dot{r} \\ \dot{e}_{la} \\ \dot{e}_\psi \end{bmatrix} = \begin{bmatrix} \frac{-C_{\alpha,f}-C_{\alpha,r}}{v_x m} & -v_x+\frac{C_{\alpha,r}l_r-C_{\alpha,f}l_f}{v_x m} & 0 & 0 \\ \frac{C_{\alpha,r}l_r-C_{\alpha,f}l_f}{I_Z v_x} & \frac{-C_{\alpha,f}l_f^2-C_{\alpha,r}l_r^2}{I_Z v_x} & 0 & 0 \\ 1 & x_{la} & 0 & v_x \\ 0 & 1 & 0 & 0 \end{bmatrix} \begin{bmatrix} v_y \\ r \\ e_{la} \\ e_\psi \end{bmatrix} + \begin{bmatrix} \frac{C_{\alpha,f}}{m} \\ \frac{C_{\alpha,f}l_f}{I_Z} \\ 0 \\ 0 \end{bmatrix} \delta + \begin{bmatrix} 0 \\ 0 \\ -v_x \\ -x_{la}v_x \end{bmatrix} \rho_{des} \tag{18.4}$$

This model can further be used to investigate basic stability and tracking properties of the path following scheme. It is used as well for design of the steering feedforward control law.

19 Feedforward Control

In the optimal control layout, the feedback gains are obtained solving the Riccati equation. However, these are proportional and the control law does not possess an integral term. That means constant disturbance inputs yield a steady-state offset. One approach would be to augment states such that the feedback gets integral action. However, potential risk of instability would be introduced with this approach. Furthermore, road curvature ρ_{des} appears in Equations 15.2, 15.3 and 15.6 as a disturbance input. An appropriate way in this case is using feedforward control, since ρ_{des} is known and measurable. Also the impact on the system and therefore the control variables are known. Another advantage of feedforward control is that it can react very quickly. This will eventually lead to the vehicle changing direction before it deviates from the path and an error can be measured.

19.1 Geometric and Sideslip Terms

Road curvature ρ_{des} resembles the measurable disturbance input. The geometric cornering relation of the linearized bicycle model is used to generate a steering input depending on road curvature according to Equation 6.4.

$$\delta_{FF,geo} = (l + K_{US}v_x^2)\rho_{des} = G_{FF,geo}\rho_{des} \tag{19.1}$$

The steady-state offset of e_y should be minimized. Therefore the linearized closed-loop system of the path-tracking problem is analysed. Steering input consists of error state feedback and the feedforward steering input.

$$\delta = -k_{p,1}e_{la} - k_{p,2}e_\psi + \delta_{FF,geo} \tag{19.2}$$

The system can be written in closed-loop form $\dot{\mathbf{x}} = \mathbf{A}\mathbf{x} + \mathbf{B}\rho_{des}$ with road curvature ρ_{des} as input.

$$\begin{bmatrix} \dot{v}_y \\ \dot{r} \\ \dot{e}_{la} \\ \dot{e}_\psi \end{bmatrix} = \begin{bmatrix} \frac{-C_{\alpha,f}-C_{\alpha,r}}{v_x m} & -v_x+\frac{C_{\alpha,r}l_r-C_{\alpha,f}l_f}{v_x m} & -k_{p,1}\frac{C_{\alpha,f}}{m} & -k_{p,2}\frac{C_{\alpha,f}}{m} \\ \frac{C_{\alpha,r}l_r-C_{\alpha,f}l_f}{I_Z v_x} & \frac{-C_{\alpha,f}l_f^2-C_{\alpha,r}l_r^2}{I_Z v_x} & -k_{p,1}\frac{C_{\alpha,f}l_f}{I_Z} & -k_{p,2}\frac{C_{\alpha,f}l_f}{I_Z} \\ 1 & x_{la} & 0 & v_x \\ 0 & 1 & 0 & 0 \end{bmatrix} \begin{bmatrix} v_y \\ r \\ e_{la} \\ e_\psi \end{bmatrix} + \begin{bmatrix} \frac{C_{\alpha,f}}{m}G_{FF,geo} \\ \frac{C_{\alpha,f}l_f}{I_Z}G_{FF,geo} \\ -v_x x_{la} \\ -v_x \end{bmatrix} \rho_{des} \tag{19.3}$$

The steady-state error of the system can be computed according to

$$\mathbf{e}_{SS} = \mathbf{A}^{-1}\mathbf{B}\rho_{SS} \tag{19.4}$$

Steady-state error is demonstrated with an example. Therefore a constant road curvature input of $\rho_{SS} = 0.3/v_x^2$ is chosen. It is speed dependent and yields a constant cornering acceleration of $0.3g$ invariant with speed. Feedback gains were chosen to $k_{p,1} = 0.05$, $k_{p,2} = 0.1$ and $x_{la} = 12.5$m. Obtained errors are shown in Figure 19.1.

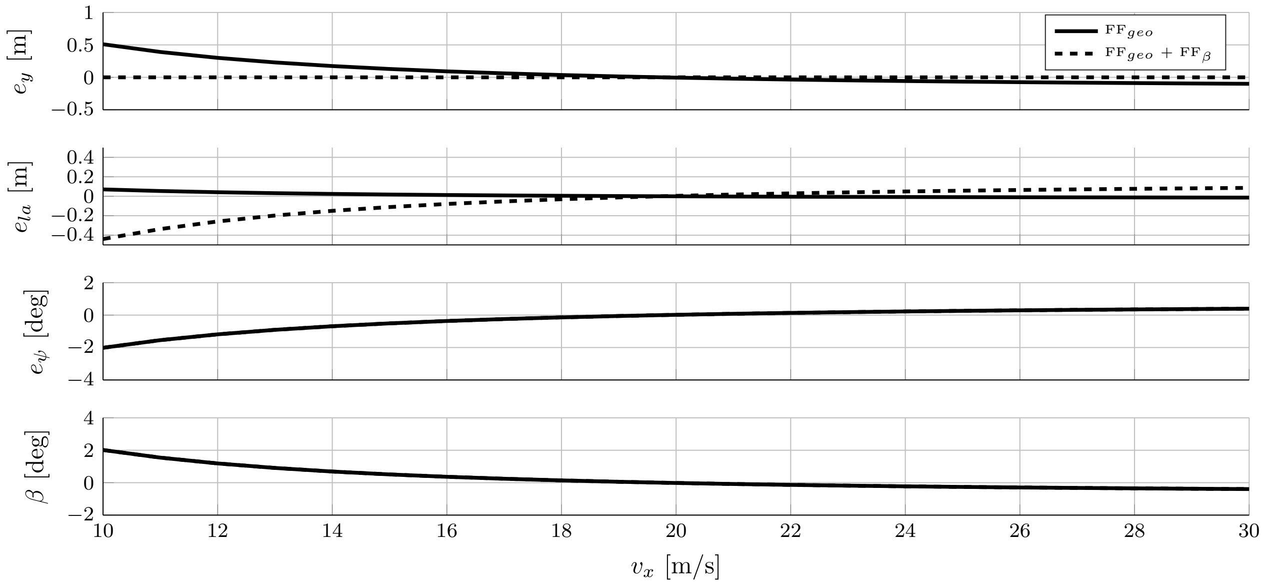

Figure 19.1: *Steady-State errors depending on speed for different feedforward controllers*

Heading and look-ahead errors remain with a nonzero steady-state offset. Also e_y shows an offset, it is not controlled directly though, but only appears as a term of the look-ahead error. The occurring steady-state offset is seen as a drawback of the error definition, which does not take body sideslip into account. As discussed in Chapter 6, the bicycle model inherits a certain body sideslip for constant cornering. Only for one particular speed which shows zero sideslip, $v_x = 19.73$ m/s, zero steady-state error can be observed as well, see also Equation 6.7. It is observed that $e_\psi = -\beta$ and therefore the steady-state steering input remains with an offset of exactly the term $k_{p,2}e_\psi$. One way to address this issue is altering the control law and adding body sideslip feedback.

$$\delta = -k_{p,1}e_{la} - k_{p,2}e_\psi - k_{p,3}\beta + \delta_{FF,geo} \tag{19.5}$$

When adding body sideslip with equal proportion as heading error feedback, $k_{p,3} = k_{p,2}$, then look-ahead error e_{la} is driven to zero. However, it is desired to drive the displacement at the CG, e_y, to zero. When substituting $e_{la} = e_y + x_{la}e_\psi$ into Equation 19.5 and assuming $e_\psi = -\beta$ it follows for the feedback steering input:

$$\delta_{FB} = -k_{p,1}e_y + k_{p,1}x_{la}\beta \tag{19.6}$$

It can be seen that in order to drive e_y to zero, the body sideslip feedback also needs to be weighted with $k_{p,1}x_{la}$ and it follows

$$k_{p,3} = k_{p,1}x_{la} + k_{p,2} \tag{19.7}$$

in order to drive e_y to zero. This approach yields two drawbacks. Firstly, body sideslip feedback is required, and also is $k_{p,3}$ dependent on $k_{p,1}$ and $k_{p,2}$. Though in the Optimal Control framework the gains are computed on-line and independent of each other. Therefore it would be preferable to know the steady-state body sideslip of the bicycle model and feedback could be avoided. Then it could be transferred into a feedforward term. This can be achieved as follows. In the equation for look-ahead error, $e_{la} = e_y + x_{la}e_\psi$, replacing x_{la} with the center of percussion, $x_{COP} = \frac{I_Z}{l_r m}$, yields a decoupling of lateral motion and yaw motion [KG12]. Therefore the front and rear axle lateral forces for steady-state cornering can be obtained from the error dynamics equations.

$$\ddot{e}_{COP} = \ddot{e}_y + x_{COP}\ddot{e}_\psi = \dot{v}_y + v_x\dot{e}_\psi + x_{COP}(\dot{r} - (\dot{v}_x\rho + v_x\dot{\rho})) \tag{19.8}$$

Taking $\ddot{e}_{COP} = \dot{v}_x = \dot{\rho} = 0$ and $x_{COP} = \frac{I_Z}{l_r m}$, it follows the front axle lateral force for steady-state cornering [KG15].

$$F_{f,FF} = \frac{m l_r v_x^2}{l} \rho_{SS} \tag{19.9}$$

Using the yaw rate derivative the rear axle steady-state force can be computed.

$$F_{r,FF} = \frac{m l_f v_x^2}{l} \rho_{SS} \tag{19.10}$$

Using the slip angle definition

$$\alpha_r = -\beta_{SS} + \frac{l_r r}{v_x} \tag{19.11}$$

together with $F_{r,FF} = \alpha_r C_{\alpha,r}$ yields

$$\beta_{SS} = \left(-\frac{m l_f v_x^2}{l C_{\alpha,r}} + l_r \right) \rho_{SS} \tag{19.12}$$

Weighted with the feedback gains, this term is used as a second feedforward input additionally to $\delta_{FF,geo}$ [KG15].

$$\delta_{FF,\beta} = \left(-\frac{m l_f v_x^2}{l C_{\alpha,r}} + l_r \right) (k_{p,1} x_{la} + k_{p,2}) \rho_{des} \tag{19.13}$$

$$G_{FF,\beta} = \left(-\frac{m l_f v_x^2}{l C_{\alpha,r}} + l_r \right) (k_{p,1} x_{la} + k_{p,2}) \tag{19.14}$$

The B matrix of the closed loop system alters to

$$\begin{bmatrix} \frac{C_{\alpha,f}}{m}(G_{FF,geo} - G_{FF,\beta}) \\ \frac{C_{\alpha,f} l_f}{I_Z}(G_{FF,geo} - G_{FF,\beta}) \\ -v_x x_{la} \\ -v_x \end{bmatrix} \tag{19.15}$$

For the linearized model this approach yields zero steady-state offset in e_y as it can be seen in Figure 19.1. Therefore, since the vehicle is located on the path, the non-zero heading error is of no concern and will remain as it has the same absolute value as the body sideslip.

19.2 Nonlinear Understeering Gradient

The feedforward steering terms, $\delta_{FF,geo}$ and $\delta_{FF,\beta}$, are a function of the linearized axle cornering stiffnesses $C_{\alpha,f}$ and $C_{\alpha,r}$ and therefore a function of the understeering gradient K_{US}. Thus a sufficient path tracking performance can only be expected up to a certain cornering acceleration, where tires are still working in their linear regime. To assess the performance, the path following controller was tested for tracking a curvature in steady-state condition. Therefore a simulation for tracking a steady-state circular path was done. The curvature was set to $\rho_{des} = 0.016$ rad/m, which means a cornering acceleration $a_{tot} = \sqrt{a_x^2 + a_y^2}$ of about $0.65g$, when tracking the curvature perfectly with a speed of 25 m/s. This represents fast cornering with utilizing about 70 % of the whole friction potential of the tire-road contact for the Prius (on dry asphalt).

Lateral error e_{la} and heading error e_ψ are controlled for this experiment, using the SDRE feedback controller together with the feedforward controller of Equation 19.1 and 19.13. Figure 19.2 shows the lateral displacement for this experiment.

The initial motion is straight line driving and after 25 meters respective one second a spiral with linear curvature rate yields to the steady-state cornering motion, which continues to the end of the simulation. Even though feedforward terms of Equation 19.1 and 19.13 are applied, there is still a significant offset of approximately 0.3 metres prevailing. The representation of cornering stiffness into a lumped linear factor does not hold for this cornering acceleration. Rather yield front and rear lateral tire force characteristics to a change in cornering stiffness, dependent on cornering accelerations and therefore dependent on slip angle, see Figure 19.3

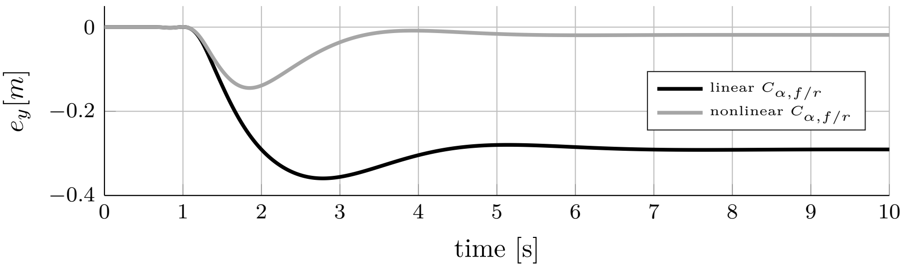

Figure 19.2: *Path tracking error comparison of feedforward control with linear and nonlinear axle cornering stiffness, the simulation was done width v_tot = 25m/s and constant curvature ρ_{des} = 0.016rad/m, yielding a cornering acceleration $a_{tot} = \sqrt{a_x^2 + a_y^2}$ of about 0.65g*

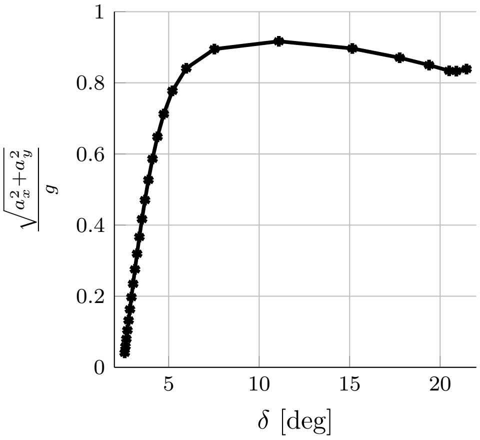

Figure 19.3: *Nonlinear handling diagram for the Prius. The diagram was created negotiating a turn with constant curvature ρ_{des} = 0.016 rad/m, for varying velocities. Velocities were kept constant with cruise control on the front wheels. The Prius shows limit understeer. Around the maximum friction an increase in steering input does have no effect, only does the front wheels slip even more. The friction limit for this curvature can be read off the diagram.*

To control lateral motion accurately at the friction limits this change in axle cornering stiffnesses $C_{\alpha,f/r}$ and therefore in understeering gradient K_{US} needs to be taken into account. Therefore, it is proposed to consider a linear description of the nonlinear tire model, at the current operating point: $C_\alpha(\mathbf{x}_j) = \frac{F(\mathbf{x}_j)}{\alpha(\mathbf{x}_j)} (\forall \alpha \neq 0)$. It is further on referred to as factorized cornering stiffness, as it is obtained by factorizing tire force: $F(\mathbf{x}_j) = C_\alpha(\mathbf{x}_j)\alpha(\mathbf{x}_j)$. Figure 19.4 shows this concept.

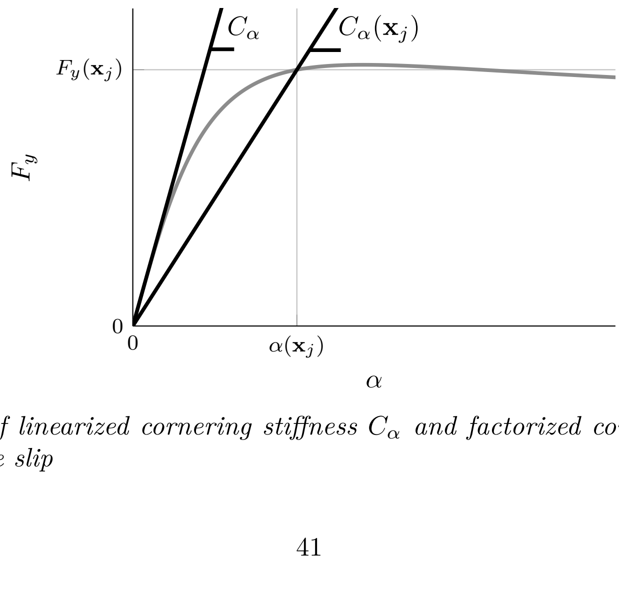

Figure 19.4: *Comparison of linearized cornering stiffness C_α and factorized cornering stiffness $C_\alpha(\mathbf{x}_j)$, at operating point $\mathbf{x}_j$ with large slip*

Respective tireforces are obtained using Equation 13.7. The lumped factorized front and rear axle cornering stiffness is obtained in real-time and replaces $C_{\alpha,f/r}$ in 19.1 and 19.13.

$$C_{\alpha,f} = \frac{F_{y,fl}\cos\delta + F_{x,fl}\sin\delta}{\alpha_{fl}} + \frac{F_{y,fr}\cos\delta + F_{x,fr}\sin\delta}{\alpha_{fr}}, \quad (\forall \alpha_i \neq 0) \tag{19.16}$$

$$C_{\alpha,r} = \frac{F_{y,rl}}{\alpha_{rl}} + \frac{F_{y,rr}}{\alpha_{rr}}, \quad (\forall \alpha_i \neq 0) \tag{19.17}$$

In the case of $\alpha_i = 0$, the linearized lateral tire stiffness from the i-th tire is substituted.

Besides the influence of steering and load transfer, also the impact of driving or braking forces is considered. Through the combined slip tire characteristics, driving or braking forces have significant influence on the cornering stiffness. Using this method the axle cornering stiffness required for calculating the feedforward input becomes dependent on state feedback via the controller tire model. As it is to expect that cornering stiffness changes low frequent, no influence of the transient path tracking is expected. The improvement in path tracking can be seen in Figure 19.2. Steady-state error is decreased by approximately 90% in this case.

A further advantage of this concept is that influences of propulsive or braking forces changing the lateral axle stiffness are taken into account via the combined slip tire model within the controller. As can be seen in Figure 7.1, the amount of longitudinal slip applied to a tire has a major influence on its lateral slip stiffness. An increase in longitudinal slip yields a decrease in lateral tire stiffness. Therefore the understeering gradient K_{US} is a function of longitudinal slip applied to the wheels. This nonlinear relation is dependent on the specific tire model. Figure 19.5 shows for the Prius tire model the specific case where slip is only applied to the rear axle, λ_r. This represents braking actuation only on the rear axle or rear wheel drive.

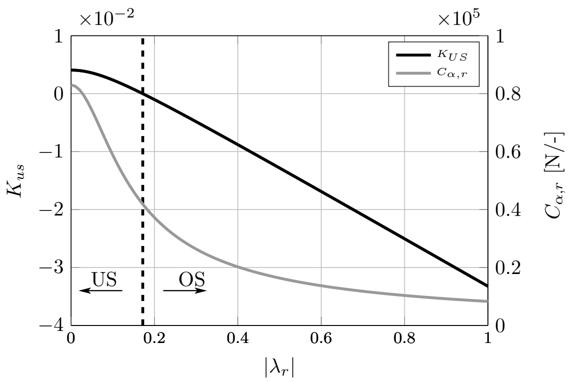

Figure 19.5: *Dependence of $C_{\alpha,r}$ and K_{US} on rear axle longitudinal slip λ_r as a result of the combined slip tire characteristics, for $\alpha_r = 0$*

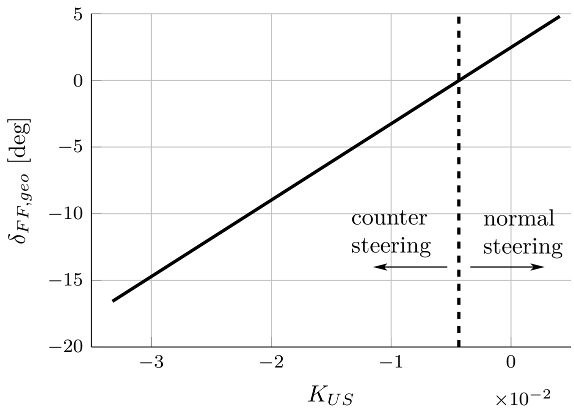

Figure 19.6: *Feedforward Steering input $\delta_{FF,geo}$ dependent on K_{US} according to Equation 19.1 for $v_x = 25$m/s and $\rho_{des} = 0.0016$rad/m*

It can be seen that due to λ_r the understeering gradient drops significantly and for $|\lambda_r|$ greater than 0.18 the understeering gradient drops below zero and the vehicle becomes oversteered according to Equation 6.4. Figure 19.6 shows the feedforward steering input for the respective range of understeering gradient from Figure 19.5, for tracking a curvature ρ_{des} of 0.016 rad/m, with a speed v_x of 25 m/s. It can be seen that for K_{US} smaller than -0.0042 the feedforward steering input becomes negative, representing a counter steering input to adapt for the oversteering vehicle condition. This is an advantage of using the nonlinear understeering gradient in terms of the factorized cornering stiffness.

Part V
Simulation and Tuning

The SDRE controller developed in Part IV is used to perform path following tasks in Simulation. Different paths are chosen as well as different controller setups. Focus is to assess the performance dependent on different error states to be penalized. The aim of tuning is to minimize lateral path tracking offset e_y, see Chapter 15.3. All simulations are done using Matlab Simulink. The vehicle model represents the Prius using respective parameters, see Appendix A. The speed during the simulations is kept constant with the longitudinal controller as described in Chapter 17. Rear wheel drive is chosen for the experiments.

It is started with control for steady-state conditions in order to gain basic understanding of the controller behaviour and the steady-state offset for large cornering accelerations. After that transient, actual path tracking manoeuvres are considered. Basic path tracking elements, representing elementary pieces of arbitrarily complex paths, are investigated. As a relevant manoeuvre for real collision avoidance scenarios, a lane-change is chosen as well. Also parameter variation robustness is tested with the lane change path. Finally, body sideslip control is considered.

20 Steady-state Cornering when only Steering

Results for steady-state cornering with cornering acceleration greater than $0.5g$ for different path curvatures are obtained using simulation, see Figure 20.1. Offset error e_{la}, heading error e_ψ and curvature error e_ρ are penalized within the SDRE feedback controller. Therefore, state weighting in $\mathbf{Q}$ and actuator weighting in $\mathbf{R}$ were tuned heuristically. Speed is kept constant with the output feedback slip controller, and an axle differential is taken into account as mentioned above.

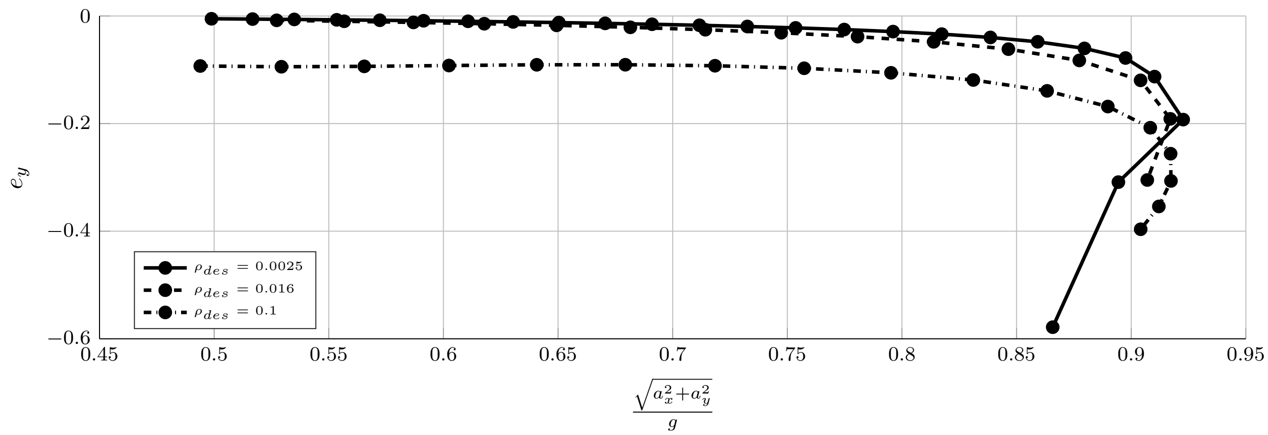

Figure 20.1: *Steady-state lateral error for cornering at the limits of handling with the Prius*

The path used for simulation consists of an initial straight driving part, followed by a smooth transient piece, yielding into the steady-state cornering part with constant curvature. The transition from straight line driving into the turn is defined with a low curvature rate in order that transient oscillations are minimized, and the vehicle reaches to steady-state quickly. Displacement error is measured after transients vanished. This setup, using SDRE controller together with feedforward controller shows stable path tracking up to the limits of handling for the Prius. The offset error e_y does not exceed 0.3 m up to the very maximum of tire-road friction. Only when exceeding this limit using a too large desired cornering speed, the longitudinal controller oversaturates the front tires. As a result, the vehicle state drops into an equilibrium at lower cornering acceleration, with greater steering input and significant displacement error of greater than 0.3 meters.

This limit understeering behaviour is predicted from the handling diagram in Figure 19.3. To avoid this behaviour, desired velocity should be decreased in such situations. Differential braking actuators can be used in order to reduce speed whilst cornering. However, cornering speed that exceeds a_{max} due to the friction limits, is neglected in this research, see Chapter 9.1. Aside this case, where cornering speed is too large, it is concluded that during steady-state cornering, only steering input is required to control the vehicle laterally. Only for the case, where the cornering acceleration should be optimized to its global optimum, further actuation may be required. However, aiming for the global optimum also requires high fidelity vehicle modelling taking into account suspension dynamics, roll stiffness and compliances to be of practical advantage. Eventually, the expected gain in peak cornering acceleration is marginal. More complex models in turn would also bring robustness issues. Therefore, and due to the fact that in relevant driving scenarios for this project, transients are more important, further optimizing of the peak cornering performance is not relevant for this project.

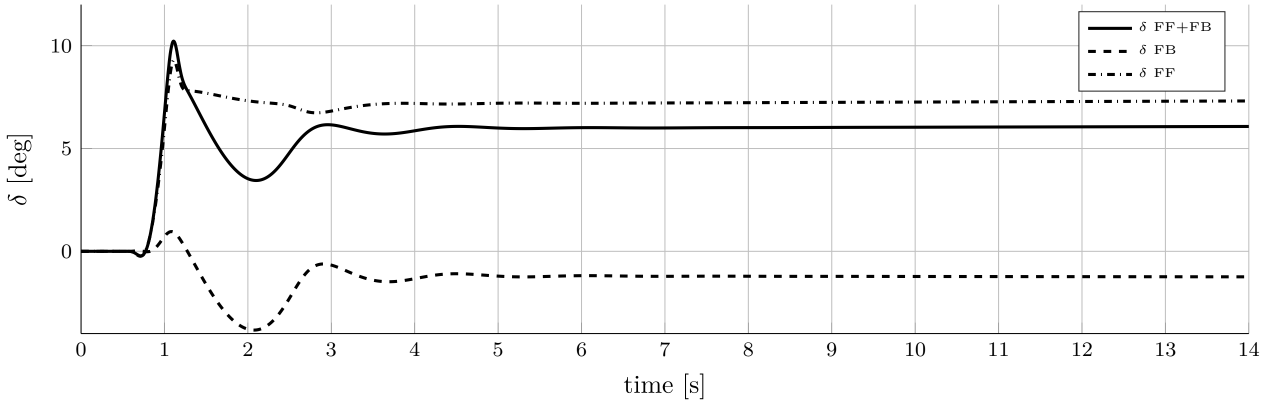

Figure 20.2: *Feedforward and feedback contribution to steady-state steering input*

Figure 20.2 shows the steering input for the one respective trim with $\rho_{des} = 0.016$ rad/m and $\frac{a_{tot}}{g} \approx 0.85$. It can be seen, that the feedforward term holds main contribution. It is therefore important to keep in mind, that the controller highly depends on the cornering stiffness values coming from the underlying nonlinear tire model. This determines that, for application in any car, performance significantly depends on accuracy of the tire model. This model dependency is a known drawback of model based control. The setup yields overall satisfying performance for steady-state cornering. Consequently transient cornering and additional slip input is treated in the subsequent chapters.

21 Transient Cornering

Transient cornering for path tracking means that the vehicle has to follow a change in desired curvature from one constant value to another. Especially for collision avoidance manoeuvres this change needs to be as quick as possible. Therefore the task of path tracking in evasive manoeuvring boils down to the curvature rate, that can be achieved by the vehicle. For constant total velocity this is $\dot{\rho}_{des} = \dot{r}/v$. As shown in Chapter 9.2, for the linear bicycle model, additional wheel slip input adds yaw moment and therefore improves curvature response. To accomplish this for the fully nonlinear model, feedforward control was added, which would compensate for the $\dot{\rho}_{des}$ disturbance term in Equation 16.18.

21.1 Wheel Slip Controller

As the steering controller can minimize offset error in steady-state conditions, there is no need for feedforward slip input when cornering in steady-state with constant road curvature. It is rather required to use wheel slip inputs for transient sections in order to track curvatures accurately. The required yaw moment for a certain velocity can be obtained dependent on $\dot{\rho}_{des}$.

$$M_{Z,des} = \frac{I_Z}{v_{tot}} \dot{\rho}_{des} \tag{21.1}$$

The actual yaw moment of the vehicle can be determined using the tire forces according to Equation 13.7.

$$M_Z = (F_{y,fl} + F_{y,fr})l_f - (F_{y,rl} + F_{y,rr})l_r \tag{21.2}$$

The lack of actual yaw moment with respect to desired yaw moment has to be compensated via feedforward slip inputs. Since only differential braking is considered, there will be only negative slip inputs on the corresponding inner wheels with respect to turning direction. These inner wheels have to generate a certain amount of longitudinal force $F_{x,in,FF}$

$$\Delta M_Z = M_{Z,des} - M_Z \tag{21.3}$$

$$= F_{x,in,FF} l_t \tag{21.4}$$

where

$$F_{x,in,FF} = \begin{cases} F_{x,fl,FF} + F_{x,rl,FF}, & \dot{\rho}_{des} \geq 0 \\ F_{x,fr,FF} + F_{x,rr,FF}, & \dot{\rho}_{des} < 0 \end{cases} \tag{21.5}$$

As a measure to distribute the input between front and rear inner wheels load transfer is taken into account and the input is put proportional to the tire load. This is to avoid that one of the tires gets overly saturated.

$$F_{x,f,in,FF} = F_{x,in,FF} \frac{F_{z,f,in}}{F_{z,f,in} + F_{z,r,in}} \tag{21.6}$$

$$F_{x,r,in,FF} = F_{x,in,FF} \frac{F_{z,r,in}}{F_{z,f,in} + F_{z,r,in}} \tag{21.7}$$

Then the slip inputs are obtained,

$$\lambda_{f,in,FF} = \frac{F_{x,f,in,FF}}{C_{\lambda,f,in}} \tag{21.8}$$

$$\lambda_{r,in,FF} = \frac{F_{x,r,in,FF}}{C_{\lambda,r,in}} \tag{21.9}$$

where the longitudinal stiffness is obtained using $F_{x,i}$ from the tire model and λ_i as well as δ from the plant inputs. The concept of factorized stiffness, as described in Chapter 19.2 for lateral cornering stiffness, is applied here for obtaining longitudinal tire stiffness respectively.

$$C_{\lambda,fl} = \frac{F_{x,fl}\cos\delta}{\lambda_{fl}} \qquad C_{\lambda,fr} = \frac{F_{x,fr}\cos\delta}{\lambda_{fr}} \tag{21.10}$$

$$C_{\lambda,rl} = \frac{F_{x,rl}}{\lambda_{rl}} \qquad C_{\lambda,rr} = \frac{F_{x,rr}}{\lambda_{rr}} \tag{21.11}$$

In the case of $\lambda_i = 0$, the linearized longitudinal tire stiffness from the i-th tire is substituted. Furthermore, via the combined slip relation, too large longitudinal slip would compromise lateral performance. Therefore a saturation of the slip inputs is implemented to avoid excessive longitudinal slip.

21.2 Curvature Tracking

Tracking a step like input in curvature for the controller is investigated first. The feedforward slip input only adds when $\dot{\rho}_{des} \neq 0$, which means only one sample in terms of a step input. To account for that, and better show the influence of the feedforward controller, the step input would be stretched over 0.1 seconds. The desired value was chosen to achieve a certain steady-state cornering acceleration when tracking the curvature perfectly, see Table 21.1.

Table 21.1: Testcases for curvature response, curvature values in [rad/m]

$\frac{a_{tot}}{g}$	**10m/s**	**20m/s**	**30m/s**
$\approx$ **0.2**	0.0200	0.0050	0.0022
$\approx$ **0.5**	0.0500	0.0120	0.0055
$\approx$ **0.8**	0.0750	0.0200	0.0090

The input for $0.2g$ represents rather normal driving in highway conditions. The cases for $0.5g$ and $0.8g$ represent cases, which rather do not appear under normal driving conditions. They rather occur in collision avoidance scenarios. Figure 21.1 shows the responses in curvature. Only e_ρ is penalized. Different controllers are compared:

- Steering feedback input: δ_{FB}
- Steering feedback and feedforward input: $\delta_{FB} + \delta_{FF}$
- Steering feedback and feedforward input together with wheel slip feedback input: $\delta_{FB} + \delta_{FF} + \lambda_{FB}$
- Steering feedback and feedforward input together with wheel slip feedback and feedforward input: $\delta_{FB} + \delta_{FF} + \lambda_{FB} + \lambda_{FF}$

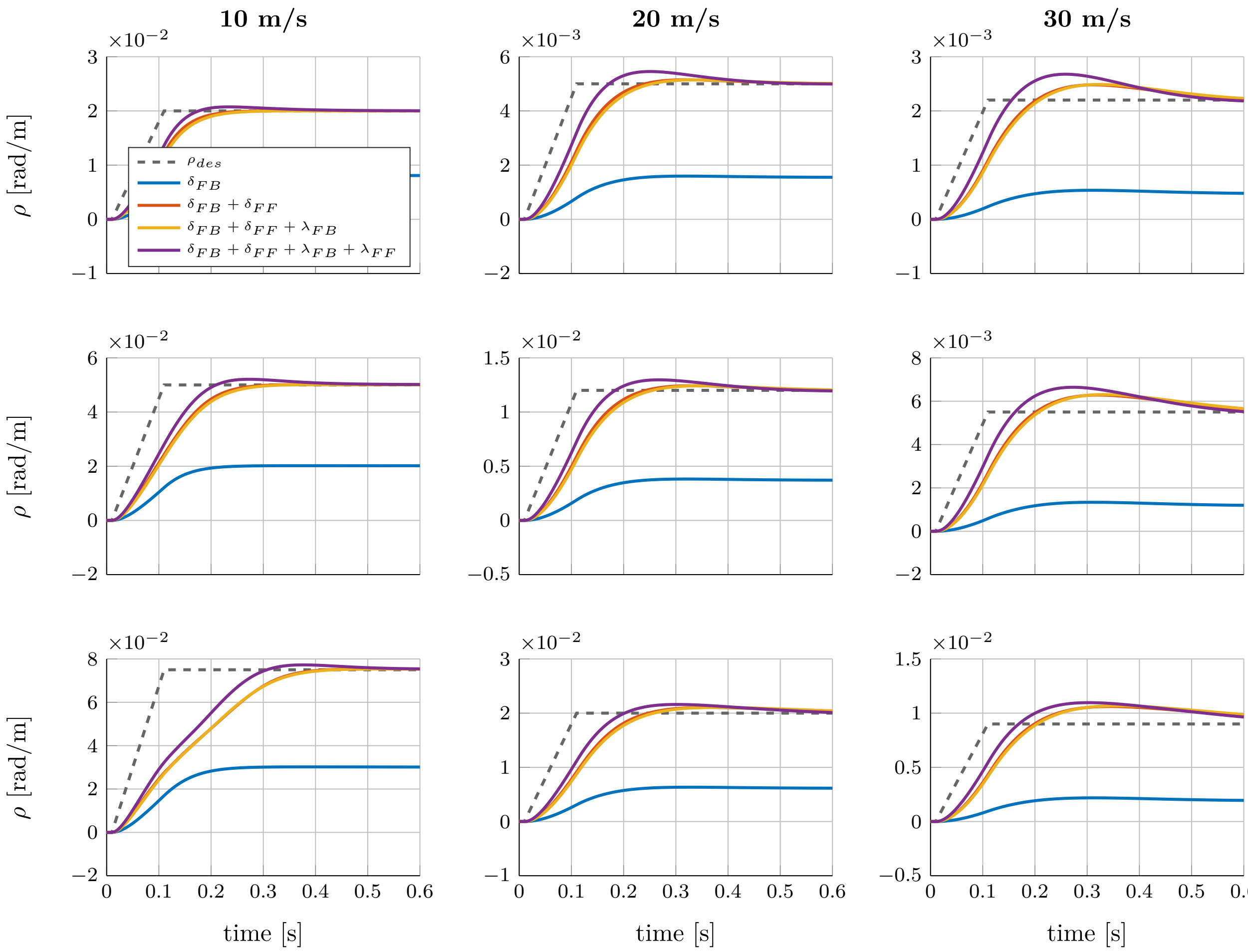

Figure 21.1: *Controller curvature response for variation in speed and cornering acceleration*

The data shows that using feedforward steering input does not improve the initial curvature rate of the vehicle for low velocities. For greater velocities only feedback steering input yields a poor response in comparison. However this is due to the fact that the total steering input is low and brings the vehicle in a different steady-state equilibrium with smaller curvature. Furthermore it can be seen that feedback slip input does achieve no significant improvement in the response. However, when also adding the feedforward term of wheel slips, then a larger initial curvature rate can be achieved for all cases. The rise time is shortened. This proofs the results from the step response investigation for the open loop bicycle model as discussed in Chapter 9.3.

21.3 Path Tracking

Path tracking performance is to be assessed. In the first place, just changing from one cornering equilibrium to another one should be tested. Any more complex path can be assembled out of sequences of different cornering equilibria with transitions inbetween, as discussed in Chapter 9.2. The transition should be linear, as in Figure 21.2. This guarantees a linear change in feedforward steering input without oscillations when travelling along the path [Kri12]. Three initial controller setups are chosen to compete with each other in path tracking performance:

- LQR controller with only steering input as a benchmark (see Chapter 18),
- SDRE controller with only steering input and
- SDRE controller with steering input and wheel slip input.

A single linear change in curvature from one cornering equilibrium to another is tested first. Furthermore, the controller setup is altered in order to investigate the influence of the different error states. Afterwards, also a lane change manoeuvre is investigated, which consists of two equilibrium changes in a row, and represents a relevant scenario for collision avoidance.

21.3.1 Single Linear Transition

A basic path setup was chosen, as can be seen in Figure 21.2, where the initial equilibrium has zero curvature representing straight line driving. The second equilibrium is set for a cornering acceleration of 0.86 g which represents 95% of the maximum capabilities of the Prius according to the handling diagram, see Figure 19.3. The transition between the equilibria was chosen with a rate larger than could only be achieved via steering. This is done in order to invoke wheel slip inputs. This rate was set to be 0.86 g/s and therefore the Prius would be brought from straight line driving into limit handling condition within one second. The path setup can be seen in Figure 21.2. Respective controller setups are shown in Table 21.2.

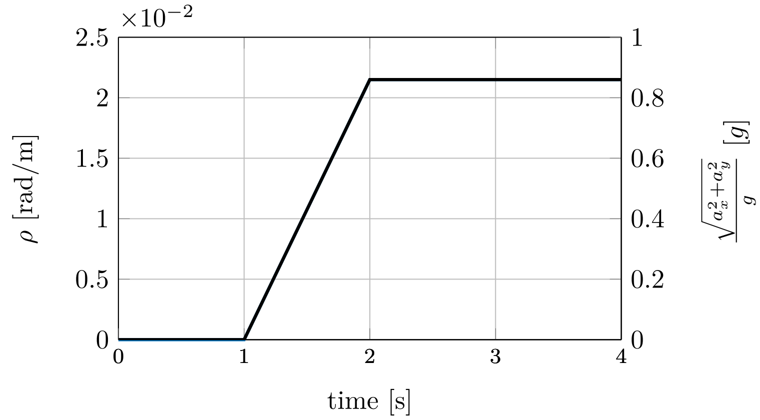

Figure 21.2: *Basic simulation path setup for constant speed of 20 m/s along the path*

Table 21.2: Initial Controller Setups

Setup	Lateral Controller	Penalized States	Actuators	FF δ-Controller	FF λ_i-Controller
1	LQR	e_{la}, e_ψ	δ	nonlinear	
2	SDRE	e_{la}, e_ψ	δ	nonlinear	
3	SDRE	e_{la}, e_ψ	δ, λ_i	nonlinear	x

Firstly, only lateral error e_{la} and heading error e_ψ are penalized. To compare the linear LQR controller with the nonlinear SDRE controller, $\mathbf{Q}$ and $\mathbf{R}$ were tuned in order to provide equal gains for the unexcited systems. Gains for the respective states can be seen in Figure 21.3.

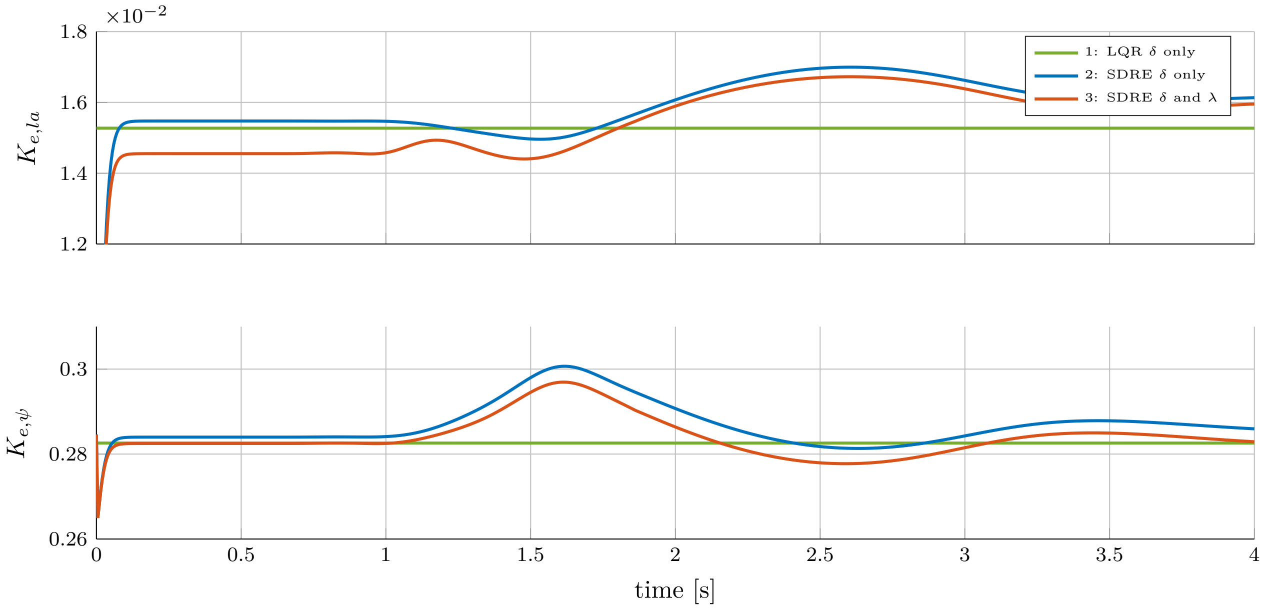

Figure 21.3: *Gains for the penalized states of the basic path tracking experiment*

The gains for the nonlinear controller change over time, dependent on the vehicle states. This shows the advantage of the nonlinear controller, and in Figure 21.4 can be seen, that in fact the LQR controller shows the largest lateral error e_y. All setups achieve the same steady-state offset for the second equilibrium. This is due to the fact that identical feedforward steering terms are used for all setups.

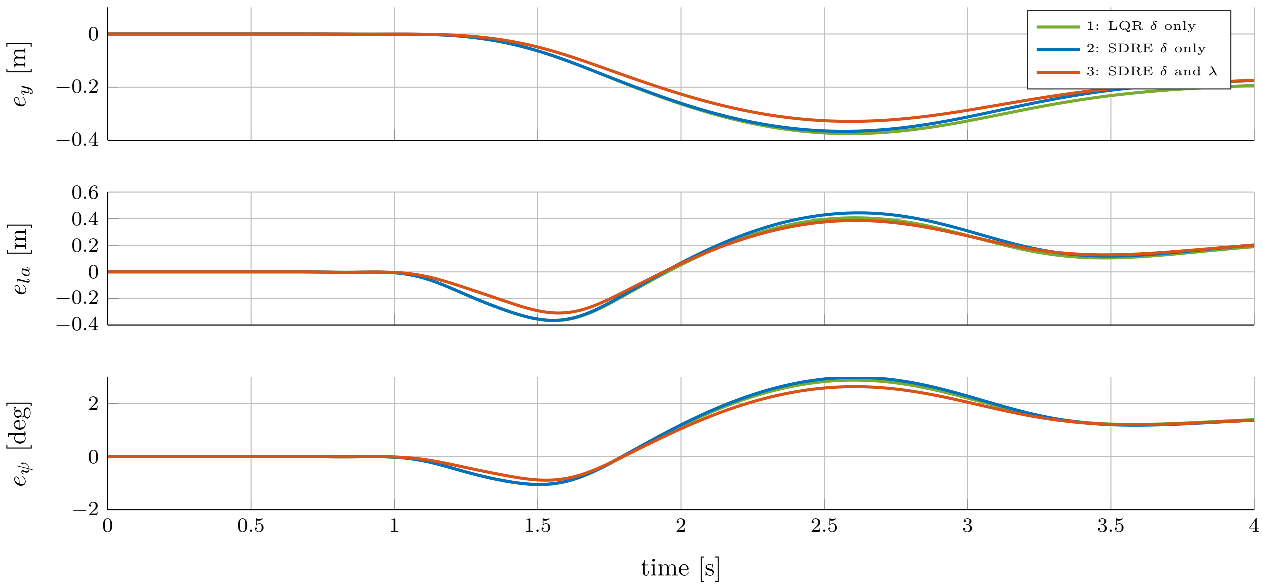

Figure 21.4: *Errors for the basic path tracking experiment*

Finally, the best performance is obtained with the nonlinear controller and using all inputs. Due to the feedforward wheel slip inputs, additional yaw moment is accessed. This allows to track the path curvature even better. In this particular experiment, use of differential braking reduces the maximum absolute error by 9%. In the following simulation the use of curvature error e_ρ in the controller is investigated. Therefore only the nonlinear controller is used with respective setups, see Table 21.3.

For Setup 4 only the heading error e_{la} is penalized. For Setup 5 also heading error e_ψ is penalized, and expected to add additional damping and path tracking performance. With Setup 6 the benefit of also penalizing the

Table 21.3: Controller Setups for test of curvature error e_ρ

Setup	Lateral Controller	Penalized States	Actuators	FF δ-Controller	FF λ_i-Controller
4	SDRE	e_{la}	δ, λ_i	nonlinear	x
5	SDRE	e_{la}, e_ψ	δ, λ_i	nonlinear	x
6	SDRE	e_{la}, e_ψ, e_ρ	δ, λ_i	nonlinear	x
7	SDRE	e_{la}, e_ρ	δ, λ_i	nonlinear	x

curvature error e_ρ is investigated. The latter one however has a similar effect as the heading error, as it determines where the vehicle is going to be in the future and if it will deviate from the path. Therefore with Setup 7 it should be investigated if the curvature state can substitute the functionality of the heading error. The results can be seen in Figure 21.5.

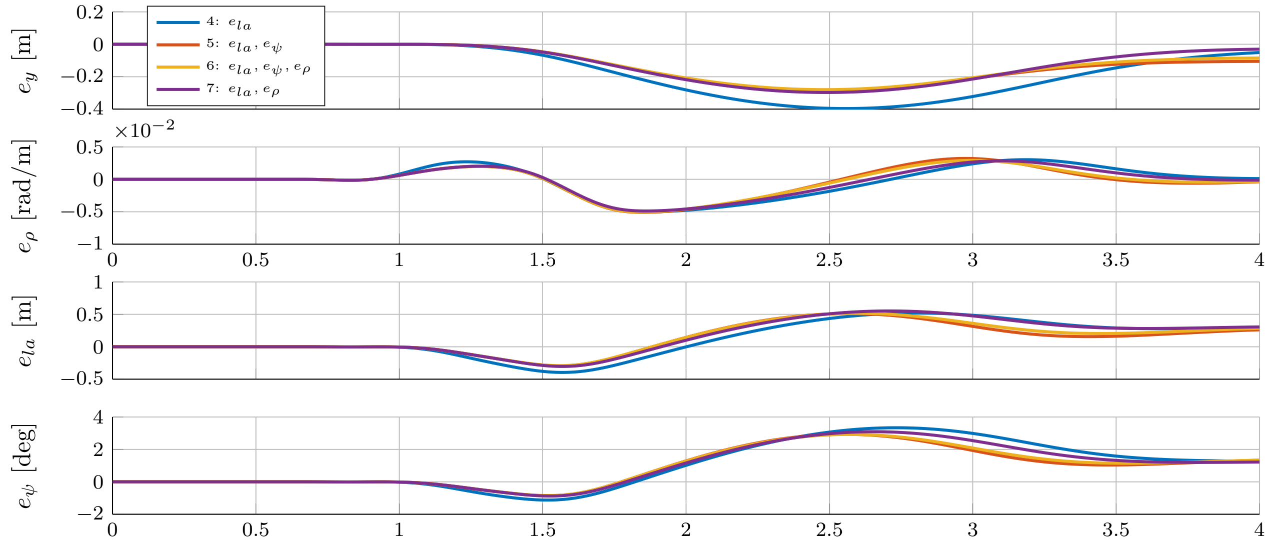

Figure 21.5: *Errors for the basic path tracking experiment*

Looking at the lateral offset e_y, it can be seen that Setup 4 yields the poorest path tracking performance in comparison. Taking into account the heading error as well for Setup 5 yields the expected performance improvement. Also taking into account curvature error in terms of Setup 6, yields further improvement, which is rather marginal however. When increasing the gain for the look-ahead error slightly, then the combination of e_{la} and e_ψ in Setup 7 can achieve up to the same performance as Setup 5, see the respective gains in Figure 21.6.

The results show, that the curvature error can possibly substitute the functionality of the heading error. This has to be tested in practical application as well however. For further simulation it was chosen to make use of all three error states.

21.3.2 Lane Change

As a practically relevant example, a lane change manoeuvre was chosen to demonstrate the effect of the controller. The path was defined in order that it could represent an evasive collision avoidance manoeuvre for a vehicle travelling with 20 m/s. The lane change has an offset of approximately four meters and extends over a distance of about thirty meters. For a vehicle travelling with 20 m/s that means the avoidance manoeuvre takes place over a time frame of about 1.5 seconds. The path together with the curvature profile and heading profile can be seen in Figure 21.7.

Furthermore, there is straight pieces of path added ahead of the lane change and proceeding the lane change. In the simulation the manoeuvre therefore starts after one second of straight line driving. The curvature profile

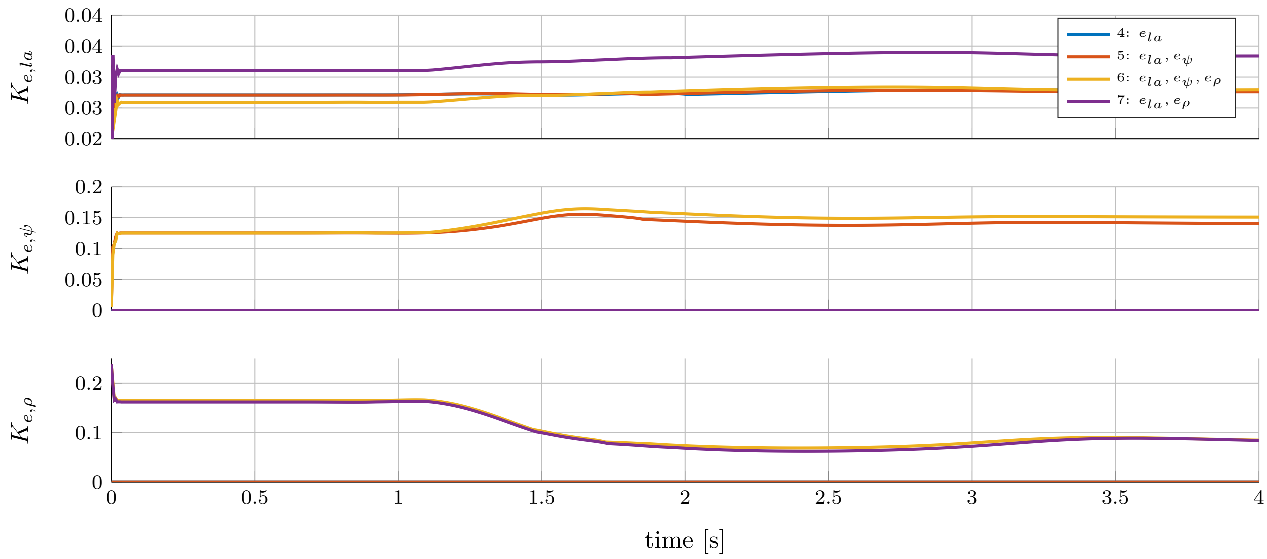

Figure 21.6: *Gains for the penalized states of the basic path tracking experiment*

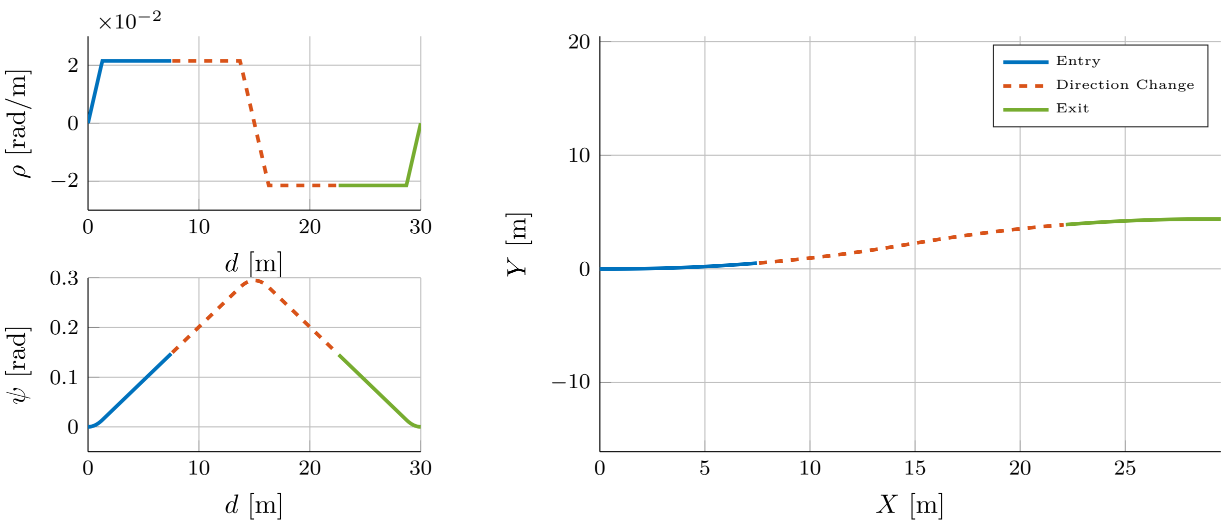

Figure 21.7: *Lane change path*

starts with a steep linear transition up to the maximum curvature. The latter one again is chosen that the Prius reaches up to 95 % of its friction limit. Then, the direction change is again resembled by a linear transition and subsequent the minimum curvature is reached before the lane change exit occurs. The setup with and without wheel slip inputs are compared for this path, see Table 21.4.

Table 21.4: Initial Controller Setups

Setup	**Lateral Controller**	**Penalized States**	**Actuators**	**FF δ-Controller**	**FF λ_i-Controller**
8	SDRE	e_{la}, e_ψ, e_ρ	δ	nonlinear	
9	SDRE	e_{la}, e_ψ, e_ρ	δ, λ_i	nonlinear	x

The actual trajectory achieved in the simulation can be seen in Figure 21.8.

Evolution of the vehicle states is shown in Figure 21.9. The excitation in lateral velocity remains smaller with the controller of Setup 9, meaning the motion is more stable.

Evolution of the errors is shown in Figure 21.10. It can be seen that when entering the lane change to the left, the lateral error e_y remains small and below 0.2 metres. The acceleration, as can be seen in Figure 21.11, rises

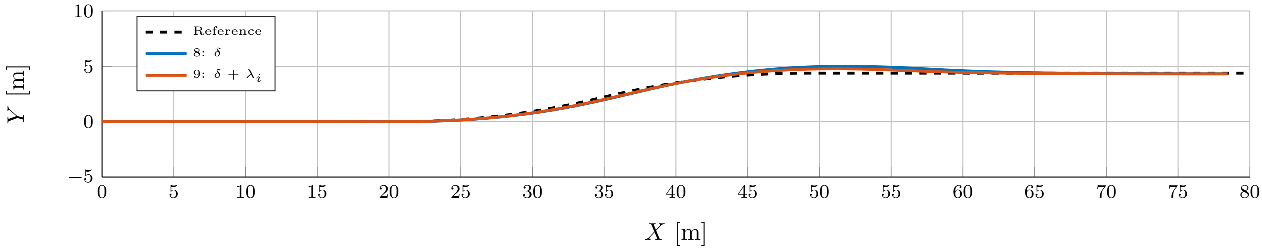

Figure 21.8: *Globale position during lanechange manoeuvre*

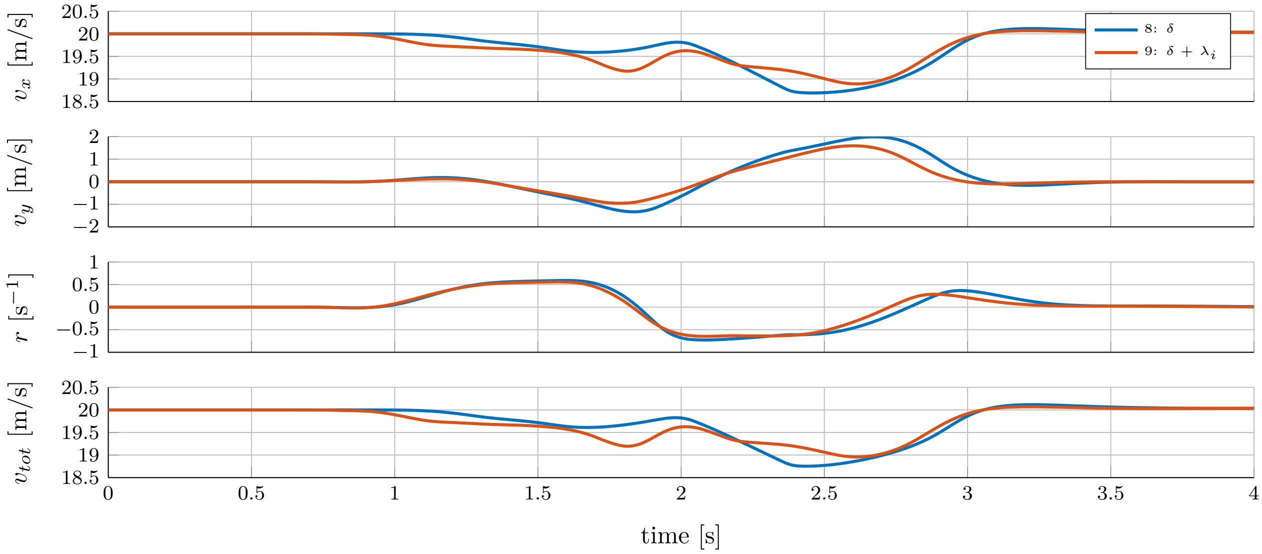

Figure 21.9: *Vehicle state during lanechange manoeuvre*

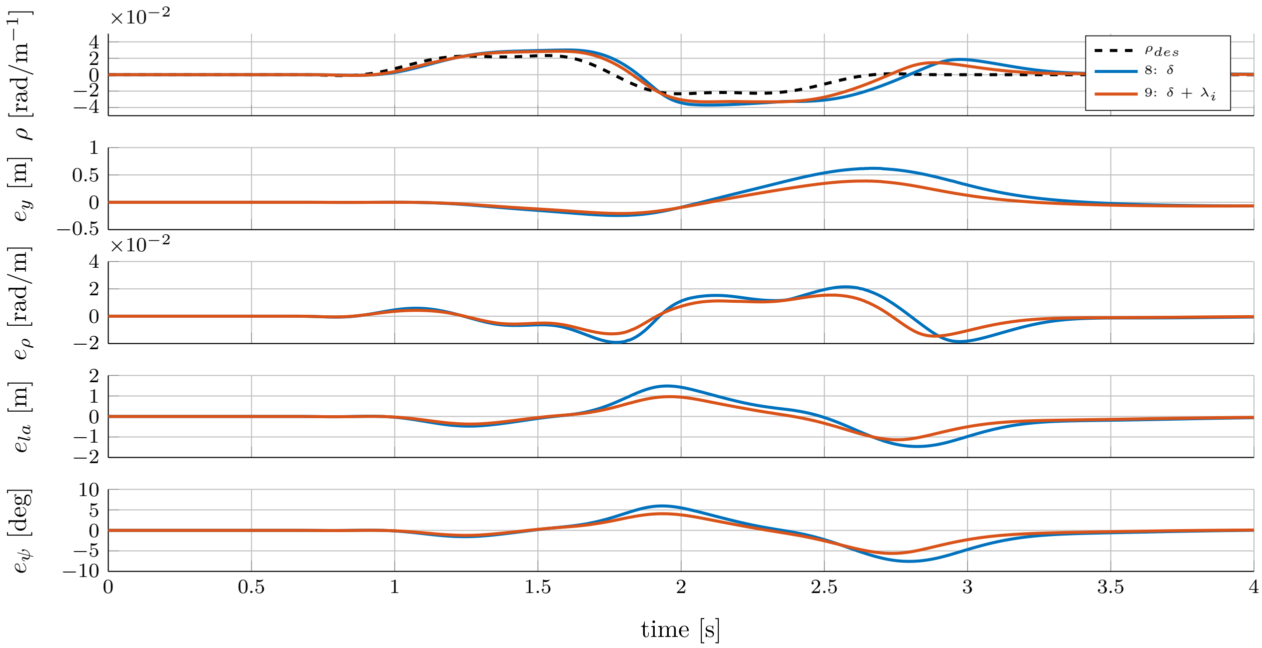

Figure 21.10: *Error state during lanechange manoeuvre*

up to almost one g and therefore reaching the ultimate friction limits of the Prius, at about 1.5 seconds. At this situation the reference path requires to decrease yawing motion again, and ultimately a change towards

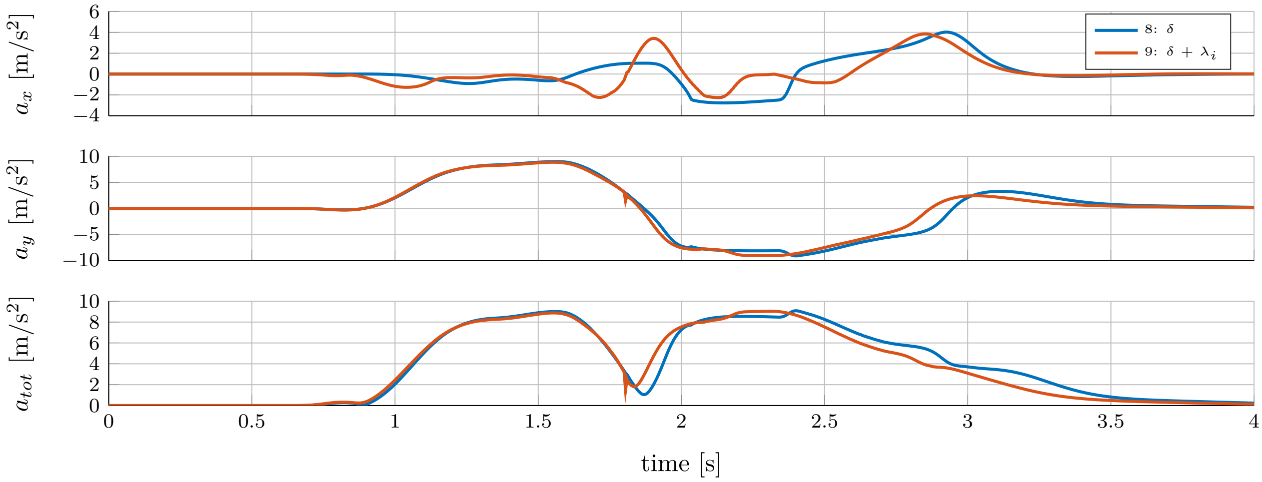

Figure 21.11: *Acceleration during lanechange manoeuvre*

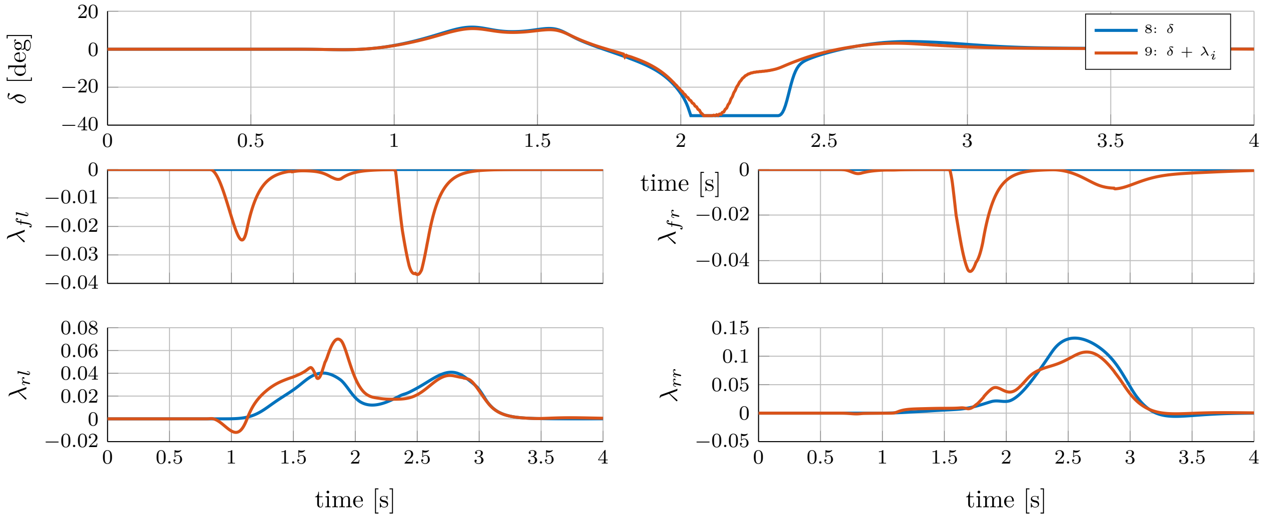

Figure 21.12: *Actuator inputs during lanechange manoeuvre*

negative curvature. With the tires close to saturation the required buildup in negative yaw moment proceeds slow. This yields overshoot towards the left side of the path which is about two times as large as the overshoot before. In this particular scenario the slip input can reduce the maximum lateral error by approximately 50 percent. Also does the vehicle remain stable and the course of cornering acceleration remains smooth, with both setups.

Figure 21.12 shows the actuator inputs. To be noted is that the relatively large amount of rear wheel slip throughout the whole experiment originates from the cruise controller applied to the rear wheels. The front wheel slip input clearly indicates the effort, which the wheel slip controller is making to improve yaw response. For the left front wheel a peak appears at one second, where the vehicle has to turn to the left. After that the vehicle has to change direction and the corresponding slip input on the front right wheel can be seen at around 1.75 seconds. At the end of the manoeuvre the yawing motion has to be stopped to bring the vehicle in constant heading again. The respective slip input appears in the left front wheel at 2.5 seconds. Of relevance is also that due to the slip input, less control in terms of steering is required as it can be seen from the graph. Without slip input the steering input remains for 0.35 seconds within the mechanical limit stop of -35 degree. However, the simulation shows that the controller can reliably track a single lane change up close to the friction limits, whereas slip input even improves path tracking performance.

21.4 Parametric Robustness

The performance of the model based controller is largely dependent on model accuracy. In reality however the controller has no access to absolute accurate information of model parameters. Therefore it should be tested in terms of robustness against parameter variation. Three prominent examples are chosen: vehicle mass, tire-road friction and tire-model correspondence [AJJ16].

Vehicle mass varies for instance with fuel fill level and even more drastically with number of passengers or amount of cargo in the vehicle. Furthermore an accurate real-time estimation of vehicle mass is costly. For the simulation vehicle mass and inertia inside the plant were increased by 10% and parameters inside the controller kept the same. The above used lane change manoeuvre is used here as well with controller Setup 9. The evolution of the errors can be seen in Figure 21.13. The path tracking performance decreases only slightly and the system remains stable, giving the indication of the controller to be rather insensitive to changes in vehicle mass.

In terms of variation in road friction a simulation is done where the plant shows lower friction than by the controller anticipated. In real application this could happen if sudden friction change appears due to change in road surface for instance. Furthermore accurate and quick friction estimation is difficult. Therefore the state of road friction is always afflicted by inaccuracy and uncertainty as input of the controller. For the simulation friction in the plant is lowered by 10%. The error states of the experiment can be seen in Figure 21.13.

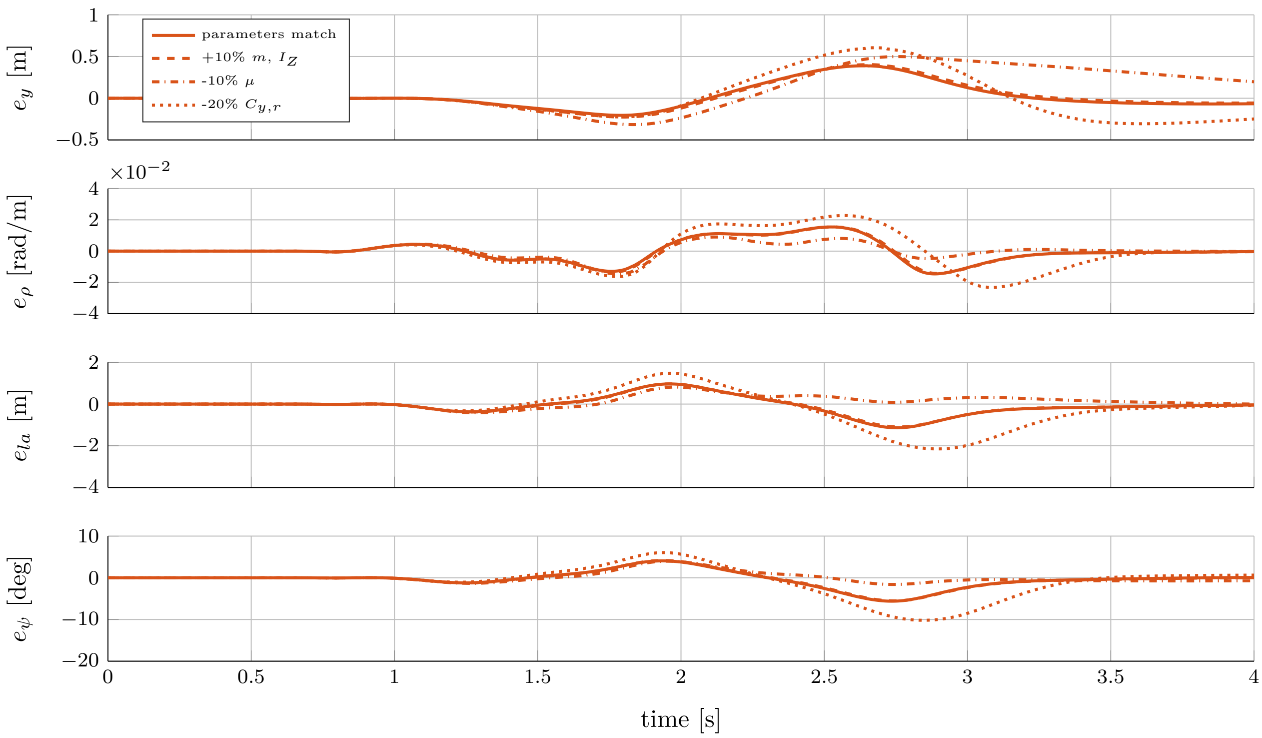

Figure 21.13: *Errors during lane change manoeuvre for plant parameter variation*

Path tracking performance drops significantly and an approximately 18% larger maximum lateral offset e_y is the result. Since the desired lane change path is intended for the expected tire road friction limit, the drop in friction experienced by the plant essentially yields an unachievable path. Therefore the errors grow significantly showing how sensitive the vehicle dynamics are to friction change when operating at the limits of handling.

Correspondence between tire model and plant is never fully given. This is due to the fact that even an experimentally well matched tire model does not account for changes in environmental conditions during operation and operational conditions of the tire itself. Examples are tire temperature, tire wear and inflation pressure. In worst case scenario the controller tire model can be far off with tire lateral stiffness value for instance which is a vital parameter to achieve reasonable lateral control performance. Therefore the controller was also tested with a change in rear tire lateral stiffness by minus 20%. This essentially represents a vehicle with smaller understeering gradient. Results can be seen in Figure 21.13 showing the largest lateral error. Especially from the large heading error can be seen that significant yawing oscillation occurs, but stability remains however.

22 Body Sideslip Control

In the previous chapters of this report the focus lies on minimizing path tracking errors e_ρ, e_{la} and e_ψ, for steady-state and transient cornering whilst the vehicle is operated close to the friction limits. Therefore steering was controlled in a way, that the yaw rate changes accordingly for minimizing path tracking errors. The body sideslip is only inherited through the dynamics of the system. But for certain conditions it can be beneficial to control body sideslip, as discussed in the literature study in Chapter 8. Exploring the possibility of controlling body sideslip on top of the existent path tracking controller is the purpose of this chapter. Therefore simulation based investigation on the nonlinear bicycle model is done, and a simple way of controlling the vehicle states is described. Furthermore, any investigation from now on is done on behalf of the BMW parameters, see also Appendix B, as it is used for experimentation later.

22.1 Equilibria Investigation

In Chapter 8 it was discussed, that there exist certain equilibria in the $\beta - r$ plane for the nonlinear bicycle model. In Figure 8.1 one open loop stable equilibrium and two open loop unstable equilibria are depicted. This representation is somewhat misleading however. Basically the shape of front and rear, pure lateral slip, tire curves decide over the location and existence of these equilibria. But for sustaining large body sideslip in a manoeuvre, rear wheel drive torque is substantial to overcome the slowing of the vehicle. And the resulting longitudinal slip in the rear tires yields significant change in the lateral force response due to the combined slip tire behaviour. This means, the shape of the rear lateral tire curve changes in a sense that the cornering stiffness drops as well as the maximum lateral force. The result in terms of the bicycle model would be an oversteering vehicle with $K_{US} < 0$, which does inherit neither stable nor unstable open loop equilibria.

Looking at the problem from a controllability point of view can give further insight. Figure 22.1 shows how the stable cornering equilibria for the BMW change dependent on steering input within the state space. Greyed out in the background are the open loop state trajectories for zero steering input given as a reference.

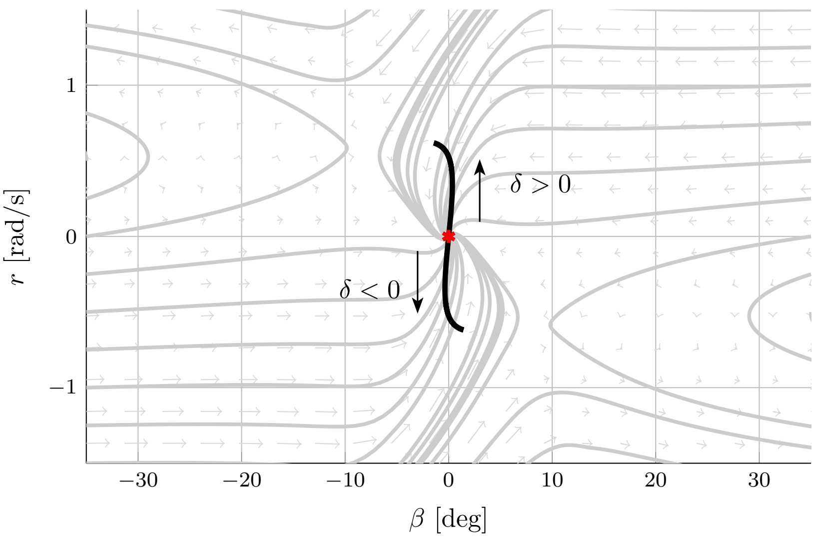

Figure 22.1: *Open loop stable equilibria of the bicycle model for ranging steering input, greyed out state trajectories for the model with zero degree steering input are given as reference*

It can be seen that steering has major control authority on yaw rate and brings an inherited, marginal body sideslip. The system is not fully controllable, but for normal cornering steering input as it changes front axle lateral force is sufficient to negotiate the vehicle. In order to get control authority over body sideslip as well, an additional actuator must be considered, that can change the rear lateral force. Eventually that is precisely what can be achieved with longitudinal slip input at the rear wheels. Through the combined slip tire behaviour, rear wheel slip lowers the cornering stiffness of the rear axle, and therefore reduces rear axle lateral force. Thus, this change in rear cornering stiffness gives control authority for body sideslip.

22.2 Feedback State Controller

Steering input exists and is determined from the path tracking controller. Furthermore, it is a function of rear axle cornering stiffness and therefore also of the body sideslip angle as demonstrated in Chapter 19.2. This means if the vehicle comes into induced oversteering, the steering controller applies counter steering in order to keep the path constraint and track the desired curvature. Thus, the steering input is considered as given. Therefore only rear wheel slip input λ needs to be computed to induce the right amount of oversteer in order to track a desired body sideslip β_{des}. Proportional feedback seems to be suited for this problem in the first place. Considering only lateral dynamics, the control error can be computed using the deviation between desired and actual body sideslip. The desired lateral velocity could be computed using the desired body sideslip.

$$v_{y,des} = \sqrt{v_x^2 + v_y^2} \sin \beta_{des} \tag{22.1}$$

However, also a yaw rate feedback should be added in order to assure that the yawing motion has the desired direction. The desired yaw rate can be computed from the path curvature.

$$r_{des} = \rho_{des} v_{tot} \tag{22.2}$$

The rear wheel slip control input can be computed.

$$\lambda_{FB} = (v_{y,des} - v_y)k_\beta + (r_{des} - r)k_r \tag{22.3}$$

When assuming the steering input to be fixed and known, coming from the path tracking controller, then this controller can be applied to the nonlinear two-degree-of-freedom bicycle model. The wheel slip input in that sense simply changes the cornering stiffness of the rear axle in order to control the body sideslip motion. Figure 22.2 shows a cloud of equilibrium points for which the controller was able to stabilize the nonlinear bicycle model with BMW parameters. The color bar indicates steering angles for the respective points. The aim was to stabilize the system with a desired positive yaw rate in order to simulate positive, left hand turning. Therefore an increased body sideslip means negative body sideslip angle and requires counter steering, respective more negative steering input. Steering was taken into account from -35 to 10 degree. As a reference also the open loop equilibria of the bicycle model with only steering are plotted in terms of a line.

The controller was tuned heuristically, with the aim to achieve a wide range of equilibria in the state space. So it is neither optimal nor complete, but still a couple of conclusions can be drawn from the result. Looking only at positive yaw rate, first of all, a wide range of equilibria is achievable, varying in both yaw rate and body sideslip. Amongst these are equilibria with very small body sideslip and yaw rate meaning that the tires operate in their linear (not saturated) region. For larger body sideslip it seems, that stabilizing the vehicle is only possible inside a smaller regime of yaw rate, as the number of equilibira is rather limited. For the understeering case, meaning a positive body sideslip angle, no equilibria appear. Only with making the vehicle more understeered, meaning reducing front axle cornering stiffness, this could theoretically be achieved.

The view given through the two-degree-of-freedom model is limited to the lateral dynamics. As the longitudinal dynamics come into play, not all off the obtained equilibria will be achievable in the end. Eventually, stabilizing a drifting vehicle means solving a three-degree-of-freedom system. So when computing slip input also the longitudinal dynamics must be regarded. Taking this into account in terms of the feedback controller, there should be the term $(v_{x,des} - v_x)k_v$ added to the input, where $v_{x,des}$ comes from Equation 17.3. Furthermore a feedforward slip input is required.

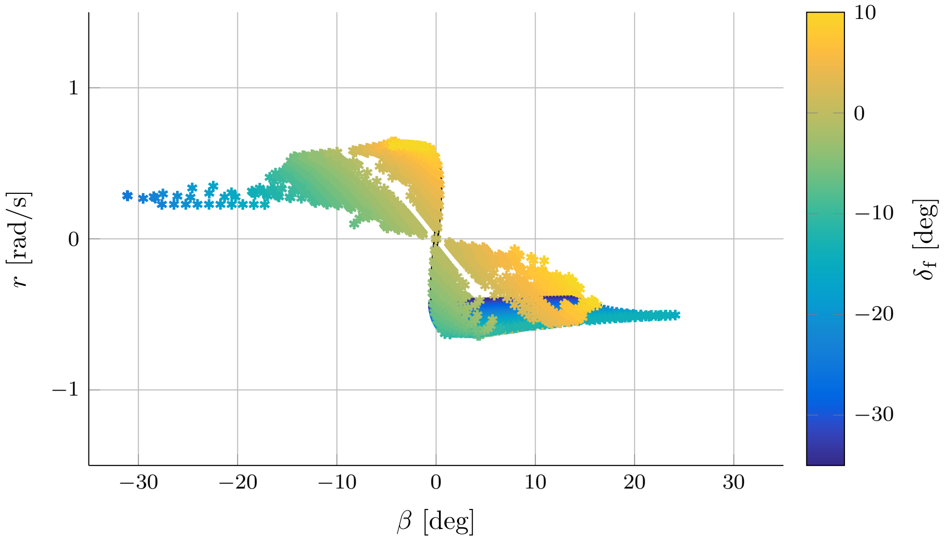

Figure 22.2: *Obatined closed loop equilibria for using the body sideslip controller within the nonlinear bicycle model*

22.3 Feedforward State Controller

The longitudinal dynamics of the nonlinear bicycle with rear wheel drive are given.

$$m\dot{v}_x = F_{x,r} - F_{y,f} \sin\delta + v_y r m \tag{22.4}$$

Substituting desired values from path tracking, desired body sideslip and $F_x = C_{\lambda,r}\lambda_{FF}$, the feedforward wheel slip input is obtained.

$$\lambda_{FF} = \frac{C_{y,f}(\delta_{ff} - \beta_{des} - l_f \frac{r_{des}}{v_{x,des}}) \sin\delta_{ff} + v_{y,des} r_{des} m}{C_{\lambda,r}} \tag{22.5}$$

The rear tire longitudinal stiffness $C_{\lambda,r}$ comes from Equation 21.11 and δ_{FF} comes from the path tracking feedforward controller.

Summarized can be said, that the body sideslip controller should be used additionally to the existing steering controller. In that sense there is a sort of task division between both controllers: the path tracking controller uses steering input to track a desired path and the body sideslip controller uses rear wheel slip input in order to control body sideslip. However the main key is, that the steering input is taken as parameter to the body sideslip controller. This circumvents the necessity to solve a nonlinear system of third order in real-time, since actually the steering input is a function of the slip input coming from the body sideslip controller itself. This simplification might influence the stability of the system especially for conditions with excessive body sideslip where longitudinal and lateral dynamics become heavily dependent on each other. Therefore the controller needs testing.

Part VI
Experiments and Results

The purpose was to test the steering controller for different scenarios.

1. In the first place it should be checked if the controller can track a path for the normal, understeering case of cornering. Focus is on minimizing the steady-state offset.
2. After that it should be checked if the steering controller can react accordingly in situations where the vehicle is brought into oversteering scenarios, as discussed in Chapter 19.2.
3. Finally the combined scenario of path tracking together with body sideslip control is to be tested, as it was discussed in Chapter 22.2.

The slip controller for transient conditions, as described in Chapter 21.1 is not considered for testing. Therefore, main attention in the experimental validation is paid to steady-state conditions and the influence of the slip input on these conditions. This limits the required actuators to steering and throttle. A rear wheel drive vehicle is required. Before the actual testing results are presented in this chapter, the experimental setup is described.

23 Experimental Setup

The first step was to make the model work on the real-time framework that TNO is using for experimental validation. Then, also a suitable test track and vehicle had to be chosen.

23.1 Real-time Implementation

The Riccati solver uses an iterative method to retreive the solution [Mad+12]. The number of iterations can be chosen, whereas an increase of numbers of iterations means convergence closer to the actual solution. Three iterations yield 80 percent accuracy and ten iterations yield a solution within 95 percent of the optimum [BMV10]. However increasing the amount of iterations also yields more computational load for the real-time hardware. The framework used at TNO consists of a dSpace AutoBox. Test runs were done in order to check if the SDC form containing six states and five actuators, as developed in Chapter 16 showed real-time feasibility. When using more then ten iterations real-time feasibility was not given. It was chosen to use five iterations for the experiments which leaves a reasonable safety margin in terms of processing capacity. Furthermore the state saturation, which was used to avoid singularity in the controller model, as described in Chapter 16.4, was tested. Therefore the model was run in the vehicle for low speed and it was checked if the solver still produced valid output.

23.2 Track

In order to spare tire and mechanical components of the testing vehicle, it was looked for a testing track equipped with a low friction surface. In that case required forces to achieve limit handling regime are much less and dynamic tests become slower. Also, smaller testing areal with less safety space next to the testing pad become applicable. The RDW Test Centre in Lelystad in the Netherlands was chosen, as it is equipped with a low friction skid pad of reasonable size. Figure 23.1 shows the skid pad test ground from top view.

The ground of the circular low friction pad consists of a polymer and appears white. Covered with water the friction with respect to vehicle tires appears to be approximately $\mu = 0.13$. The outer diameter of the pad is 38.5 metres and the inner 32.5 metres. This yields a track with of about six metres. The dashed line represents the path chosen for testing, starting at a tangential entrance and making a transition towards the steady-state

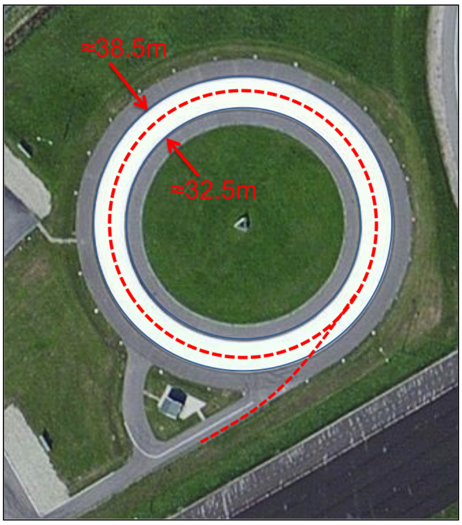

Figure 23.1: *Skid pad test ground at the RDW Test Centre in Lelystad (Netherlands), top view*

cornering on the pad, ending on the pad after one completed lap. The curvature profile of the path is equal to the one considered in Figure 9.2. However, for this test the focus lies on the steady-state cornering part. More information on the test track can be found in Appendix C.

23.3 Vehicle

A BMW 5 series, which was equipped by TNO as a vehicle dynamics testlab would be available for testing, see Figure 23.2. It could be equipped with a sophisticated steering robot allowing for precise steering input with a high bandwidth. A high precision GPS system could be used for path tracking feedback. Also vehicle state feedback was retrieved via the GPS system.

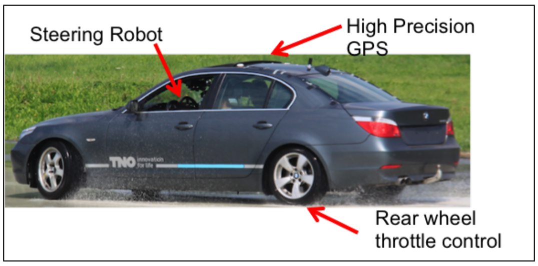

Figure 23.2: *BMW 5 test vehicle*

Most importantly the BMW possesses the rear wheel drive that makes it possible to be used for body sideslip control. However there is no traction or wheel slip control available in the car and also no wheel slip measurement. Therefore it is only possible to send a throttle setpoint to the engine control unit in order to control wheel torque and in turn regulate wheel slip. Throttle input is typically sent in percent. In this case the desired slip would be directly translated into throttle input. Vehicle parameters and testing setup is presented in Appendix B.1.

23.4 Testing Procedure and Parameter Estimation

The tests were conducted on 25.-26.08.2016. After arriving at the testsite and before starting the actual testruns, a few things had to be prepared. The GPS had to be setup in a sense that the local GPS antenna had to be positioned asides the track and connected with the car. In order to get an accurate GPS reference, random movement of the car with respect to the antenna is required for calibration. This was done by driving around the test areal for 10 minutes. After setting up the GPS and via following the outer and inner edge of the skid pad with low speed, the exact global coordinates of the test track could be retrieved. As well a self defined reference starting point and starting heading for the manoeuvres could be defined. With the respective loggings, the skid pad could be transformed into local reference with respect to the starting point and starting heading. Then a reference path was fitted to the data, it making a smooth transition from starting point into the circular pad. As a preparation, also braking manoeuvres on the test surface were undertaken and logged. Afterwards, offline friction estimates were obtained, for adaption of the friction parameter within the tire model, see Appendix C.2.

For the controller to receive path tracking error state feedback, the camera model was used, which was developed for the plant model, see Chapter 13.1. State feedback in terms of v_x, v_y and r, which is required by the camera model and also the controller, would be retrieved from the GPS system. A test run would always start from the origin with standstill. Then the test driver or the longitudinal controller respectively, would start and speed up to cornering speed within the transient phase, before entering the turn. The test run ends after maximum one lap on the pad is complete, then the test driver takes over control again and brings the car back to the origin. In between subsequent tests, controller gains and parameters could be adapted using ControlDesk software, without requiring recompilation of the model, which saved time.

Furthermore, since wheel slip feedback is not available, which is a required parameter for calculating tire forces in the controller model though, the desired wheel slip output of the controller would be used instead. This however is not accurate and introduces uncertainty within the tire model. Also an accurate tiremodel of the specific tires mounted to the BMW was not available. Instead a model for tires of similar type was used. Furthermore, in order to facilitate engaging into oversteering, degraded tires with less friction were mounted to the rear axle. Though for these tires no tire parameters were available. Consequently model uncertainty is introduced, which challenges controller robustness. Compliance in the front axle was modelled, altering the front tire cornering stiffness. After initial testing the friction inside the tiremodel was adapted to $\mu = 0.4$. This does not represent the actual friction limit measured, but yields minimized oscillatory steering control and is therefore preferable. In total, there are a few model inaccuracies related to the tire model which will affect the computation of cornering stiffness and therefore influence the control inputs. In the end, the results therefore will also give an indication on how sensitive the SDRE controller is to model inaccuracies.

23.5 Controller Setup

For the three different experiments the respective controller Setups can be found in Table 23.1

Table 23.1: Penalized states for the three chosen experiments

Setup	**Steering Controller (SDRE+FF)**	**State Controller via Throttle Input**
Path Control	$(v_{x,des} - v_x), e_{la}, e_\psi, e_\rho$	-
Driver Induced Oversteering	e_{la}, e_ψ, e_ρ	manual by driver
Combined Path and State Control	e_{la}, e_ψ, e_ρ	$(v_{x,des} - v_x), (v_{y,des} - v_y), (r_{des} - r)$

Desired speed is $v_{x,des} = \sqrt{v_{des}^2 - v_y^2}$, as explained in Chapter 17.2. Desired yaw rate is $r_{des} = \rho_{des}\sqrt{v_x^2 + v_y^2}$, as described in Chapter 22.2. Desired lateral velocity is $v_{y,des} = \sqrt{v_x^2 + v_y^2}\sin\beta_{des}$, as described in Chapter 22.2. Testing results for the three different setups is described in the subsequent chapters.

24 Path Control

With this experiment it should be shown if the steering controller is capable of tracking curvature with minimized lateral offset e_y, for cornering close to the friction limits. Figure 24.1 shows the position of the vehicle with respect to the desired path. Figure 24.2 shows states, errors and inputs of the experiment. Total cornering speed $v_{tot} \approx 6$ m/s and with a cornering radius of 35.5 metres yields a cornering acceleration of $0.1g$.

Considering the friction potential of about $\mu = 0.13$ of the skid pad, this means cornering at 77% of the friction limit.

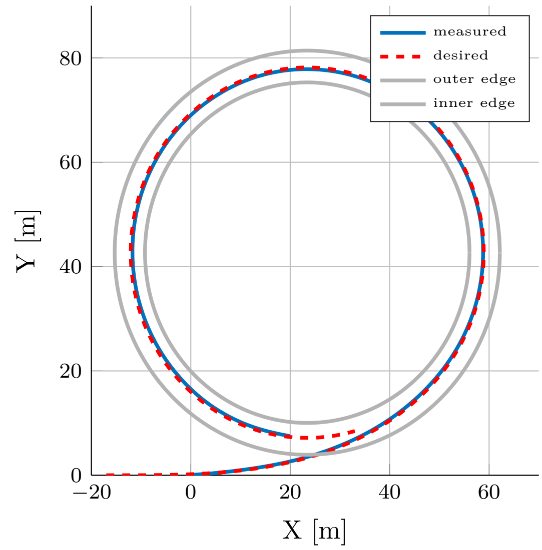

Figure 24.1: *Path Control Experiment Position*

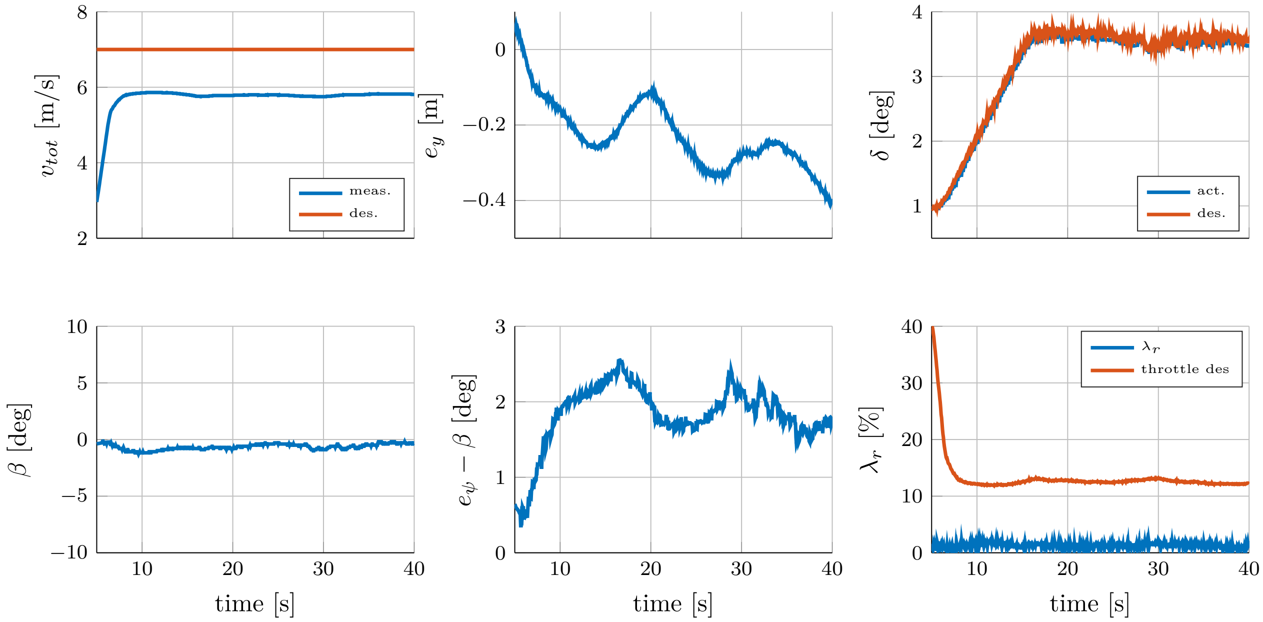

Figure 24.2: *Path Control Experiment States, Errors and Inputs*

Looking at the position of the vehicle with respect to the desired path, it is observed that it tracks the path rather accurately throughout the entire experiment. Looking at the path tracking errors of the experiment it can be seen that the deviation with respect to the path $|e_y|$ remains below 0.4 metres. Furthermore, heading error e_ψ incorporates body sideslip, due to the error definition, see Chapter 19. Thus, $e_\psi - \beta$ was plotted instead. This represents the heading of the velocity vector and it can be judged in which direction the vehicle moves with respect to the path. From the plot can be seen, that there is a steady-state offset in heading of about two degree, whereas a small oscillation with amplitude of one degree exists on top of that. Since the vehicle tracks the path without significant growing deviation, the heading error mean should be zero eventually. Therefore it can be concluded, that there exists a measurement offset in the system of about two degree. Steering input and throttle input remain smooth and steady throughout the experiment, showing a suitable tuning of the feedback gains.

The same experiment was also done with greater desired speed. This lead to spinning out of the vehicle shortly after entering the circle. As the speed approaches the maximum cornering speed given through the friction limit, small oscillation in slip input yield the rear tire lateral force potential drop and rear sideslip increases. The vehicle begins to spin and decrease in speed is penalized with increased slip input and the spinning motion gets even more amplified. This is a general drawback of rear wheel driven cars. In order to stop the runaway in sideslip, slip input would have to be decreased. This represents a case were body sideslip control should be applied in order to prevent the vehicle from spinning out. In fact it can be seen as a requirement for stabilizing an oversteering vehicle in path tracking scenarios with cornering close to the friction limits.

A steady-state offset in speed is prevailing throughout the experiment. It was concluded that this offset originates from non-modelled resistance effects that slow the vehicle. Such are rolling resistance of the tires, as well as inner resistance of the engine. The latter one means that a certain amount of throttle input is required in order to overcome the inner friction of the engine and drivetrain. Together, these effects can yield a steady-state offset in speed which is only controlled with feedback terms. Overall the experiment shows a positive performance of the controller. The achieved rather small lateral path tracking error originates from parameter uncertainties in terms of tire model.

25 Driver Induced Oversteering

In this experiment it should be tested if the steering controller can stabilize an oversteering vehicle, and at the same time retain path tracking constraint. Therefore the steering controller would be activated and the test driver manually pushes the vehicle towards oversteering, using throttle input. Figure 25.1 shows the position of the vehicle with respect to the desired path. Figure 25.2 shows states, errors and inputs of the experiment.

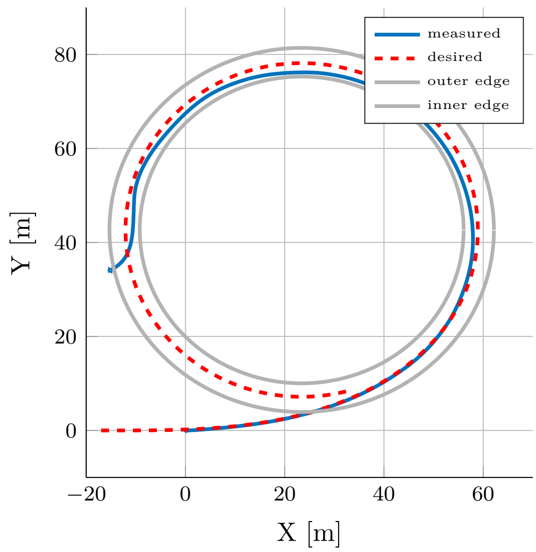

Figure 25.1: *Driver Induced Oversteering Experiment Position*

The vehicle position of the experiment gives a few indications. First of all, after the vehicle enters the circle, the driver starts to increase throttle input and the cornering happens within a different cornering equilibrium. This can be seen in terms of a larger offset with respect to the path. After three quarters of the circle, as the driver pushes the throttle further, the vehicle eventually spins out, see the kink in the graph. At this point the experiment is stopped. Task of the driver was to increase body sideslip gradually throughout the experiment. Looking at the evolution of body sideslip, this was managed well by the driver, as it shows an almost linear slope up to an absolute value of greater than 20 degree. Correlating to the body sideslip, also the lateral error $|e_y|$ increases up to two metres, meaning the vehicle negotiates a slightly sharper turn than intended. The reason for that lies within parameter uncertainties of the tire model. For significant slip angles on the

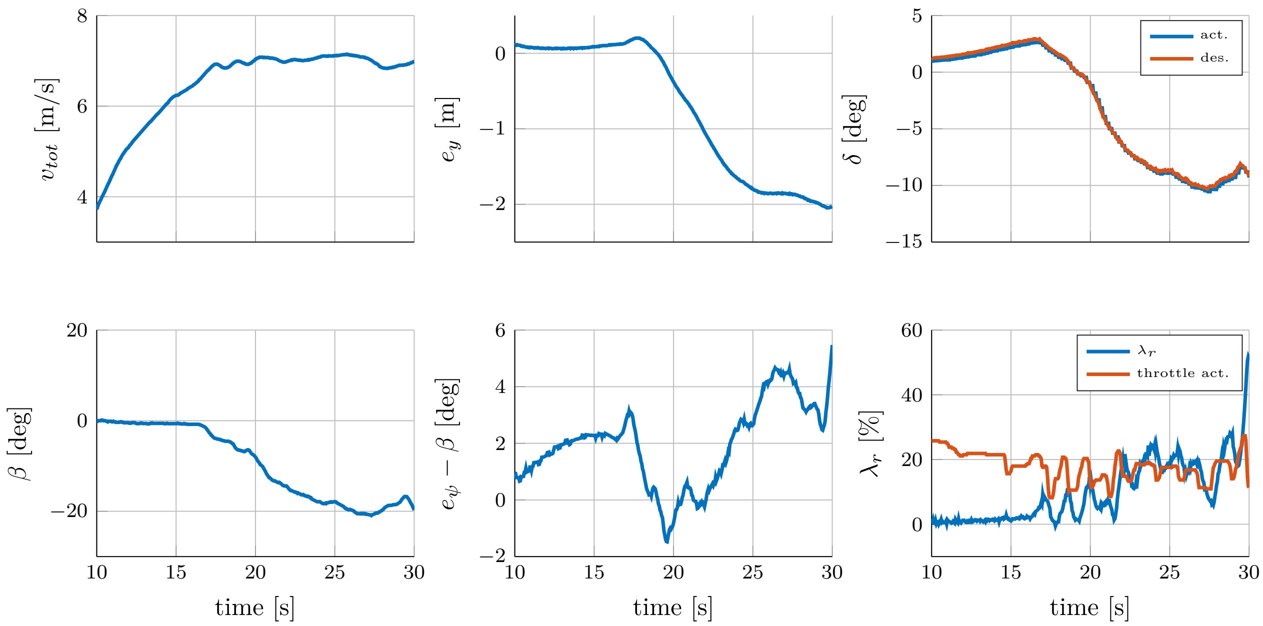

Figure 25.2: *Driver Induced Oversteering Experiment States, Errors and Inputs*

tires in the range of saturation, the modelled force response is not accurate any more. The heading e_ψ shows an oscillation within an amplitude of six degrees, set off by approximately 2 degree, as seen in the previous experiment. Looking at the steering input it can be observed that from the same time, as the body sideslip is increased, the steering input decreases gradually. At 19 seconds when the bodysideslip reaches approximately -7 degree, the steering input is zero. After that counter steering is applied, which allows further on for stabilizing the vehicle in an unstable cornering equilibrium up to an absolute body sideslip of 20 degree.

The throttle input gives notable insight into the manual control of such a manoeuvre. At about 15 seconds the vehicle enters the low friction pad. The driver increases throttle input and the buildup in sideslip is triggered. From then on the driver controls the sideslip with fine throttle oscillations between 10 and 20 percent. Whereas the absolute body sideslip increases strictly further up to 10 degree, no strict increasing throttle input is required. At this point, at around 22 seconds, the driver gives a rather significant throttle push, whilst body sideslip increases further and from now on the driver controls the throttle with corrections in notable smaller amplitude. At this point also the longitudinal slip λ_r makes a significant jump. It seems that force response characteristic changes within this range of body sideslip. From this it is assumed that for high body sideslip β and therefore also rear tire sideslip α_r, in the range of tire saturation, the control of body sideslip appears smoother with less feedback action. For larger sideslip the change in longitudinal slip λ_r has less impact on the lateral motion.

For further increase of absolute body sideslip beyond 25 degree, the steering input appears oscillatory and together with driver throttle inputs the system appeared unstable. Further controller tuning and better fitting of the tire model would be required. Though the experiment showed that the steering controller is capable of giving a smooth steering input and holding an oversteering vehicle close to the friction limits while retaining a path constraint. Moreover the achieved cornering velocity of seven meters per second means an achieved cornering acceleration of 0.14 g. This in fact even exceeds the measured friction limit of $\mu = 0.13$. Reaching this maximum in lateral grip was observed for a range of absolute body sideslip angle of 5 to 20 degree.

26 Combined Path and State Control

After validating the performance of the steering controller, also the body sideslip controller using throttle input should be tested. This would yield fully autonomous combined path and vehicle state control. The test runs were done in the sense that every run was started with the controller setup for path tracking, see Table 23.1.

After entering the low friction pad, the state controller would be engaged manually via the real-time Control Desk interface. At this moment, a step input in sideslip is given. In the experiment to be discussed here the step is -20 degree. Figure 25.1 shows the position of the vehicle with respect to the desired path. Figure 25.2 shows states, errors and inputs of the experiment.

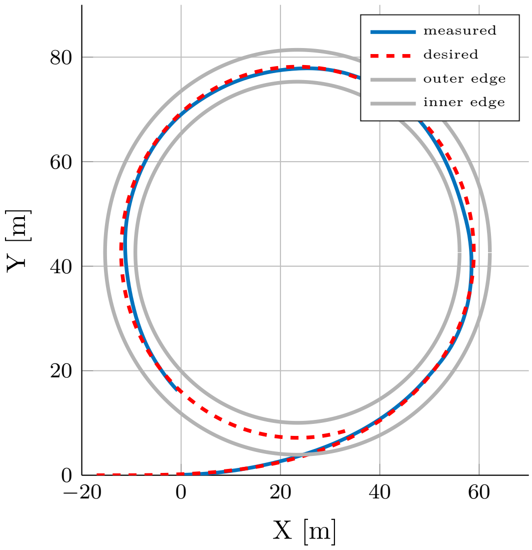

Figure 26.1: *Combined Path and State Control Experiment Position*

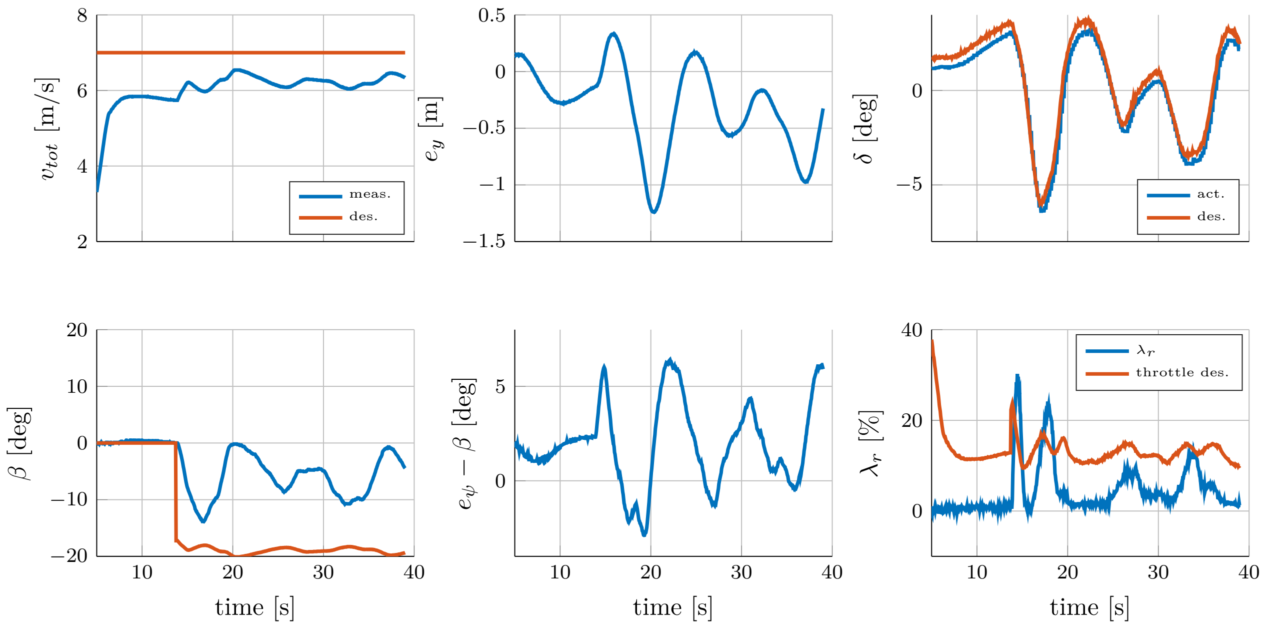

Figure 26.2: *Combined Path and State Control Experiment States, Errors and Inputs*

From the position of the vehicle, it can be seen that the path constraint is retained, as the whole circle is completed. A certain lateral oscillation prevails while the vehicle is brushing the reference path from the inside of it. Desired speed for the experiment is $v_{des} = 7$ m/s, whereas a steady-state offset can be observed which is comparable to the first experiment with path tracking only. Looking at the body sideslip it can be seen that the state controller attempts to follow the step input seen by a steep slope in sideslip. After reaching a maximum absolute value of 13 degree, the sideslip drops again, about three seconds after the step input. An oscillation in body sideslip follows ranging between maximum zero and minimum -11 degree. The lateral offset e_y mirrors this oscillation meaning that for increase in body sideslip the vehicle increases lateral offset and vice versa. It resembles the same behaviour as seen in the second experiment, where the driver pushes towards oversteering and the vehicle increases lateral offset. As the vehicle in that sense moves closer and further from the path, the heading, $e_{psi} - \beta$, shows the same trend.

Also the steering input shows the same trend as the body sideslip, as it corrects for the build-up in lateral error and heading error. However, as investigation shows the feedback weighting was chosen rather large and shows overcompensation yielding the relatively large oscillations in steering. This in turn also enforces oscillations in body sideslip. However, the presumably most relevant contributor to the oscillations in body sideslip becomes apparent when looking at the rear axle slip λ_r. The desired slip which is used as throttle input shows the desired increase, as the step input is applied. However for the wheel slip to react to the input takes 0.2 seconds. This time delay originates from the dynamics of engine and drivetrain and also results in reduced damping of the system. An overshoot in wheel slip up to 30% follows, which is above the desired value of about 25%. As a result the desired wheel slip is over-adjusted via the controller and the actual wheel slip drops back to almost zero, and is then increased rapidly again. This is the reason for the large oscillation in body sideslip at this moment. Following the trend of the wheel slip, it can be seen that there exists a steady-state offset between desired slip in terms of throttle input, and actual slip. Except when the desired wheel slip reaches a certain threshold of about 15 %, then the wheels start to spin rapidly and the offset is reduced rapidly. The offset is assumed also to cause the steady-state offset in body sideslip, that can be seen from the graph. This highly nonlinear relation between throttle input and wheel slip response is expected to be induced by the longitudinal force characteristic of the tire as well as the combustion engine dynamics whose torque response is not linear either. This result strongly calls for use of a slip controller in order to accurately regulate wheel slip.

Looking at the throttle input generated by the test driver for the second experiment in Figure 25.2, it gives an indication on how the throttle input should look like in order to control wheel slip more accurately. Furthermore, it appears that the step input in desired body sideslip is responsible for harsh wheel slip input and initiates the oscillation. Instead should a ramp input yield a smoother body sideslip response and faster damping out of transients. Looking back at the graph, in fact it can be seen that at the time of 25 seconds transients have reduced. This is due to the fact that wheel slip enters a stage where it appears less oscillatory, with maximum 13% and minimum 3% between 25 and 35 seconds. In this stage body sideslip ranges between -5 and -10 degree. This shows a sustained autonomous drift over a substantial time frame, when at the same time considering the path constraint of the vehicle. Giving the fact that there was no wheel slip controller available for the experiment and the controller was not tuned to the optimum yet, this is seen as a positive result.

27 Results

Summarized there is a few things that limited the performance in the experiments

1. **Wheel Slip Controller**
   A low level wheel slip controller would be required in order to track the desired wheel slip coming from the state controller.
2. **Tuning Steering Feedback**
   Too large gains in the SDRE feedback controller yield steering overcompensation as the vehicle increases lateral path tracking offset slightly due to increased sideslip.
3. **Ramp Input**
   A ramp input instead of step input for desired body sideslip reduces transient oscillations in body sideslip.
4. **Wheel Slip Feedback**
   Wheel slip feedback increases tire model accuracy within the SDRE controller and therefore improves feedback steering input.
5. **Parameter Estimation**
   Accurate parameter estimation for tire model and vehicle model improve feedback and feedforward input.

However testing showed promising results and proved the controller concept could work for the intended purpose in the scope of autonomous driving in general.

Part VII
Conclusion and Recommendation

28 Conclusion

The research problem is to track a desired path, whilst the tires operate in limit handling condition. The latter one means large tire sideslip essentially. In the scope of autonomous driving, large tire sideslip can occur in scenarios like an evasive lane change, where the vehicle has to avoid an unpredictable situation. In such a situation, a reference path will be represented in terms of a curvature profile. It was found suitable to assess the path tracking capabilities of a vehicle based on its actual curvature, which is the quotient of yaw rate and speed of the vehicle. In order to track evasive paths, the vehicle has to possess a good curvature response. An investigation on behalf of the bicycle model was done with different actuator setups. It could be concluded that differential wheel slip inputs show a comparable improvement in curvature response with rear wheel steering. Thus steering and differential wheel slip inputs (only negative, for braking) were considered as actuators for path tracking. Positive slip (driving torque) would be considered for controlling speed to keep the vehicle within the limit handling regime.

After choosing a suitable error definition, a feedback controller was developed using the State Dependent Riccati Equation technique. However feedforward steering input appeared to be necessary for minimizing steady-state errors, and account for body sideslip angle of the vehicle. Using nonlinear cornering stiffness obtained from a tire model in real-time, the path tracking controller was shown in simulation to reliably track steady-state curvatures up to the the friction limits, with lateral offset smaller 0.3 meters. Furthermore through taking the changes in cornering stiffness into account in real-time, the controller is capable of reacting to a drop in rear cornering stiffness. This means the controller applies counter steering in case of oversteering. The use of differential braking inputs for a lanechange manoeuvre could lower the maximum path tracking error by 33%.

Furthermore from simulation it became apparent that rear wheel driven or oversteering vehicles could not be stabilized at the limits of friction. This results from the longitudinal controller, as it does not possess any sideslip feedback. Therefore it does not reduce the throttle when sideslip begins to rise, indicating a spinning out of the vehicle. This reason and also the initial literature investigation suggests that body sideslip control can be beneficial in certain scenarios. Thus it was decided that further investigation into body sideslip control was necessary, and the scope of the project switched towards this direction in the remainder of the project.

Cornering equilibria of the nonlinear bicycle model were investigated. It was concluded that the phase portrait representations of the unstable drift equilibria are somewhat misleading, as they only result from the particular slip curve shape of the pure lateral slip tire model. In contrast, the combined slip tire behavior was added to the bicycle model. Combined with a simple proportional feedback controller this allows for stabilizing the bicycle in numerous equilibria of body sideslip angle and yaw rate. Amongst these are also closed loop equilibria within the linear range of the tire meaning small tire sideslips. A feedforward wheel slip term was added in order to produce the required amount of propulsion force for sustaining the drift. The SDRE steering controller and proportional body sideslip controller were implemented and tested in a BMW test vehicle and showed promising results.

Testing track was a low friction circular pad for steady-state cornering tests. The steering controller showed to stabilize the vehicle up to the friction limits and can also stabilize an oversteering vehicle via counter steering whilst still satisfying the path tracking constraint. This was shown up to an absolute body sideslip angle of 20 degree. For completely autonomous manoeuvres where also speed is controlled automatically, the body sideslip controller becomes necessary to stabilize an oversteering vehicle and prevent spinning out. In the control scheme the steering input would be used to reduce path tracking errors and the rear wheel slip input would be used to control body sideslip. This task separation was demonstrated to work well in experiment. During a path following task, the vehicle was able to autonomously engage into a drift and as well leave the drift, whilst at all times regard the path tracking constraint. This was shown for a slip angle of minus 7.5 degree and could be sustained for approximately ten seconds. The results proof that the control concept is working. Also considering that no actual wheel slip controller was available in the experiment and only the desired wheel slip would be used as throttle input, the result is promising.

29 Recommendation

The path following controller showed good performance. Therefore recommendations mainly originate from the testing of the body sideslip controller.

1. **Wheel Slip Controller**
   For future experiments a wheel slip controller should be used. So far only was the desired slip input used to control the throttle of the BMW. Data acquisition after testing showed that there was a much larger error between desired slip and actual slip than expected. This had negative influence on tracking body sideslip. The use of a wheel slip controller will therefore increase the control performance significantly.
2. **Desired Body Sideslip**
   So far a body sideslip controller was developed and the desired input was chosen randomly only for testing its functionality. The next step would be to make an investigation on which cornering equilibrium is actually desired for what condition. This goes together with finding the quantitative advantage of controlling body sideslip in transient manoeuvres. The desired scenario would be to have a body sideslip setpoint dependent on path curvature and rate in path curvature.
3. **Differential Braking**
   For the body sideslip controller rear wheel slip input was used only. Applying also differential braking input would give more authority over tracking a desired body sideslip. Especially for transient manoeuvres which appear in typical collision avoidance scenarios this would be relevant.
4. **SDRE Control**
   The body sideslip controller should be integrated within the SDRE framework in order to adapt the control input to the model nonlinearities.
5. **Modelling Drivetrain**
   Tests within this research were done on low friction surface. On surfaces with large friction such as dry asphalt the accelerations occuring will be much larger and therefore load transfer becomes significant. Due to different normal loads on the driven wheels, dynamics of the rear axle differential will have a great influence on wheel slip and must be regarded.

References

[09] *European status report on road safety: towards safer roads and healthier transport choices.* WHO Regional O ce for Europe. 2009.

[AJJ16] M. Alirezaei, S. Jansen, and J. Janssen. “Experimental evaluation of collision avoidance system using state dependent Riccati equation technique”. *IAVSD 2016.* 2016.

[Ali+13] M. Alirezaei et al. “Experimental Evaluation of Optimal Vehicle Dynamic Control based on the State Dependent Riccati Equation Technique”. *2013 American Control Conference (ACC).* June 2013, pp. 408–412.

[Ali15] M. Alirezaei. “Advanced Control Application for Automotive Active Safety Systems”. Lecture Notes, TU Delft. 2015.

[And+10] S. J. Anderson et al. An optimal-control-based framework for trajectory planning, threat assessment, and semi-autonomous control of passenger vehicles in hazard avoidance scenarios. *Int. J. Vehicle Autonomous Systems* **8**.2/3/4 (2010), 190–216.

[Ber95] D. P. Berstekas. *Dynamic Programming and Optimal Control.* Athena Scientific, 1995.

[BG13] C. G. Bobier and J. C. Gerdes. Staying within the nullcline boundary for vehicle envelope control using a sliding surface. *Vehicle System Dynamics* **51**.2 (Feb. 2013), 199–217.

[BMV10] B. Bonsen, R. Mansvelders, and E. Vermeer. “Integrated Vehicle Dynamics Control Using State Dependent Riccati Equations (SDRE)”. TNO Report. June 2010.

[CDM96] J. R. Cloutier, C. N. DSouza, and C. P. Mracek. “Nonlinear regulation and nonlinear H-infinity control via the state-dependent Riccati equation technique”. *International Conference on Nonlinear Problems in Aviation and Aerospace, 1 st, Daytona Beach, FL.* 1996, pp. 117–130.

[Clo+] J. R. Cloutier et al. “State-Dependent Riccati Equation Techniques: Theory and Applications”. *Workshop Notes: American Control Conference.*

[E V] P. T. E. Velenis. “Minimum Time vs Maximum Exit Velocity Path Optimization During Cornering”. *2005 IEEE international symposium on industrial electronics.*

[Efs08] J. L. Efstathios Velenis Panagiotis Tsiotras. Optimality Properties and Driver Input Parameterization for Trail-braking Cornering. *European Journal of Control* 4 (2008), 308–320.

[EP09] J. Edelmann and M. Plöchl. Handling Characteristics and Stability of the Steady-State Powerslide Motion of an Automobile. *Regular and Chaotic Dynamics* **14**.6 (2009), 682–692.

[ES98] C. Edwards and S. K. Spurgeon. *Sliding Mode Control: Theory and Applications.* Taylor & Francis Ltd, 1998.

[Fal+08] P. Falcone et al. “Low Complexity MPC Schemes for Integrated Vehicle Dynamics Control Problems”. *AVEC ’08.* 2008.

[Fal+10] P. Falcone et al. “On Low Complexity Predictive Approaches to Control of Autonomous Vehicles”. *Lecture Notes in Control and Information Sciences: Automotive Model Predictive Control.* Vol. 402. Springer-Verlag Berlin Heidelberg, 2010, pp. 195–210.

[Fra08] E. Frazzoli. Discussion on: ’Optimality Properties and Driver Input Parameterization for Trail-braking Cornering’. *European Journal of Control* 4 (2008), 321–328.

[GBD02] T. J. Gordon, M. C. Best, and P. J. Dixon. An automated driver based on convergent vector fields. *Proc Instn Mech Engrs* **216** (2002), 329–347.

[Gil92] T. D. Gillespie. *Fundamentals of Vehicle Dynamics.* Society of Automotive Engineers, Inc., 1992.

[Gra+] A. Gray et al. “Predictive Control for Agile Semi-Autonomous Ground Vehicles using Motion Primitives”. *2012 American Control Conference.*

[GTP96] J. Guldner, H.-S. Tan, and S. Patwardhan. Analysis of Automatic Steering Control for Highway Vehicles with Look-down Lateral Reference Systems. *Vehicle System Dynamics* **26**.4 (1996), 243–269.

[HC13] L.-Y. Hsu and T.-L. Chen. An Optimal Wheel Torque Distribution Controller for Automated Vehicle Trajectory Following. *IEEE TRANSACTIONS ON VEHICULAR TECHNOLOGY* **62**.6 (July 2013), 2430–2440.

[HG05] Y.-H. J. Hsu and J. C. Gerdes. “Stabilization of a Steer-by-wire Vehicle at the Limits of Handling using Feedback Linearization”. *Proceedings of IMECE2005: 2005 ASME International Mechanical Engineering Congress and Exposition.* Nov. 2005.

[Hin13] R. Y. Hindiyeh. “Dynamics and Control of Drifting in Automobiles”. PhD thesis. Stanford University, Mar. 2013.

[HM90] R. A. Hess and A. Modjtahedzadeh. A Control Theoretic Model of Driver Steering Behavior. *IEEE Control Systems Magazine* (Aug. 1990).

[Hoe16] R. van Hoek. "Vehicle State Estimation Using the State Dependent Riccati Equation Technique". MA thesis. Eindhoven University of Technology, 2016.

[ime08] T. Ç. imen. "State-Dependent Riccati Equation (SDRE) Control: A Survey". *Proceedings of the 17th World Congress*. The International Federation of Automatic Control. July 2008.

[KG12] K. Kritayakirana and J. C. Gerdes. Using the centre of percussion to design a steering controller for an autonomous race car. *Vehicle System Dynamics* (2012).

[KG15] N. R. Kapania and J. C. Gerdes. Design of a feedback-feedforward steering controller for accurate path tracking and stability at the limits of handling. *Vehicle System Dynamics* **53**.12 (2015), 1687–1704.

[Kha02] H. K. Khalil. *Nonlinear Systems Third Edition*. Prentice-Hall, Inc, 2002.

[Klo10] M. Klomp. "Longitudinal Force Distribution and Road Vehicle Handling". PhD thesis. Chalmers University of Technology, 2010.

[Koš+98] J. Košecká et al. "A Comparative Study of Vision-Based Lateral Control Strategies for Autonomous Highway Driving". *Department of Electrical Engineering and Computer Sciences*. University of California at Berkeley, 1998.

[Koš96] J. Košecká. *Vision-based Lateral Control of Vehicles Look-ahead and Delay Issues*. 1996.

[Kri12] K. (Kritayakirana. "Autonomous Vehicle Control at the Limits of Handling". PhD thesis. Stanford University, June 2012.

[LC08] D.-C. Liaw and W.-C. Chung. A feedback linearization design for the control of vehicle's lateral dynamics. *Nonlinear Dyn* **52** (2008), 313–329.

[Lie+] E. K. Liebemann et al. *Safety and Performance Enhancement: The Bosch Electronic Stability Control (ESP)*. Tech. rep. Paper Number 05-0471. Robert Bosch GmbH Germany.

[LL94] M. F. Land and D. N. Lee. Where we look when we steer. *Letters to Nature* **369** (June 1994), 742–744.

[Mad+12] A. K. Madhusudhanan et al. "Solving Algebraic Riccati Equation Real Time for Integrated Vehicle Dynamics Control". *2012 American Control Conference*. June 2012, pp. 3593–3598.

[NS11] S. Nazari and B. Shafai. "Robust SDC Parameterization for a Class of Extended Linearization Systems". *2011 American Control Conference*. June 2011, pp. 3742–3747.

[Ono+06] E. Ono et al. Vehicle dynamics integrated control for four-wheel-distributed steering and four-wheel-distributed traction/braking systems. *Vehicle System Dynamics* **44**.2 (Feb. 2006), 139–151.

[Ono+13] E. Ono et al. Bifurcation in Vehicle Dynamics and Robust Front Wheel Steering Control. *IEEE TRANSACTIONS ON CONTROL SYSTEMS TECHNOLOGY* **21**.4 (July 2013), 1258–1269.

[OUH95] U. Ozguner, K. Unyelioglu, and C. Hatipoglu. "An Analytical Study of Vehicle Steering Control". *Control Applications, 1995., Proceedings of the 4th IEEE Conference on*. IEEE, 28-29 Sep 1995.

[Pac12] H. Pacejka. *Tire and Vehicle Dynamics*. Ed. by I. Besselink. 3rd. Elsevier Ltd., 2012.

[Pad] R. Padhi. *Optimal Control, Guidance and Estimation*. Indian Institute of Science, Bangalore, Department of Aerospace Engineering, Lecture Notes.

[Par09] E. Parliament. *REGULATION (EC) No 661/2009 OF THE EUROPEAN PARLIAMENT AND OF THE COUNCIL*. Official Journal of the European Union. July 2009.

[PI11] S. C. Peters and E. F. andKarl Iagnemma. "Differential flatness of a front-steered vehicle with tire force control". *IEEE/RSJ International Conference on Intelligent Robots and Systems*. IEEE, Sept. 2011.

[PT90] H. Peng and M. Tomizuka. "Vehicle Lateral Control for Highway Automation". *American Control Conference, 1990*. IEEE, 23-25 May 1990, pp. 788–794.

[PW] H. Pang and L. Wang. "Global Robust Optimal Sliding Mode Control for a Class of Affine Nonlinear Systems withUncertainties Based on SDRE". *Second International Workshop on Computer Science and Engineering*.

[Raj12] R. Rajamani. *Vehicle Dynamics and Control*. Ed. by F. F. Ling. Springer Science+Business Media, 2012.

[RSG00] E. J. Rossetter, J. P. Switkes, and J. C. Gerdes. Experimental Validation of the Potential Field Lanekeeping System. *International Journal of Automotive Technology* (2000).

[SCS00] R. Sharp, D. Casanova, and P. Symonds. A Mathematical Model for Driver Steering Control, with Design, Tuning and Performance Results. *Vehicle System Dynamics, 33:5,* **33**.5 (2000), 289–326.

[Tho+13] P. Thomas et al. “Identifying the causes of road crashes in Europe”. *57th AAAM Annual Conference Annals of Advances in Automotive Medicine*. Sept. 2013.

[TJ10] J. Tjønnås and T. A. Johansen. Stabilization of Automotive Vehicles Using Active Steering and Adaptive Brake Control Allocation. *IEEE TRANSACTIONS ON CONTROL SYSTEMS TECHNOLOGY* **18**.3 (May 2010), 545–558.

[TKG11] K. L. Talvala, K. Kritayakirana, and J. C. Gerdes. Pushing the limits: From lanekeeping to autonomous racing. *Annual Reviews in Control* **35** (2011), 137–148.

[Trz08] M. Trzesniowski. *Rennwagentechnik*. 1st ed. Vieweg+Teubner, 2008.

[Vel+09] E. Velenis et al. Steady-state drifting stabilization of RWD vehicles. *Control Engineering Practice* **19** (2009), 1363–1376.

[VFT09] E. Velenis, E. Frazzoli, and P. Tsiotras. “On Steady-State Cornering Equilibria for Wheeled Vehicles with Drift”. *CDC/CCC 2009. Proceedings of the 48th IEEE Conference*. Institute of Electrical and Electronics Engineers, MIT, 2009, pp. 3545–3550.

[VHG10] C. Voser, R. Y. Hindiyeh, and J. C. Gerdes. Analysis and control of high sideslip manoeuvres. *Vehicle System Dynamics* **48** (2010), 317–336.

[VTL07] E. Velenis, P. Tsiotras, and J. Lu. “Modeling aggressive maneuvers on loose surfaces: The cases of Trail-Braking and Pendulum-Turn”. *Control Conference (ECC), 2007 European*. July 2007, pp. 1233–1240.

[Wei16] E. W. Weisstein. *Curvature*. A Wolfram Web Resource. http://mathworld.wolfram.com/Curvature.html. June 2016.

[Xio+12] L. Xiong et al. Vehicle dynamics control of four in-wheel motor drive electric vehicle using gain scheduling based on tyre cornering stiffness estimation. *Vehicle System Dynamics* **50**.6 (June 2012), 831–846.

A Toyota Prius Parameters

Table A.1: Vehicle Parameters of Toyota Prius 2012

Parameter	Value	Unit	Designation	Source
l	2.7	m	wheelbase	TNO parameterfile
l_t	1.5	m	track width	TNO parameterfile
m_f	966	kg	nominal load on front axle	TNO parameterfile
m_r	688	kg	nominal load on rear axle	TNO parameterfile
m	1654	kg	nominal total vehicle mass	$m_f + m_r$
I_Z	2865.6106	kg m^2	yaw moment of Inertia	TNO parameterfile
l_f	1.1231	m	x-distance CG to front axle	$l\frac{m_r}{m}$
l_r	1.5769	m	x-distance CG to rear axle	$l\frac{m_f}{m}$
h_{CG}	0.54	m	nominal CG height	TNO parameterfile
$C_{\alpha,f}$	117620	N/rad	front axle lateral stiffness	derived from TNO Prius MF tire model
$C_{\alpha,r}$	169960	N/rad	rear axle lateral stiffness	derived from TNO Prius MF tire model

B BMW 5 Parameters and Testing Setup

Table B.1: Vehicle Parameters of BMW

Parameter	Value	Unit	Designation	Source
l	2.888	m	wheelbase	TNO parameterfile
l_t	1.570	m	track width	TNO parameterfile
m_f	927.8	kg	nominal load on front axle	TNO parameterfile
m_r	972.2	kg	nominal load on rear axle	TNO parameterfile
m	1900	kg	nominal total vehicle mass	$m_f + m_r$
I_Z	3498	kg m^2	yaw moment of Inertia	TNO parameterfile
l_f	1.478	m	x-distance CG to front axle	$l\frac{m_r}{m}$
l_r	1.410	m	x-distance CG to rear axle	$l\frac{m_f}{m}$
h_{CG}	0.544	m	nominal CG height	TNO parameterfile
$C_{\alpha,f}$	122440	N/rad	front axle lateral stiffness	derived from TNO MF tire model of BMW similar tire
$C_{\alpha,r}$	213630	N/rad	rear axle lateral stiffness	derived from TNO MF tire model of BMW similar tire

Figure B.1: *TNO BMW 5.45 (E60) vehicle dynamics test lab, with automatic gearbox*

Figure B.2: *Steering robot installation*

C Testtrack

Figure C.1: *Skid Pad with artificial irrigation*

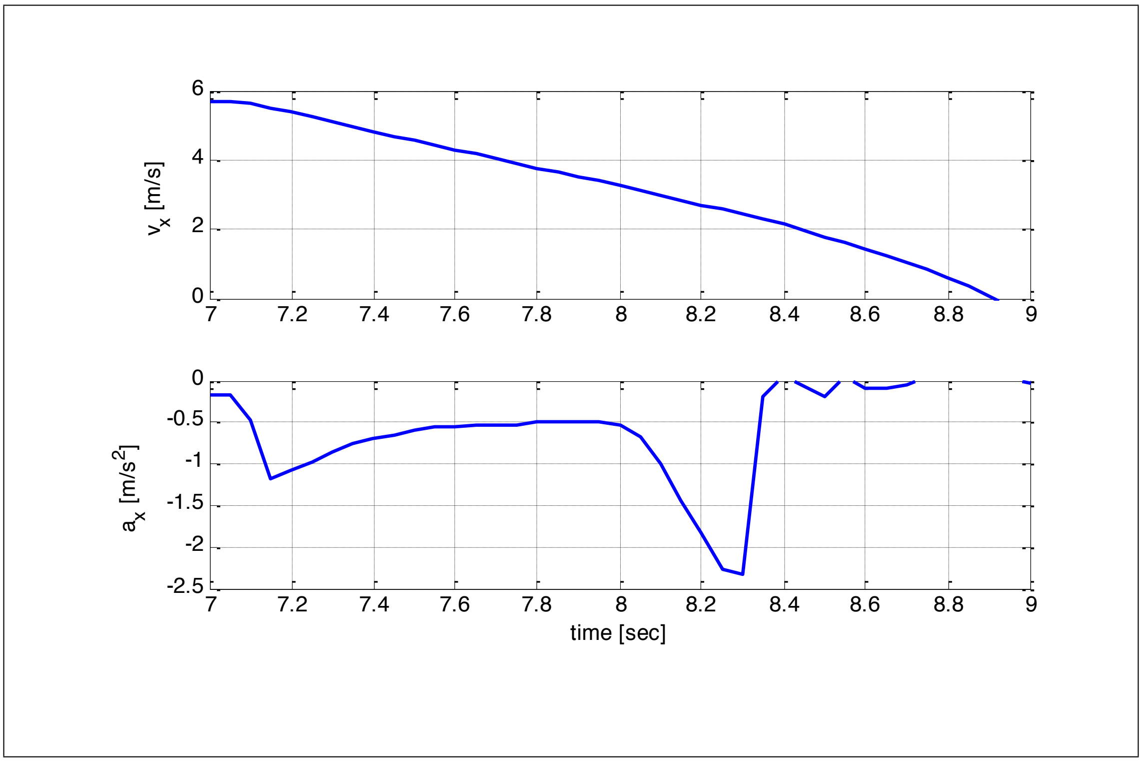

Figure C.2: *Progressive braking manoeuvre on the low friction skid pad surface. The friction estimate is determined by the first peak of the longitudinal acceleration with about -1.3 m/s^2. The second peak represents full wheel lock at almost stand still, where the water below the wheels is pushed away, and therefore larger absolute acceleration is measured.*

D Alternative Error Definition

An alternative error definition accounting for body sideslip β is presented. Heading and look-ahead error both yield zero when the vehicle is located on the path and the total velocity vector points in the direction of the path. See the error definition in Figure D.1.

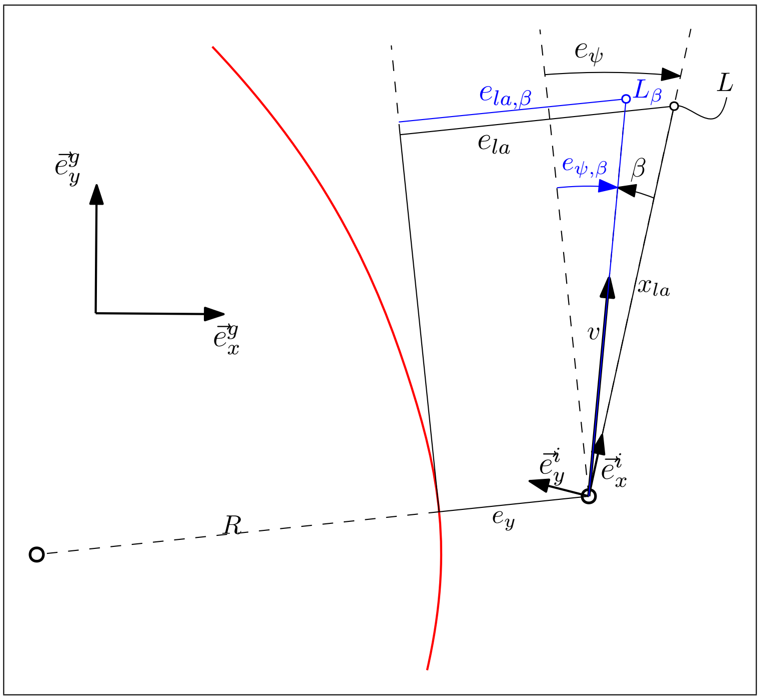

Figure D.1: *Error definition*

The nonlinear state equations can be obtained using

$$e_\psi = e_{\psi,\beta} + \beta, \tag{D.1}$$

as can be seen from the figure. It follows:

$$\dot{e_{\psi,\beta}} = [v_x cos(e_{\psi,\beta} + \beta) + v_y sin(e_{\psi,\beta} + \beta)]\rho_{des} - r - \dot{\beta} \tag{D.2}$$

$$\dot{\beta} = \frac{1}{1 + (\frac{v_y}{v_x})^2} \frac{\dot{v_y} v_x - v_y \dot{v_x}}{v_x^2} \tag{D.3}$$

$$\dot{e_{la,\beta}} = \dot{e_y} + x_{la} cos(e_{\psi,\beta}) \dot{e_{\psi,\beta}} \tag{D.4}$$

$$\dot{e_y} = -v_y cos(e_{\psi,\beta} + \beta) + v_x sin(e_{\psi,\beta} + \beta) \tag{D.5}$$

This error definition is dependent on β-feedback. A linearized model was tested by [KG15] and it was concluded that stability margins are reduced in comparison to the normal error definition.